Idrees, Muhammad Danish

Acoustic analysis of engine exhaust ducts: a comprehensive empirical/1D simulation approach

School of Technology and Innovations
Master's thesis
Industrial Systems Analytics

Vaasa 2023

UNIVERSITY OF VAASA
School of Technology and Innovations
Author: Idrees, Muhammad Danish
Title of the Thesis: Acoustic analysis of engine exhaust ducts: a comprehensive empirical/1D simulation approach
Degree: Master of Science
Programme: Industrial Systems Analytics
Supervisor: Maciej Mikulski, Jeyoung Kim
Industrial Instructor: Zengxin Gao
Year: 2023 **Pages:** 111

ABSTRACT :
Internal combustion engines, renowned for their instantaneous and high-energy output, are in high demand in the heavy-duty sector, especially within the marine industry. However, they pose significant challenges with atmospheric and noise emissions. Excessive noise impacts human health and has adverse effects on harbor environmental due to the significant noise emissions produced by vessels. One of the main causes that deliberately contributes to this noise is the exhaust stack. Studying how noise behaves in these exhaust ducts can help improve their design and reduce these noise emissions.

This thesis aims to study the behavior of low-frequency acoustic in exhaust ducts through experiments and simulations, while ignoring thermal and mean-flow effects. The study is based on two experiments: one using the main exhaust pipe of the W4L20 medium-speed engine, and the other using a plastic pipe (3.2 m), called the reference experiment. The thesis focuses mainly on the reference experiment. This reference experiment was modeled using the 1D modeling software GT-SUITE. The aim of this study is to identify the parameters that affect the accuracy of noise measurements with a perspective to use them to calibrate airflow simulation models. To this end, a unique approach is adopted to define the acoustic source in the GT model using input data obtained from experiment. In addition, a comparative analysis between the GT model and experimental results has been conducted to identify discrepancies. The thesis also includes a fundamental analysis of the experimental results for the main exhaust pipe. The emphasis is on understanding the phenomenon of acoustic propagation through complex airflow paths.

Experimental results showed that the fundamental mode of wave propagation remained dominant. In the reference experiment, this mode succeeded in exciting the resonance frequencies of the plastic pipe. However, this mode failed to excite the resonance of the exhaust pipe. During noise propagation, it was observed that the effect of pipe bends on the SPL was negligible. Furthermore, simulation results based on the GT model showed that the reliability of these results depends on the accuracy of the input data measured during the experiment. Measurements taken outside the source opening are very sensitive to sensor placement. They showed 8 to 10 dB difference in SPL at a small distance of only 9 mm. It was concluded that for duct-based simulations, input data should be measured from inside the source pipe. The parametric study using the GT-model showed that the resonant frequencies decrease with increasing pipe length. However, the increase in pipe diameter and pipe bend had no significant effect on the frequency spectrum.

KEYWORDS: Acoustic analysis, low-frequency, cut-off frequency, measurement, data acquisition, FFT, frequency spectrum, complex acoustic pressure, complex acoustic impedance, source characterization, GT-SUITE, parametric study

Acknowledgments

This Master's thesis was conducted on behalf of the University of Vaasa as part of Work Package 3 of the Silent Engine project. I express my sincere gratitude to all those who have made significant contributions to the successful completion of this thesis.

I am profoundly grateful to Professor Maciej Mikulski, my thesis supervisor, for allowing me to work under his guidance. His invaluable advice and unwavering support have been instrumental in the successful completion of this thesis. I would also like to extend my heartfelt gratitude to my second supervisor, Jeyoung Kim, a Ph.D. student who supported me with the writing and encouraged me throughout the process. In addition, I express my deep gratitude to my colleague, Touraj Hashempour, for his support in the modeling and simulation area.

I am obliged to my industrial instructor, Zengxin Gao, Sr. Noise Expert at Wärtsilä, for his central role in setting up the experimental setup and assisting with the measurement techniques used in this thesis. In addition, I also thank Carlo Pestelli, Sr. R&D Manager for Noise and Vibration, for his consistent guidance and, sharing the valuable code needed to perform FFT.

Finally, I would like to express my appreciation to the VEBIC engine laboratory team for their exceptional assistance in conducting this loudspeaker experiment. In particular, I would like to thank Pauli Valkjäarvi, whose continuous support was crucial throughout the experimental process.

In addition, I would like to acknowledge that the results of this work were achieved in the "Partnership model - Silent Engine" project, which was co-funded by Business Finland (NextGenerationEU funding).

Contents

Figures

Tables

Abbreviations

ADC	Analog to Digital converter
BNC	Bayonet Neill-Concelman
CCP	Conventional Coupler probe
EN	Exhaust Noise
FFT	Fast Fourier Transform
GT	Gamma Technologies
IL	Sound Intensity Level
IMO	International Maritime Organization
ISO	International Organization for Standardization
NOx	Nitrogen Oxides
NVH	Noise, Vibration, and Harshness
PM	Particulate Matter
PP	Pressure Pressure
PU	Pressure Velocity
PVC	Polyvinyl Chloride
PWL	Sound Power Level
RCCI	Reactivity Controlled Compression Ignition
RMS	Root Mean Square
SI	International System of Units
SOLAS	International Convention for the Safety of Life at Sea
SPL	Sound Pressure Level
TM	Transfer Matrix
VEBIC	Vaasa Energy Business Innovation Centre
WP	Work Package

Greek Symbols

γ	Specific heat ratio
λ	Wavelength
ω	Angular frequency of wave
ξ	Particle displacement

Latin Symbols

ρ	Density of the medium (air)
ω	Angular frequency of wave

Other Symbols

A	Pipe cross-sectional area
a	Duct cross-sectional area
a_f	Amplitude correction factor
c	Speed of Sound
C_p	Specific heat capacity at constant pressure
C_v	Specific heat capacity at constant volume
e_f	Energy correction factor
f	Frequency
$F(s)$	Sampling frequency
f_0	Centre frequency
F_{max}	Maximum frequency
I	Measured sound intensity
I_{ref}	Reference sound intensity
j	Imaginary number
K	Stiffness of the medium (air)
k_c	Modified wave number

k_o	Wave Number
L	Length of pipe
M_0	Mach number
N	Block size
n_{lines}	Number of spectral lines
p	Pressure inside the medium (air)
$p(t)$	Sound pressure in time domain
p_1, p_2	Sound pressure at state 1 and 2
P_s	Source pressure
Pr	Prandtl number
R	Geometric radius
res	Frequency resolution
Δr	Distance between two microphones
S	Cross-sectional area of orifice
T	Time period
Δt	Time step
U	Particle Velocity of fluid
u	Volumetric flow rate of fluid
u_1, u_2	Volumetric flow rate at state 1 and 2
v	Dynamic viscosity of fluid
$v(t)$	Particle velocity in time domain
W	Measured sound power
W_{ref}	Reference sound power
$winsize$	Window size
x	Coordinate along axial direction
Z	Acoustic Impedance
z	Specific acoustic Impedance
Z_s	Source impedance

1 Introduction

1.1 Background

Industries face significant challenges as the world transitions to cleaner and more sustainable energy sources. Transportation, with a particular focus on the marine industry, is a sector at the crossroads of this transition. Traditionally reliant on internal combustion engines as its primary propulsion systems, the marine industry now faces the challenge of excessive noise emissions. Advanced combustion concepts such as reactivity-controlled compression ignition (RCCI) and low-carbon fuels have attracted much interest due to their superior thermal efficiency and very low emissions (NOx and PM). Surprisingly, it's not air pollution that is the biggest obstacle to the development of these next generation of engines, but rather the issue of noise. The consequences of excessive noise emissions are multifaceted, affecting both human populations and marine ecosystems.

The International Maritime Organization (IMO) has established guidelines in resolution MSC.337(91), known as the code on noise levels on board ships. These guidelines referenced (International Maritime Organization, 2012) define a maximum noise level of 70 dB(A) for listening posts, which encompass various areas such as navigating bridge wings and windows, during the ship's normal operating conditions. Apart from this the Danish Maritime Authority has established its own guidelines for noise levels on ships. These guidelines (Danish Maritime Authority, 2006) specify noise limits and recommended limits for various areas such as listening stations, external recreation areas, and rescue stations. According to the regulation, the noise limit for listening stations is 70 dB(A) and 75 dB(A) for external recreation areas and rescue stations. Additionally, the recommended limits are 5 dB lower than the specified limits for each respective area. On top of that, the International Convention for the Safety of Life at Sea (SOLAS) (International Maritime Organization , 1974) has implemented a strict noise limit of 110 dB(A), measured from a mere 1-meter distance from the engine. Meeting

this demanding standard is already challenging, particularly for machinery setups with twin engines. In anticipation of forthcoming regulations by 2025, industries are pledging to lower noise emissions below the 100 dB(A) threshold.

In response to this legislation on industrial machinery, the Silent Engine consortium (SilentEngine, 2022), aims to revitalize the Finnish powertrain industry to meet the standards set for the combined areas of noise/vibration and sustainability. A new set of robust and state-of-the-art NVH solutions will be applied to the internal combustion engine using the latest measurement techniques and simulation tools. The subject of this study is the W4L20 medium-speed internal combustion engine, located at the engine laboratory of the Vaasa Energy Business Innovation Center (VEBIC). The primary project goal is to decrease the overall engine noise by 5 dB, with the approach divided into three distinct work packages that target specific aspects of noise emissions. Work package 3 (WP3) focuses on the exhaust noise (EN) emitted by the engine. The aim is to explore new ways to reduce engine EN without compromising engine performance. This work, based on acoustic analysis of the exhaust duct, is directly related to this goal of WP3 and will contribute to the overall understanding of acoustics based on complex air paths.

1.2 Formulating the Problem

The world of acoustics is complex, with many factors influencing the nature and behavior of sound. This complexity becomes particularly apparent when performing experiments on a larger scale. This is especially true when dealing with exhaust ducts that extend over a distance of 15 meters. In these situations, it is both time-consuming and costly to modify the geometric parameters of such long exhaust ducts for in-depth analysis. Furthermore, creating controlled experimental conditions, especially those that accurately mimic a free-field environment, is not possible. As a result, such experiments are prone to uncertainty. They lack the repeatability and flexibility required for accurate and thorough analysis to reduce noise levels.

In WP3 of the Silent Engine (SilentEngine, 2022) consortium, a model-based design methodology has been proposed to overcome this problem. It involves the establishment of a 1D model of the exhaust pipe using the acoustic simulation capabilities of GT-SUITE. The model would be able to explore the drastic changes in the exhaust pipe and make reliable predictions of airborne noise in a time and cost-efficient manner. However, this model-based approach requires high-precision input data to make reliable acoustic predictions. This input data can be obtained from the experimental measurements. The reliability and accuracy of the model will be tested by validating it with the experimental results. After the verification, this model can be optimized by performing a parametric study to achieve maximum noise reduction. This thesis adopts the same methodology as proposed in WP3 of the Silent Engine project. Instead of using an exhaust pipe, the methodology is applied to a reference experiment using a plastic pipe, with a loudspeaker acting as the acoustic source to mitigate the thermal and flow effects produced by a running engine.

The main objective of this thesis is to analyze the acoustic behavior of noise in-ducts at low frequencies. This objective is pursued through a dual-track approach that combines experimentation and simulation. In the experimental approach, the influence of complex air paths, such as bends, on SPL and propagation modes is studied. Results obtained from experiments involving exhaust pipe and plastic pipe setups are critically analyzed. In parallel, the acoustic simulation approach involves modeling a reference experiment within GT-SUITE. The aim of this study is to understand the parameters that affect the accuracy of noise measurements from the perspective of using them to calibrate airflow simulation models. This work highlights the sensitivity of acoustic parameters based on their measurement locations during the experiments. Additionally, the gap between the idealized acoustic environment (free field) and the actual experimental conditions is explored. The transfer matrix method in GT-SUITE for calculating acoustic results in linear solutions is also investigated. A parametric study using the established GT model assesses the influence of parameters such as pipe diameter, length, and bends on acoustic behavior. This work will directly contribute to the goals of Silent Engine WP3

and help to further refine the methodology of modeling and simulation of complex airflow paths in GT-SUITE. To achieve these objectives, the following four research questions will be addressed in details.

1. What disparities emerge when validating GT-model-based results against outcomes from experimental data?
2. What is the most appropriate location for sensor placement to measure the input data to make reliable model-based acoustic predictions?
3. How do bends impact acoustic behavior in different sections of exhaust pipes?
4. How does the GT model-based parametric study, which involves varying the pipe's diameter, length, and angle of bend, influence the SPL?

1.3 Structure of Thesis

The thesis follows a structured framework consisting of five main chapters: "Review of Related Literature", "Objects and Methods", "Results and Discussion", "Summary and Outlook", and "Conclusions". Chapter 2, "Review of Related Literature," lays the foundation for understanding acoustic properties and their conversion into units. It emphasizes the importance of representing the frequency spectrum in terms of octaves and narrow bands. In addition, this chapter explores basic acoustic concepts such as acoustic impedance and resonance. The theoretical framework of this thesis is also explained in this part. This includes the calculation of the cutoff frequency and an overview of the possible propagation modes under the conditions set for the analysis. Furthermore, the measurement techniques used in the experiments and the principles followed by the sensors are also covered in this chapter. Chapter 3 of the thesis focuses on the objectives and methods used during the experiments, data analysis and 1D modeling of the reference experiment in GT-POWER. It shows how the experiments were performed and how the source settings were set during the experiments. In addition, the signal processing of the pressure and particle velocity signals collected by the sensor is explained. The purpose and procedure of data analysis is detailed in this part of the thesis. Applications used in signal processing such as windowing and spectral leakage and their significance are also discussed. Impedance calculation from the FFT output and

normalization techniques are also included in this chapter. Finally, this chapter ends by explaining the transfer matrix method used for 1D modeling of the reference experiment in GT-POWER. Chapter 4 of the thesis is dedicated to discussion and results. The first part of this section focuses on the validation of the results obtained by post-processing the data. In addition, a comparative analysis is carried out considering different positions of the sensor relative to the source to see how the sound pressure evolves. The spectral analysis of the results of the reference experiment and the exhaust pipe experiment is presented in this chapter. The simulation results obtained from the GT model of the reference experiment are compared with the experimental results. Discrepancies in the results are discussed and the underlying factors are explained. Furthermore, a parametric study based on the model is also performed in this section. Chapter 5 summarizes these results and provides conclusive answers to the proposed research questions. It also contains suggestions in the form of a perspective on how to improve the accuracy of model-based simulation on the basis of measurements. The final chapter, Chapter 6, provides a brief conclusion.

2 Review of Related Literature

2.1 Propagation of sound through fluids

The inherent nature of fluids, which include both gases and liquids, lies in their ability to deform without stress. Unlike solid materials, fluids are not able to transmit shear forces. They respond to physical changes only due to their inertia. Sound waves are a notable example of compressional oscillations propagating through fluids. These waves oscillate back and forth in the direction of propagation, with no net flow, and are coupled with variations in pressure, density and temperature as depicted in Fig. 1. The quantity perceived as sound is the pressure fluctuation with respect to static pressure caused by sound waves traveling through the medium (Finn Jacobsen P. M., 2013).

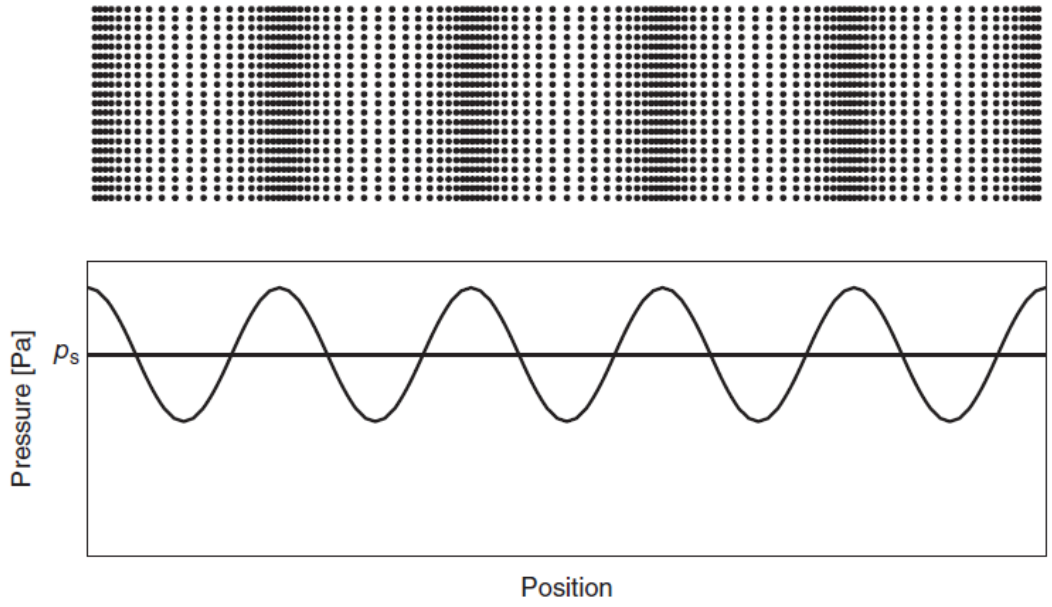

Figure 1. Sound pressure fluctuations can be seen relative to static pressures, resulting in regions of high pressure termed "compressions" and regions of low pressure termed "rarefactions" (Finn Jacobsen P. M., 2013).

Jacobsen and Juhl (2013) provided valuable insights on acoustics in their book. They explained that in acoustics, fluid oscillations are typically very small. They considered

sound at 120 dB, which is close to the pain threshold under standard conditions. At this level, very small changes in pressure and density of the fluids were observed, about 2×10^{-4} and 1.4×10^{-4}, respectively. Furthermore, temperature changes were minimal, and particle velocity measured around 50 mm/s at 1000 Hz. These facts illustrate that the sound perceived by the human ear results from very minute perturbations in the physical properties of a fluid.

2.1.1 Sound Measurement Units

The pascal is not recommended for sound pressure measurements, despite being the fundamental unit of pressure. This recommendation arises from the wide dynamic range of the human auditory system, which spans from 20 µPa to 20 Pa. As a result, using pascals for measurements often leads to confusion due to the resulting values in decimal notation (see Fig. 2).

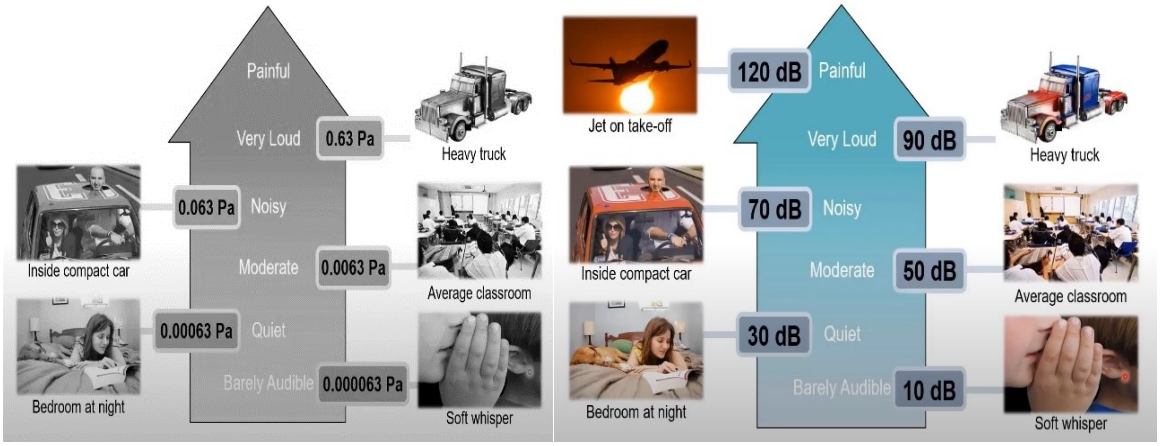

Figure 2. Comparison of sound pressure levels from various sources, measured in pascals and decibels (Basics: What is a decibel (dB) anyway? Why is it used?, 2021).

This problem can be solved by using a decibel scale. A decibel scale squeezes the human hearing range into the 0-120 dB range and expresses measurements in whole numbers. The conversion of the unit from pascal to decibel have been expressed in Eq. (1) and Eq. (2).

$$SPL = 10log\left(\frac{rms\ pressure}{ref.pressure}\right)^2 dB \quad (1)$$

The simplification of the Eq. (1) results the Eq. (2),

$$SPL = 20log\left(\frac{rms\ pressure}{ref.\ pressure}\right) dB \quad (2)$$

Where, $rms\ pressure$ is the root mean square of the pressure in pascal. The $ref.\ pressure$ is the reference pressure and always taken as 20 µPa. It is the minimum sound pressure level that can be perceived by the human ear also referred to as 0 dB. The dB scale operates on a logarithmic basis is not an absolute unit. It is a logarithmic ratio between the measured quantity and a standardized reference value (Brüel & Kjær, 1984). Another important advantage of sound representation in the decibel scale is its ability to reflect human hearing more accurately, since human sensitivity is logarithmic in nature. Table 1 highlights an interesting observation about unit conversion to decibels.

Table 1. Unit conversion of the pressure along linear and decibel scale is shown (Basics: What is a decibel (dB) anyway? Why is it used?, 2021).

Parameter	Linear Scale	Decibel Scale
Hearing threshold 1kHz	$20e^{-6}$ Pa	0 dB
Calibration	1 Pa	94 dB
Doubling the pressure	2 Pa	100 dB
Doubling again	4 Pa	106 dB
Pain threshold	20 Pa	120 dB

As shown in Tab. 1, doubling the pressure from 1 Pa to 2 Pa results in a 6 dB increase on the decibel scale, raising the SPL from 94 dB to 100 dB. However, when the pressure is reduced from 200 Pa to 100 Pa, there is only a 6 dB decrease on the decibel scale. This

difference in dB illustrates the logarithmic relationship between pressure in pascals and decibels. The dB scale can also be used to express other acoustic properties. These include sound power, sound intensity, and particle velocity. The sound intensity level (IL) and power level (PWL) can be obtained by using Eq. (3) and Eq. (4).

$$IL = 10log\frac{I}{I_{ref}}\ decibels \tag{3}$$

The IL is the sound intensity level in decibels and should not be confused with intensity (I) in watts per square meter. Similarly, the sound power level can be calculated by Eq. (4).

$$PWL = 10log\frac{W}{W_{ref}}\ decibels \tag{4}$$

Table 2. Sound pressure, sound power, and sound intensity can all be expressed in decibels (dB) even though they represent different physical quantities (Sound Pressure, Sound Power, and Sound Intensity: What's the difference?, 2019).

Quantity	**Measurement Unit**	**Reference Values**
Sound Pressure	Pa (Pascal)	dB (ref=20×10^{-6} Pa)
Sound Power	W (Watts)	dB (ref = 1×10^{-12} W)
Sound Intensity	W/m^2	dB (ref = 1×10^{-12} W/m^2)
Particle Velocity	m/s	dB (ref =5 × 10^{-8} m/s)

Reference values for different acoustic properties can be found in Tab.2. In acoustics, direct measurement of sound intensity can be difficult. Sound pressure is therefore a parameter often used for measurement. This parameter is similar to voltage in electronic circuits. Sound intensity, or power, is proportional to the square of sound pressure.

Consequently, the conversion of linear quantities (sound pressure, particle velocity and displacement) to the dB scale uses 20log for conversion, as shown in Eq. (2). On the other hand, the levels of second-order (quadratic) quantities are calculated using the tenfold logarithm of the ratio of their rms value to the reference value (F. Alton Everest, 2015).

2.1.2 Frequency and Wavelength

Sound is often represented by sinusoidal waves as depicted in Fig. 1. This is because of their simplicity and regularity. Many natural sounds, especially pure tones, can be approximated by simple sinusoidal oscillations. These waves are mathematically easy to analyse and understand. Therefore, they are a common choice for representing sound. This representation of the sound in a sinusoidal waveform makes it easier to study its properties, such as frequency, time period, and wavelength.

Time period is the time it takes the sound wave to complete one cycle, usually represented by T, and is one second for pure tone. The frequency of the sound is the number of cycles that a periodic wave goes through in one second and is usually represented by Hertz or cycles per second. The range of human hearing for a healthy young individual typically extends from about 20 Hz to 20,000 Hz, which encompasses a wide range of audible sounds (Peters, 2011). For a pure tone, which has only one cycle, the frequency is one and is represented by Eq. (5)

$$f = \frac{1}{T} \tag{5}$$

The wavelength of the periodic wave, on the other hand, is the minimum distance between two points of the wave at which the air particles are in phase with each other.

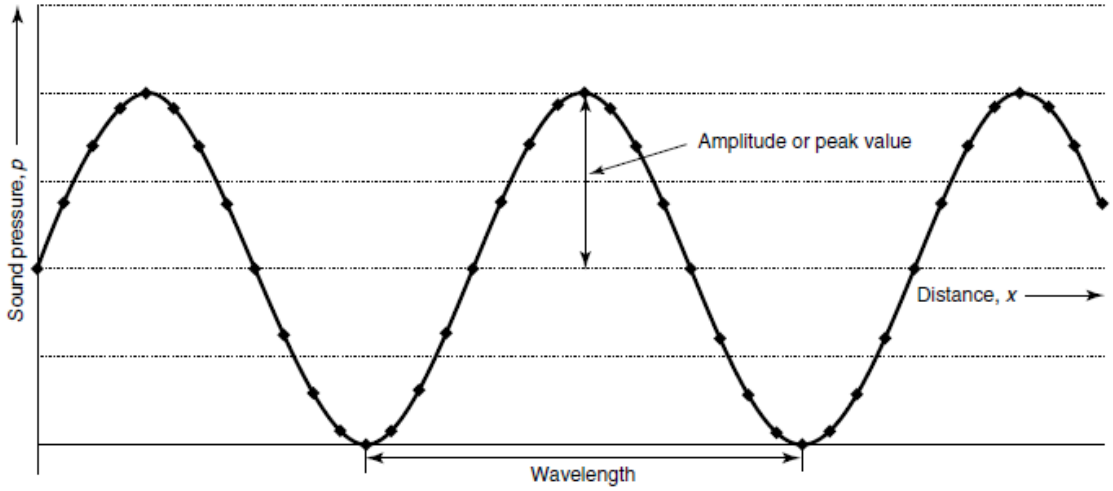

Figure 3. Wavelength is depicted between two consecutive troughs (Peters, 2011).

It can be said that the wavelength denoted by ‘‘λ’’ is the distance the wave travels to complete one cycle (Peters, 2011). So, the wave velocity can be expressed by Eq. (6).

$$c = \frac{\lambda}{T} = f\lambda \tag{6}$$

By re-arranging the Eq. (6),

$$\lambda = \frac{c}{f} \tag{7}$$

The frequency and wavelength of a periodic wave are inversely proportional to each other, as given in Eq. (7). The smaller the frequency is, the longer the wavelength will be. The frequency of a sound gives it a distinctive sound. For example, a lower-frequency sound can be heard as the distant rumbling of thunder, while a higher-frequency sound can be heard as a whistle. (Brüel & Kjær, 1984).

2.1.3 Frequency Spectrum

In acoustics, frequency spectra can be analysed and displayed in a variety of ways. This depends on the application and the level of detail required. Octave and narrow band frequencies are two common methods of representing frequency spectra. In this thesis, most of the sensor readings are filtered in 1/3 octave band frequencies and some of the results are in narrow band spectrum. The term "octave band" comes from music theory, where it refers to a range of frequencies between notes of the same name that are exactly doubled in frequency (Octaves in Human Hearing, 2020). This is shown in the following Fig. 4.

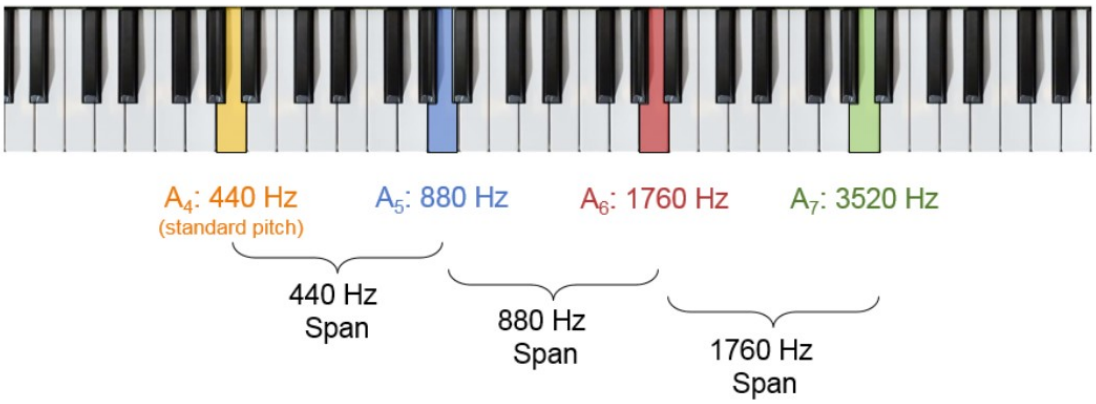

Figure 4. In music, notes of the same name exhibit a doubling of frequency (Octaves in Human Hearing, 2020).

Furthermore, octave bands are groups of frequencies that help to quantify the way humans distinguish between frequencies. Each octave represents the total level of energy in the frequency band. The human ear has a spiral-shaped organ called the cochlea. It is responsible for detecting frequencies. This spiral-shaped organ is divided into a group of frequencies ranging from 20 Hz to 20 kHz. These frequencies are grouped logarithmically, like octave bands. This indicates that humans cannot process discrete frequencies. Rather, they can process the group or bucket of frequencies. The human hearing range is divided into eleven octave bands. Each band contains a frequency that is twice as high as the previous band (Octaves in Human Hearing, 2020). These bands are referred to as 1/1 octave bands, as shown in Tab. 3.

Table 3. The frequencies of the 1/1 octave bands within the human hearing range are categorized into lower, upper, and center frequencies (Octaves in Human Hearing, 2020).

Centre frequency	Lower Frequency	Upper Frequency	Band Range
16	11	22	11
31.5	22	44	222
63	44	88	44
125	88	177	89
250	177	355	178
500	355	710	355
1000	710	1420	710
2000	1420	2840	1420
4000	2840	5680	2840
8000	5680	11360	5680
16000	11360	22780	11360

Each 1/1-octave band can be divided into three bands, called 1/3-octave bands, to better match the way the human ear perceives frequencies. This finer resolution allows for a more detailed analysis of the frequency content. Table 4 lists the upper and lower cut-off frequencies of the 1/3-octave bands.

Table 4. The 1/3 octave bands are characterized by their upper, lower, and center frequencies, providing a more detailed and refined representation of the frequency content across the spectrum (Octaves in Human Hearing, 2020).

Centre Frequency	Lower Frequency	Upper Frequency
12.5	11.2	14.1
16	14.1	17.8
20	17.8	22.4
25	22.4	28.2

Centre Frequency	Lower Frequency	Upper Frequency
31.5	28.2	35.5
40	35.5	44.7
50	44.7	56.2
63	56.2	70.8
80	70.8	89.1
100	89.1	112
125	112	141
160	141	178
200	178	224
250	224	282
315	282	355
400	355	447
500	447	562
630	562	708
800	708	891
1000	891	1122
1250	1122	1413
1600	1413	1778
2000	1778	2239
2500	2239	2818
3150	2818	3548
4000	3548	4467
5000	4467	5623
6300	5623	7079
8000	7079	8913
10000	8913	11220
12500	11220	14130
16000	14130	17780
20000	17780	22390

The centre frequencies f_0 of an n[th] octave band are obtained by successive multiplication or division of 1,000 Hz with $2^{(\frac{1}{n})}$ (Jaouen, ei pvm). For example, the centre frequencies for a one-third octave band can be obtained by using Eq. (8).

$$Centre\ freq.before\ 1000\ Hz = \frac{1000}{(2)^{\frac{1}{3}}} = 793.7, (preferred: 800) \tag{8}$$

The lower and upper frequency bounds of a given n[th] octave band with a centre frequency f_0, are calculated as $f_0/(\sqrt{2})^{\frac{1}{n}}$ and $f_0 \times (\sqrt{2})^{\frac{1}{n}}$, respectively. For instance, if the centre frequency f_0, is 1000Hz, then the lower and upper frequency bounds can be given by Eq. (9) and Eq. (10).

$$Lower\ freq.bound = \frac{f_0}{(\sqrt{2})^{\frac{1}{3}}} = \frac{1000}{1.12246} = 891 \tag{9}$$

$$Upper\ freq.bound = f_0 \times (\sqrt{2})^{\frac{1}{3}} = 1000 \times 1.12246 = 1122 \tag{10}$$

Octave bands exhibit narrower spans at lower frequencies to enhance the ear's precise distinction, leveraging its heightened sensitivity in this range. Conversely, at higher frequencies, the bands broaden, posing a challenge for the ear to discriminate between frequencies. as depicted in Fig. 5 (Octaves in Human Hearing, 2020). It visually illustrates this phenomenon, showcasing the deliberate modulation of band widths across the audible spectrum. This strategic variation optimizes the auditory system's efficiency, aligning octave band characteristics with the intricacies of human hearing for a more accurate and nuanced perception of sound frequencies.

The narrow-band spectrum is used for the detailed analysis of the frequency component. Most commonly, 0.3125 frequency steps (frequency resolution) are used. This means that each frequency component is separated by 0.3125 Hz. Narrowband frequencies are characterized by focusing on specific frequency points or smaller frequency ranges within a broader spectrum. In contrast to octave bands, which group frequencies into logarithmic intervals, narrow band frequencies provide a more precise analysis of individual frequency components. This level of detail is critical when performing a detailed analysis of noise, especially in the low-frequency region of the spectrum

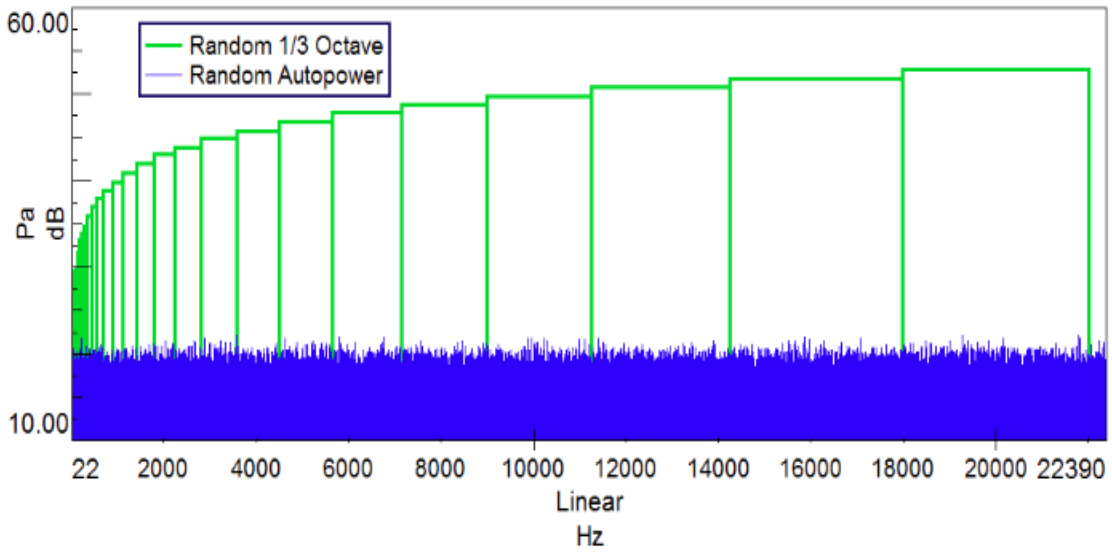

Figure 5. The X-axis is represented in a linear format, showcasing the random white noise expressed both in octaves and as an auto power (Octaves in Human Hearing, 2020).

The choice between using octave bands and narrow-band frequencies depends on the specific goals of the analysis. Octave bands are useful for a quick overview and rough analysis of the spectrum, while narrow-band frequencies are useful for examining specific characteristics of a signal, such as resonance and harmonics at individual frequency components. For instance, Fig. 6 shows the amplitude of the sound pressure level along each frequency component. The harmonics in the spectrum reflect the resonant behaviour of the sound wave.

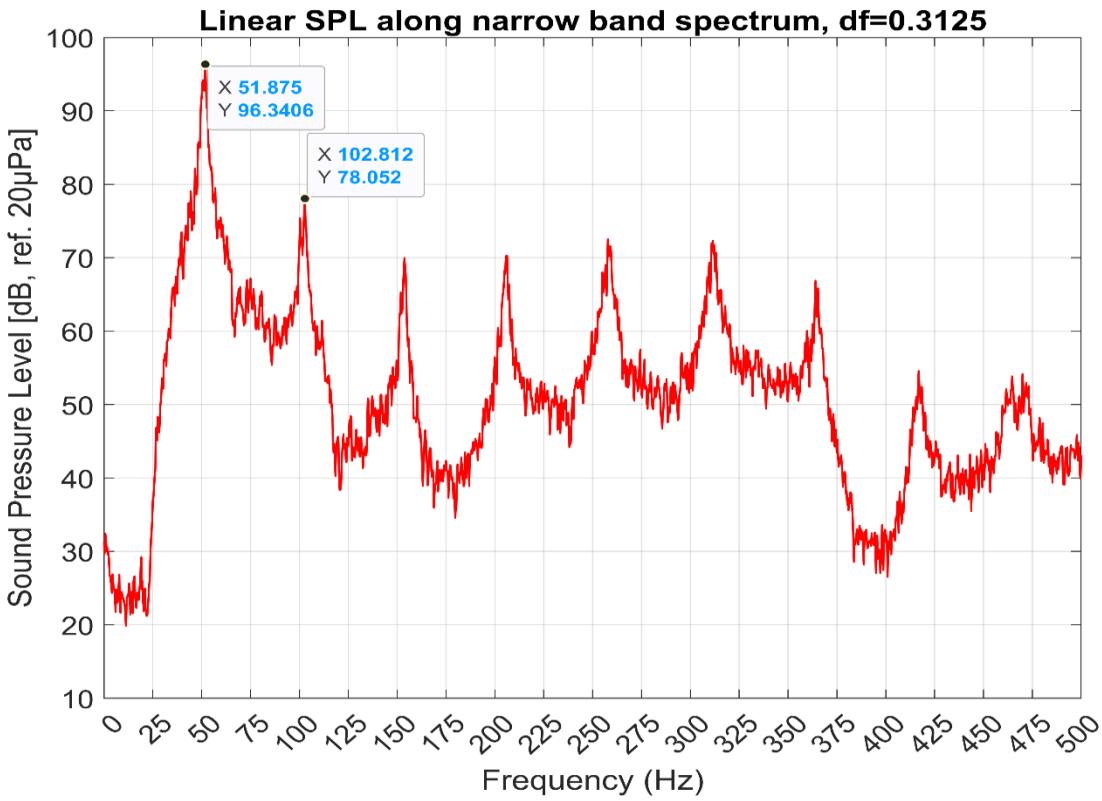

Figure 6. Harmonics are easily visible at different discrete values of the frequencies in given narrow band spectrum, at frequency step of 0.3125 Hz.

2.1.4 Particle Velocity

Particle velocity plays a critical role in acoustic analysis, particularly as it relates to sound pressure, sound intensity, and acoustic impedance. An understanding of particle velocity is essential to gain insight into the physical properties of a sound wave, including its direction, intensity, phase, waveform, wavelength, and source. When the surface of a source expands and contracts sinusoidally, the increased pressure causes air particles to move outward. This perturbation propagates outward at the speed of sound. During the next half of the sinusoidal motion, the source reverses direction, creating a pressure drop that pulls nearby particles toward it. This results in sinusoidal particle motion, called particle velocity, at any point in space (István L. Vér, 2005).

Particle Velocity is a vector quantity that describes the speed and direction at which particles move in a given medium. It is typically measured in m/s. In the case of one-dimensional sound propagation, the particle velocity direction is axial and can be positive or negative. The sign depends on whether the particles are moving away from or toward the source direction. The velocity of particles should not be confused with the velocity of the wave moving through the medium. The wave moves rapidly, but the particles only oscillate around their original positions at relatively low particle velocity as shown in Fig. 7. It is important to note that the velocities of individual molecules are different from particle velocities, which are mainly determined by temperature and molecular weight (Particle velocity, 2021).

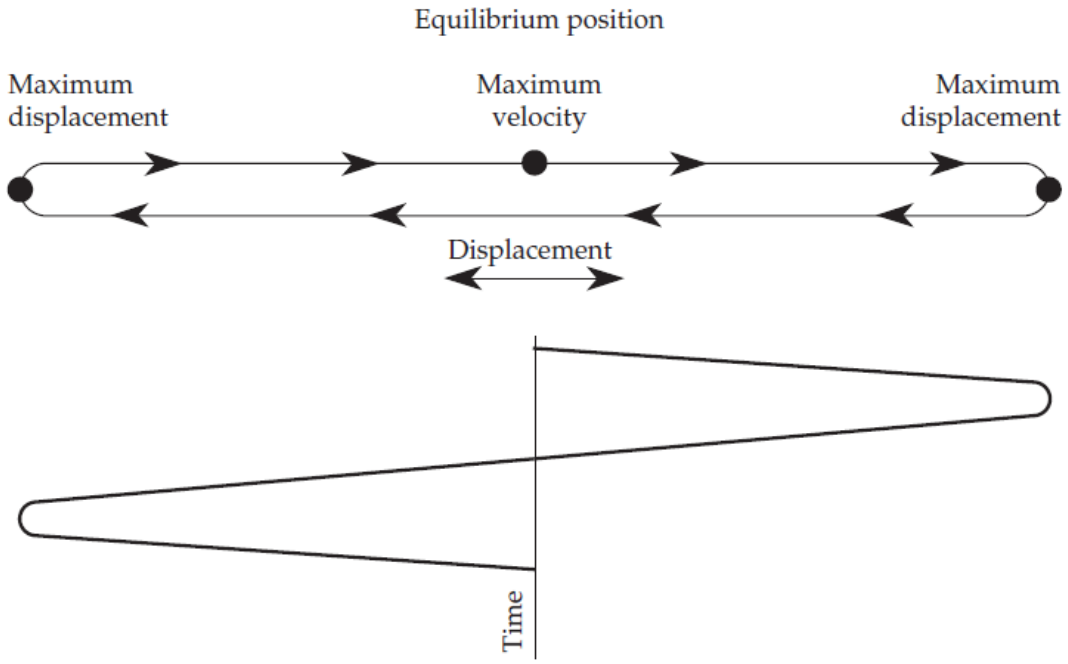

Figure 7. The interaction between the elastic forces and the inertia of the air particle causes it to vibrate around its equilibrium position when a sound wave passes through it (F. Alton Everest, 2015).

Moreover, in the context of plane waves, which occurs at significant distances from a point source in a free space. The sound pressure and particle velocity reach at their maximum and minimum values at the same time and are said to be in phase. However, the particles oscillate back and forth along the direction of wave propagation and their

velocities are always perpendicular to the imaginary spherical surface (wave front) in space (István L. Vér, 2005).

2.1.5 Sound Intensity

In engineering acoustics, sound intensity is an important quantity that represents the continuous flow of power carried by a sound wave through a small hypothetical area in space. It is expressed in watts per square meter (W/m^2) (István L. Vér, 2005). Sound intensity measurements play an important role in sound source localization. They help to determine the position of sound sources in an environment as illustrated in Fig. 8. It is done by analyzing the direction and magnitude of the sound intensity vector.

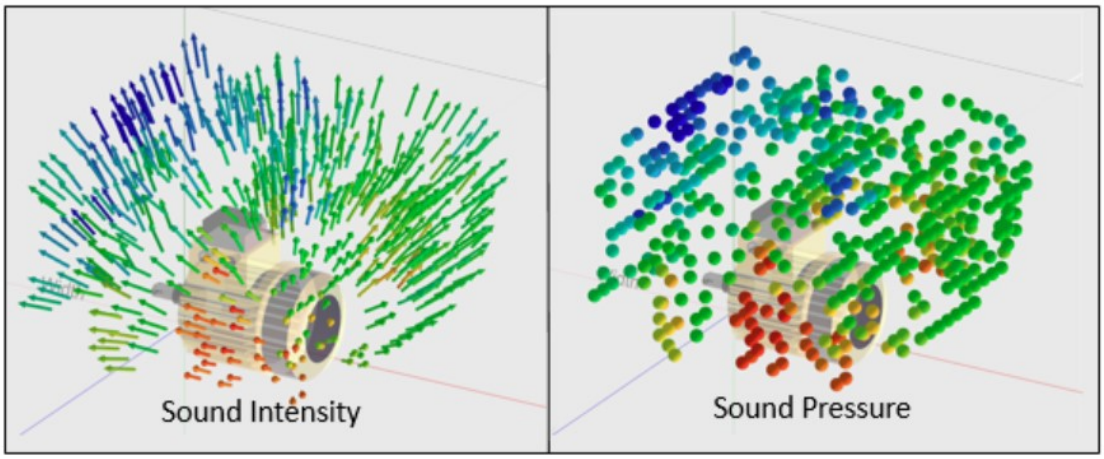

Figure 8. Sound intensity (left) indicates the direction of noise from the electric motor, while sound pressure (right) represents only the pressure magnitude (Sound Pressure, Sound Power, and Sound Intensity: What's the difference?, 2019).

Moreover, sound intensity measurements are instrumental in calculating the sound power emitted by sound sources. This knowledge is essential for understanding the sound energy output of various devices, machinery, or systems. The direction of sound intensity at a point is vectoral, meaning the plane of the small area can vary from being perpendicular to the direction of the wave's travel to being parallel to it. When the plane is perpendicular, sound intensity reaches its maximum value (I_{max}), and it becomes zero

when the plane becomes parallel. In between, the component of I_{max} changes with the cosine of the angle formed between the direction of travel and a line perpendicular to the area (István L. Vér, 2005). Typically, it is computed by multiplying the measured sound pressure level (scalar) with the particle velocity (vector), as shown in the Eq. (11).

$$\boldsymbol{I} = p(t).\boldsymbol{v}(t) \left[\frac{W}{m^2}\right] \tag{11}$$

The sound intensity is commonly expressed in decibels, with the reference value set at $1x10^{-12}$ W/m^2. There are two main types of the sound intensity probes:

1. Pressure velocity probe (PU): It consists of one microphone and one particles velocity sensor.
2. Pressure-Pressure probe (PP): It consists of two microphones separated by a spacer (Sound Intensity, 2020).

During the experimentations, both sensors are used and their measurement techniques will be elaborated in the forthcoming subsections.

2.1.6 Concept of Acoustic Impedance

Acoustic impedance and specific acoustic impedance quantify the resistance of a system to acoustic flow caused by an acoustic pressure applied to the system. The SI unit for acoustic impedance is the pascal-second per cubic meter (Pa-s/m^3) (Acoustic impedance, 2023). Specific acoustic impedance and acoustic impedance describe different conditions. Specific acoustic impedance is mainly used in unbounded environments such as room acoustics and outdoor sound propagation, while acoustic impedance is employed for enclosed spaces like pipes.

Specific acoustic impedance (z) is also known by characteristic impedance, and wave impedance is a measure of a medium's resistance to wave propagation and is influenced

by both the properties of the medium and the type of waves traveling through it. It is expressed using the Eq. (12) for a plane wave propagating through the medium.

$$z = \sqrt{K \times \rho} \tag{12}$$

Where, K is the stiffness of the medium in N/m^2 and ρ is the density of the medium in kg/m^3. For the gases, instead of the stiffness, the term adiabatic bulk modulus is used, in ideal conditions it is given by Eq. (13).

$$K = \gamma \times p \tag{13}$$

In above mentioned Eq. (13), K is the adiabatic bulk modulus of the medium and γ represents the ratio of specific heat capacities (C_p/C_v) for the gases. Pressure is denoted by p. The adiabatic bulk modulus is directly related to the speed of sound in the gases by Eq. (14).

$$c = \sqrt{\gamma \times \frac{p}{\rho}} \tag{14}$$

By re-arranging the above Eq. (14), it becomes Eq. (15),

$$\gamma = \frac{c^2 \rho}{p} \tag{15}$$

Substituting the Eq. (15) into Eq. (13) gives Eq. (16),

$$K = c^2\rho \tag{16}$$

By putting the value of the K in Eq. (12), specific acoustic impedance z becomes

$$z = \rho \times c \tag{17}$$

The specific acoustic impedance is a function of air density and the speed of sound as it travels through the medium, and it is affected by air temperature due to variations in density and speed. The unit of specific acoustic impedance is the rayl (Ry), with values for air 428 Ry at 0°C and 413 Ry at 20°C, and for water 14.8 MRy. Specific acoustic impedance plays a critical role in sound wave propagation and energy transmission through a medium. It determines how sound travels from one medium to another, such as from air to the walls of a room. A medium with a low impedance will allow a large sound pressure to produce a significant particle velocity, while a medium with a high impedance will result in a relatively smaller particle velocity for the same sound pressure. This impedance greatly influences the way sound behaves in different acoustic environments (Acoustic Impedance, 2009).

Specific acoustic impedance characterizes the medium and represents the point impedance, indicating the pressure-velocity relationship at a particular point in unbounded space. However, when the medium itself vibrates, like in a standing wave inside a pipe, a different impedance called acoustic impedance is needed. It is analogous to mechanical flow impedance in a hydraulic system and determines the ratio of fluid pressure to fluid flow. Acoustic impedance (flow impedance) (Z) is the ratio of the average sound pressure across a hypothetical finite surface to the volumetric flow rate of the fluid and is dependent on the geometry of the medium (Acoustic Impedance, 2009). If p is the external pressure causing the particle of fluid to flow with particular

velocity U, through a pipe with cross-section area A, then the acoustic impedance Z will be written in the form of Eq. (18).

$$Z = \frac{p}{U \times A} = \frac{p}{u} \tag{18}$$

Furthermore, this acoustic impedance can be related with specific impedance by Eq. (19).

$$Z = \frac{z}{A} \tag{19}$$

2.1.7 Acoustic Resonance

The resonance of a pipe is a result of constructive interference between the incoming sound waves and the waves reflected within the pipe. When the frequency of the generated sound matches one of the natural resonant frequencies of the pipe, the sound waves reinforce each other, leading to an amplification of the sound's amplitude. This effect is particularly pronounced at the resonant frequencies, resulting in a louder and more sustained sound.

Pipe resonance is influenced by a variety of factors, including pipe length, geometry, sound velocity, pipe impedance, and material properties. Among these factors, length and sound velocity are particularly important. They determine the frequencies at which resonances occur, known as harmonics. (Acoustic Resonance, 2023). For open-ended pipes, these resonant frequencies can be calculated using the formula given in Eq. (20).

$$f = \frac{nc}{2L} \tag{20}$$

Where, f is the resonant frequency in Hertz and n indicates the positive integer (1,2, 3…) representing the node of resonance. The speed of sound in air is expressed by c which is approximately 343 m/s at 21°C and L is the length of the pipe in meters. For instance, if the length of the pipe is 3.190 m, as used during the experimentation, and the speed of sound is approximately 343 m/s corresponding to a room temperature of 21°C, the fundamental resonant frequency and its subsequent harmonics can be calculated as expressed in Eq. (21).

$$f_1 = \frac{343}{2\times3.19} \approx 53.847\ Hz,\ \ f_2 = 2f_1 \approx 107.69\ Hz,\ f_3 = 3f_1 \approx 161.541\ Hz, \ldots\ldots \quad (21)$$

Where, f_1 is the first resonant frequency is also called the fundamental frequency. The wavelength of this frequency is twice the length of the pipe. It is clear from the relationship between resonance frequency and pipe length expressed in Eq. (20) that resonant frequencies decrease as length increases.

2.2 Theoretical Framework of Experimentation

During the acoustic analysis inside the duct only linear behavior of the sound waves and the region of the plane waves have been considered to reduce the computational complexity. Plane waves mean that the frequency ranges before the cut-off frequency are analyzed. The cut-off frequency depends on the geometry and speed of the sound traveling through a given duct. Moreover, all acoustic parameters considered are determined by assuming a hard-walled pipe with only acoustic flow (no mean flow) during the experiment. Since there is no mean flow inside the pipe, fluid flow (air) is supposed to be stable and stationary.

2.2.1 Cut-off Frequency and Mode of Propagation

The term "cut-off frequency" denotes a critical point in the frequency response of a system, delineating the transition between distinct modes of propagation that a system

can support. At this frequency, the energy transmission through the system experiences a significant reduction, attributed to factors such as reflection or attenuation caused by other phenomena (WIKIPEDIA The Free Encyclopedia, 2023).

In this work, acoustic analysis inside ducts focuses on two key aspects: duct geometry and the frequency range studied. More specifically, the study is limited to low-frequency noise, from 25 Hz to 500 Hz. The aim is to identify the characteristics of waves propagating in this frequency range, and to understand their dominant mode of propagation. In the low-frequency region, the primary mode of acoustic propagation within a duct is referred to as the fundamental mode, or the mode with the least attenuation. This occurs when the wavelength λ significantly exceeds a characteristic dimension a of the duct's cross-section. For a hollow circular hard-walled duct with negligible mean flow, the criterion for the excitation of the first axisymmetric mode is met by the condition in Eq. (22).

$$\lambda > 3.4126(a) \tag{22}$$

This condition can be represented by the non-dimensional product $k_o a$, known as the Helmholtz number based on the duct radius, as expressed in Eq. (23).

$$k_o a < 1.8412, \qquad and \quad k_o = \frac{2\pi f}{c_o} \tag{23}$$

The term "low frequency" in acoustics means that the Helmholtz number based on the characteristic duct size is less than unity. The cut-off frequency is determined by the Helmholtz number based on the characteristic dimension of the duct. Therefore, the fundamental mode predominates, when the frequency is less than this Helmholtz number (Dokumacı, 2021). For a speed of sound at 20°C propagating through a pipe with

an internal diameter of 0.076m (or a radius of 0.038m), the cut-off frequency is calculated by Eq. (24).

$$f_c = \frac{1.8412 c_o}{2\pi a} = \frac{1.8412 \times 343}{2 \times \pi \times 0.038} = 2646\ Hz \tag{24}$$

Below this cut-off frequency, all frequencies will have wavelengths longer than the duct's characteristic dimension. Sound waves predominantly propagate in one direction, perpendicular to the duct's cross-section, forming planar wave fronts. This simplifies the analysis as all acoustic variables remain constant on the plane, with pressure and particle velocity in phase during propagation.

The fundamental mode (n = 1) is the dominant mode of propagation under the cut-off frequency. It exhibits a simple pattern with one antinode and one node along the duct's length, resembling a standing wave. Higher-order modes (n > 1) may influence the sound field at higher frequencies, but within the low-frequency range (25 to 500 Hz), the fundamental mode should prevail (Dokumacı, 2021).

2.2.2 One-dimensional equation for the plane waves

Generally, when a disturbance in a thin cross-sectional element of fluid is considered in a duct, its motion can mathematically be described by assuming the following:

a. the amount of fluid in the element remains constant
b. the net longitudinal force is balanced by the inertia of the fluid in the element
c. the compressive process in the element is adiabatic (no heat flow)
d. the undisturbed fluid is stationary (no fluid flow).

Using these assumptions, can help to derive the equation of wave motion as expressed in Eq. (25).

$$\frac{\partial^2 p}{\partial x^2} - \frac{1}{c^2}\frac{\partial^2 p}{\partial t^2} = 0 \tag{25}$$

In Eq. (25), p represents the sound pressure, x is used for coordinate, and t for time. This equation is commonly referred to as the acoustic wave equation. Similar wave equations can be derived by replacing p in Eq. (25) with other acoustic quantities such as particle displacement ξ, particle velocity u, condensation s, fluctuating density ρ', or fluctuating absolute temperature T'. The derivation of these equations can be complex. However, since sound pressure can be easily measured with a microphone and is the acoustic parameter perceived by the human ear, the wave equation in terms of sound pressure is very practical. Therefore, it is usually written in terms of sound pressure, and other acoustic quantities can be derived from their relationships to sound pressure. (Crocker, 2007). Such as, they are expressed from Eq. (26) to Eq. (29).

$$p = Uz, \tag{26}$$

$$I = pU \tag{27}$$

$$I = \frac{p^2}{z} \tag{28}$$

$$I = zU^2 \tag{29}$$

Where, z= ρc (R. J. Peters, 2011).

The solution to the one-dimensional plane wave equation can be expressed by Eq. (30)

$$p = f_1(ct - x) + f_2(ct + x) \tag{30}$$

Equation (30) provides a general solution to the wave equation expressed in Eq. (25), where f_1 and f_2 can be arbitrary functions like sine, cosine, exponential, or logarithmic. It can be easily demonstrated that Eq. (30) satisfies the wave equation in Eq. (25) through differentiation and substitution. By varying the values of x and t in Eq. (30), two components can be observed: $f_1(ct - x)$represents a wave traveling in the positive x direction with a speed of c, while $f_2(ct + x)$ represents a wave traveling in the negative x direction, also with a speed of c. This solution, given in Eq. (30), is considered the general solution since it allows for the representation of various types of sound waveforms (Crocker, 2007). However, this work is mainly based on experiments. Most of the acoustic parameters have been measured with appropriate sensors to ensure the consideration of real environmental conditions.

2.3 Measurement Techniques and Sensors

Microphones are engineered with a goal of achieving a flat frequency response, meaning they have an equal sensitivity to all frequencies, unlike the human auditory system, which is not uniformly sensitive to all frequencies. However, to simulate human hearing perception, certain filters such as A-weighting, which follows a frequency-dependent curve, can be applied to microphone measurements. For this work, the focus is on analysing low-frequency noises, and therefore, all measurements taken by the microphones will be treated linearly. This approach ensures that essential information in the low-frequency range is preserved and accurately captured.

2.3.1 Particle Velocity Sensor

The particle velocity (PU) sensor, developed by Microflown Technologies, is a probe designed to directly measure the particle velocity and the sound pressure at the same point. The probe consists of two components, a microphone and a particle velocity

sensor as depicted in Fig. 9. It is capable of capturing complex near-field acoustic behavior without the need for a specially acoustically treated environment. The probe is designed to operate under real operating conditions. Moreover, it calculates the intensity by taking the time average of instantaneous product of the sound pressure and particle velocity signal unlike to PP probe, which calculates the pressure gradient (Finn Jacobsen H.-E. d., 2005). Intensity assessment and acoustic imaging, also known by the "scan and paint" technique can be performed by using this probe. In this technique, video camera is used to record the probe's movement as it scans the area of interest. Then, the intensity measurements are synchronized with the video, creating a visual overlay of intensity levels. This further helps to quantify, visualize and localize the acoustic sources (SCAN&PAINT 2D, 2023).

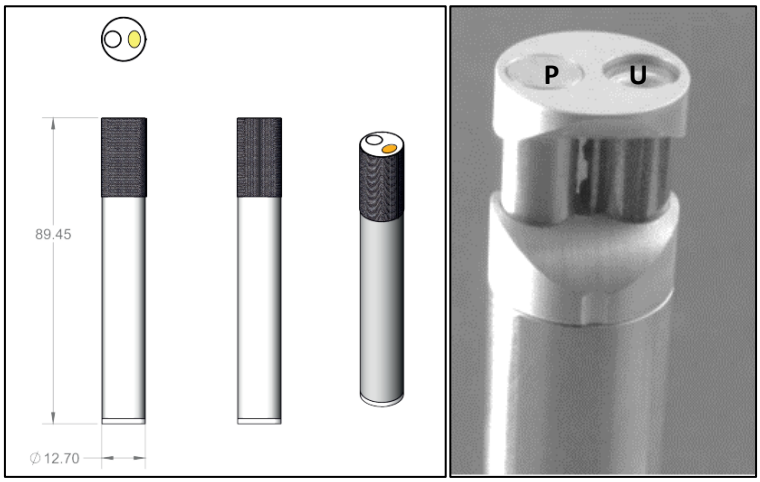

Figure 9. Particle velocity sensor can be seen on the small cylinder marked with a 'U' on the right, and the electret microphone fits inside the other cylinder (Finn Jacobsen H.-E. d., 2005).

The particle velocity sensor comprises two thin, closely-spaced platinum-coated silicon carbide wires. These wires are energized and heated to act as resistors. The resistance of the wire's changes when a particle velocity signal is applied perpendicular to them, as it alters the temperature distribution of the wires. This change in resistance is measured by the bridge circuit, which provides an electrical signal proportional to particle velocity. The electret microphone, on the other hand, works on the principle of capacitance changes induced by the vibrations of the diaphragm (Finn Jacobsen H.-E. d., 2005).

During the experiment, readings were taken by positioning the probe perpendicular to the acoustic source at a distance of 10 mm. The probe was held in a stable position and traversed the required surface in a zigzag pattern. Three separate sets of measurements were collected, depending on the method used. In the first, the probe was held still at the source opening. In the second stage, the microphone was moved over the surface area of source. For the final series of measurements, the probe, covered with a red filter for camera recognition, was moved not only to the source opening, but also to the surrounding areas. The use of a red filter made it easier for the software to detect microphone movements as a function of color. Finally, the software calculated an average value derived from these three distinct measurement methods.

2.3.2 Nor1290 Sound Intensity probe

The Nor1290 sound intensity probe, a specialized device comprised of a pair of precision microphones set exactly 12mm apart as shown in Fig. 10, is instrumental in detecting the pressure exerted by sound waves over a specific area. Both microphones of the device are phase matched and receive sound waves from the environment. The presence of a minor gap between the microphones incurs a minimal time lag in the reception of these sound waves at each microphone. The marginally earlier reception of sound waves at the first microphone leads to a phase discrepancy between the two captured signals. This discrepancy aids in deducing the directionality of the sound wave, denoting if it is advancing towards or receding from the probe (Nor150 Sound Intensity Option, 2023).

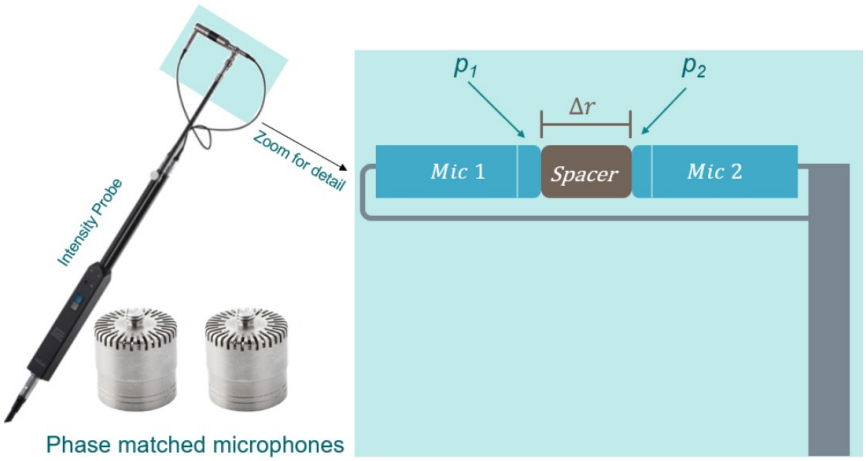

Figure 10. The intensity probe is equipped with two microphones. They are essential for obtaining directional vector information. (Sound Intensity, 2020).

2.3.2.1 Methodology for Calculating Sound Intensity

Particle velocity can be calculated using Eq. (31) below. It involves determining the pressure gradient between the two microphones based on their distance (Δr) and the pressure values at each microphone. This integrated over time and divided by the fluid medium's density (ρ) provides an estimate for particle velocity (v).

$$\boldsymbol{v} \cong -\frac{1}{\rho}\int_0^t \frac{p_2 - p_1}{\Delta r}\, dt \tag{31}$$

Whereas, the pressure component is obtained by averaging the pressure between the microphones as given in Eq. (32).

$$p = \frac{p_1 + p_2}{2} \tag{32}$$

The combination of these two equations, Eq. (32) and Eq. (33), allows the determination of the intensity by means of a PP probe as expressed in Eq. (33).

$$\boldsymbol{I} = \frac{p_1 + p_2}{2} \cdot -\frac{1}{\rho}\int_0^t \frac{p_2 - p_1}{\Delta r}\, dt \left[\frac{W}{m^2}\right] \tag{33}$$

This Eq. (33) is used to calculate sound intensity in the time domain. For accurate results, the microphones used in the measurement should be phase-matched. Phase-match means ensuring that the frequency response of two microphones is as close as possible. Ideally, when both microphones measure the same pressure wave, they should produce identical frequency, amplitude, and phase responses. However, variations in the

measured signals can occur due to small differences in microphone construction. To counteract this, specifications have been established. For instance, the maximum permissible phase difference is 0.3 degrees over the entire frequency range to ensure reliable measurements (Sound Intensity, 2020).

2.3.2.2 Influence of Spacer Length on Frequency Range

The frequency range over which intensity measurements can be made is determined by the distance between the microphones, called the spacer. Different spacer lengths are used to calculate data over different frequency ranges. The conventional rule is that the spacer length should not exceed $1/6^{th}$ of the desired wavelength, otherwise the pressure gradient estimation will become unreliable and Eq. (33) will no longer hold. For an instance, same spacer length is taken for the analysis of two different frequencies. The spacer length on the left in Fig. 11 (green) is sufficient to obtain the linear approximation of pressure change over distance change for the lower frequency sine wave. The spacer on the right (purple) is too large to accurately measure the higher frequency wave, making the linear approximation incorrect (Sound Intensity, 2020).

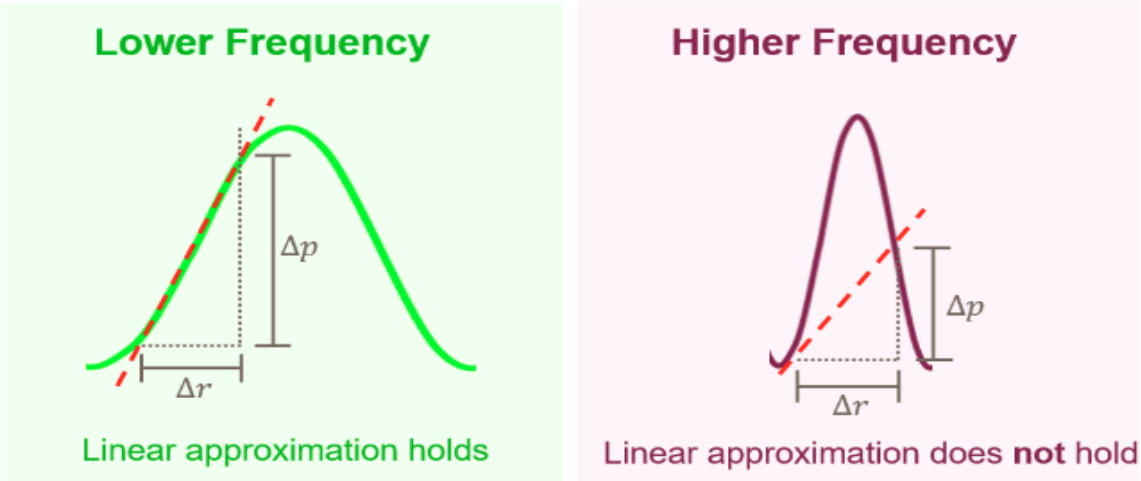

Figure 11. Linear approximation of two different frequencies with same spacer length (Sound Intensity, 2020).

The relationship between spacer distance and frequency limit is as follows:

a. A shorter spacer allows measurement of higher frequencies.

b. A longer spacer enables measurement of lower frequencies.

2.3.2.3 Effect of the directionality of the probe

The orientation of the sound intensity probe plays a crucial role in obtaining accurate measurements. Since the probe measures the pressure difference between two microphones, its orientation in the sound field significantly affects the readings. When the probe is oriented perpendicular to direction of the sound field, it captures the maximum value of intensity as depicted on the left side of Fig. 12. However, when the probe is held parallel to the surface area of the pipe opening, the sound intensity will become zero. This is because both microphones receive the same pressure value simultaneously, resulting in a zero-pressure difference and thus a zero-intensity reading (Sound Intensity, 2020).

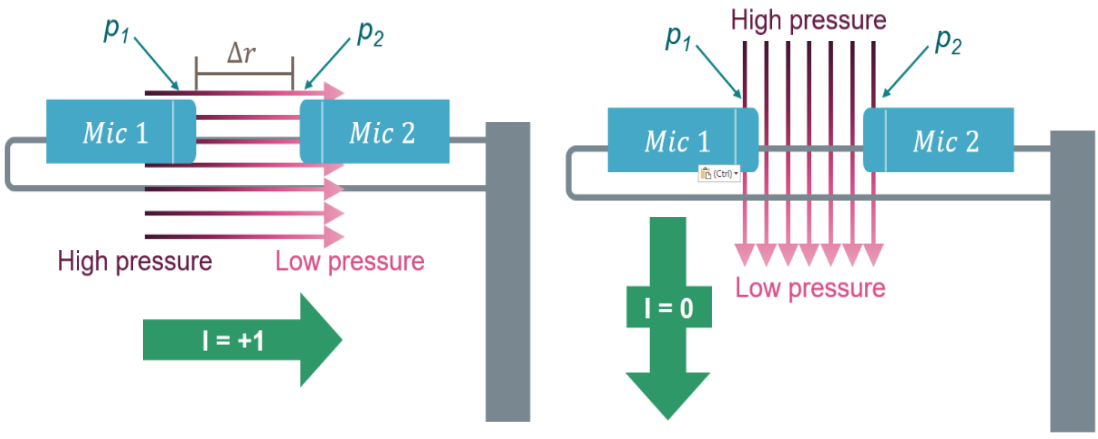

Figure 12. Figure illustrates probe orientation: Left side shows perpendicular orientation to acoustic flow, while the right side shows parallel orientation (Sound Intensity, 2020).

During the experimental procedure, measurements are made with the probe positioned approximately 100 mm from the intended sound source. It is then moved slowly over the area of interest at a constant speed of 20 cm/s. By evaluating multiple points over

the specified area, an average value is derived to provide a more comprehensive view of the sound intensity map. The positive and negative value of the sound intensity indicates the direction of the sound wave at that specific frequency. However, this work will not focus on the analysis of sound intensity, as intensity is used to determine the directionality of the sound source and to calculate the sound power level, which is not the aim of this study.

3 Objects and Methods

This chapter details the configurations and methodology used for the reference and exhaust experiments. It also explains the objectives behind conducting each of these experiments. The approach used to collect data during the experiment and to analyze the data for 1D modeling in GT-POWER is also covered. In addition, the process of 1D modeling of the reference experiment in GT-POWER will be described. The goal of this chapter is to provide a clear understanding of the experimental setups, data collection, data analysis, and modeling procedures.

3.1 Experimental Configurations

At VEBIC two different experiments were carried out to analyze the acoustic behavior inside pipes. In both experiments, a loudspeaker enclosed in a square box is used as a source to generate pink noise inside the pipes. The reference experiment was carried out on the plastic pipe, while the main experiment was performed on the exhaust pipe of the W4L20 medium-speed engine. The reference experiment is designed to reduce the complexity and test the applicability of the GT-model based approach. In addition, this reference experiment is structured to analyze the effect of different angles of pipe bend on the sound pressure level. As for the exhaust pipe experiment, it is designed to provide information on noise response at different points of the pipe geometry.

3.1.1 Sound Source Configuration

The loudspeaker box contains two components that act as a source of noise. This box is divided in two portions, upper portion of the box is reserved for the speaker and the lower one for the subwoofer as it can be seen in Fig. 13. The loudspeaker used is the hemi-dodecahedron Nor275. This speaker is used in conjunction with the power amplifier Nor280. However, this amplifier is placed outside the box.

The loudspeaker complies with the ISO140 and ISO3382 standards and is capable of generating a sound power output of up to 120 dB (Lin). The power amplifier Nor280 is used to configure the loudspeaker settings by providing options for pink, white, and red/white noise excitation with adjustable power levels, as depicted in Fig. 13. Pink noise was chosen because it concentrates most of its energy in the low-frequency range, which is favourable for studying the low-frequency spectrum. The power amplifier also has an equalization network option that compensates for the low-frequency and high-frequency roll-off of the speaker system. There is also a high-pass filter to remove low frequencies below the desired range and a low-pass filter to remove all frequencies above 12kHz. This feature protects the speakers from distortion and focuses the power to the desired frequency (Norsonic).

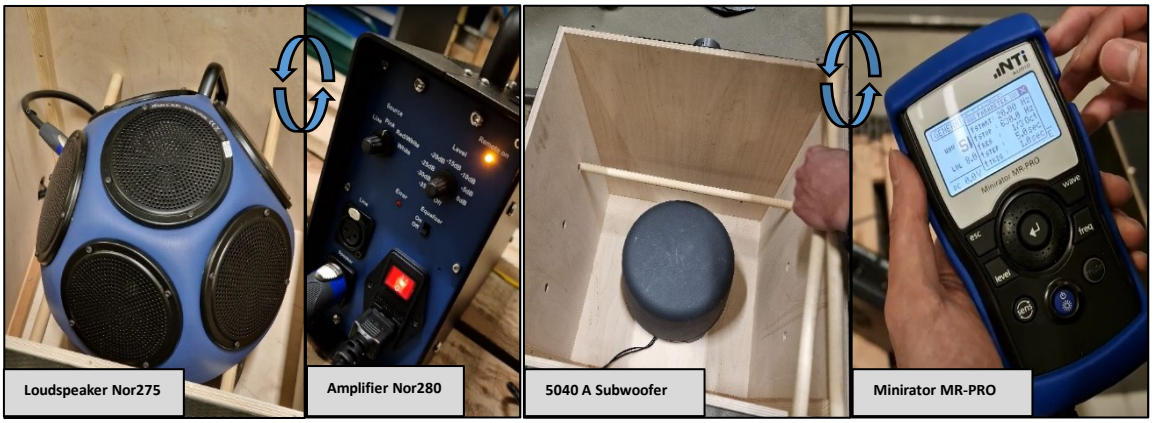

Figure 13. The subwoofer is placed at the bottom of the box, with the loudspeaker on top. The Nor280 power amplifier and the Minirator MR-PRO are responsible for configuring the required signals for the speaker and subwoofer.

During the experiment, a 5040A active subwoofer is used to generate low-frequency noise from 20Hz to 100Hz. The Minirator MR-Pro can be seen in Fig. 13 is a versatile analog audio generator. It is used to generate the necessary signals within the subwoofer. It provides a wide range of standard test signals. These include pink noise, white noise, chirp, delay, polarity, sweep, and sine wave. Both the level and frequency of these signals can be adjusted to meet the needs of the test (OPERATING MANUAL MR-PRO, 2019). The configuration settings used in this experiment are shown in Tab. 5.

Table 5. These configuration settings were adjusted by using power amplifier for loudspeaker and Minirator MR-PRO for the subwoofer.

Sound Source	Configuration settings
Nor275 Loudspeaker	Pink noise, equalizer off, amplifier (-10dB, -20dB, -30db from max)
Genelec 5040A subwoofer	Pink noise, continous, 8dBv, mid line of max and min

A consistent set of signals was used for both of the experiments. The loudspeaker generated noise in the range of 100-5kHz, while the subwoofer produced noise in the 20-100Hz range. Different amplifier settings -10 dB, -20 dB, and -30 dB were applied to the loudspeaker during the experiment conducted on the exhaust pipeline. As the GRAS 40SC was used for the pressure measurement inside in the exhaust duct. The upper dynamic range of 160 dB of the sensor supports all the mentioned settings. However, in the case of reference experiment, the main sensor used was PU probe whose upper dynamic range of 112 dB (see Tab. 6) for the pressure did not support all these settings of the amplifier. Therefore, only the -30dB level from the maximum level was selected for analysis during the reference test. This choice was made due to the dynamic limitation of the PU probe which tends to overload at higher noise levels.

Table 6. The specifications of the PU probe have been specified (PU REGULAR, 2019).

Sensor Performance	Sound Pressure	Particle Velocity
Sensitivity	65mV/pa	30V/(m/s)
Frequency Range (±1 dB)	40 - 8000 Hz	40 - 8000 Hz
Frequency Range (±2 dB)	20 - 10000 Hz	20 - 10000 Hz
Maximum Level	112 dB	125 dB

3.1.2 Experimental Configuration of the Exhaust pipeline

Experiment has been conducted in the exhaust pipeline of the medium-speed W4L20 engine by connecting the emergency relief valve with source pipe. The source pipe blue in color acts as a waveguide connecting the loudspeaker to the pipeline as depicted in Fig.14.

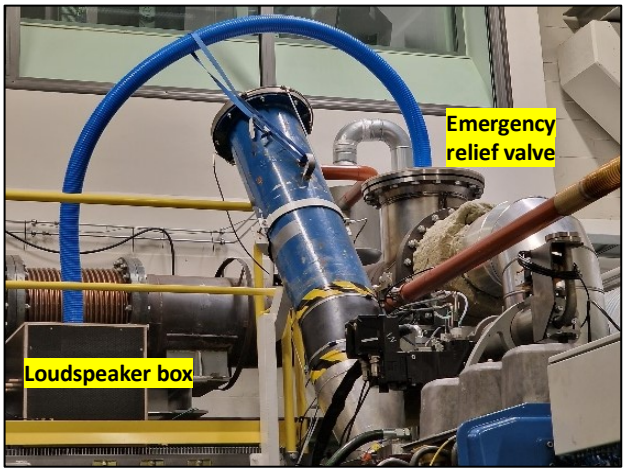

Figure 14. Loudspeaker can be seen connected to the exhaust pipeline at emergency relief valve.

The pipeline features a total of 15 holes, each with a diameter of 4mm, strategically drilled at various locations. Specifically, there are 4 holes positioned after the first bend, followed by 6 holes after the second bend, and finally, 5 holes after the third bend along the pipe's length as shown in Fig 15. The exhaust pipe is divided into three sections according to the number of bends. Section 1 is after the first bend, while section 2 is followed by the second bend, and similarly section 3 is after the third bend. The position of the drilled holes in each of these sections is marked by the numbering of the points. The GRAS 40SC CCP Probe has been employed to measure sound pressure levels at these different points. The probe is placed one by one in each these drilled holes to measure the pressure. This microphone is well-suited for accurate sound pressure measurement in diffuse fields. Its compact size, with a diameter of only 1.25mm, minimizes any potential noise caused by the presence of the probe within the sound field. As a result,

the GRAS 40SC ensures precise and reliable sound pressure measurements at each of the specified hole locations.

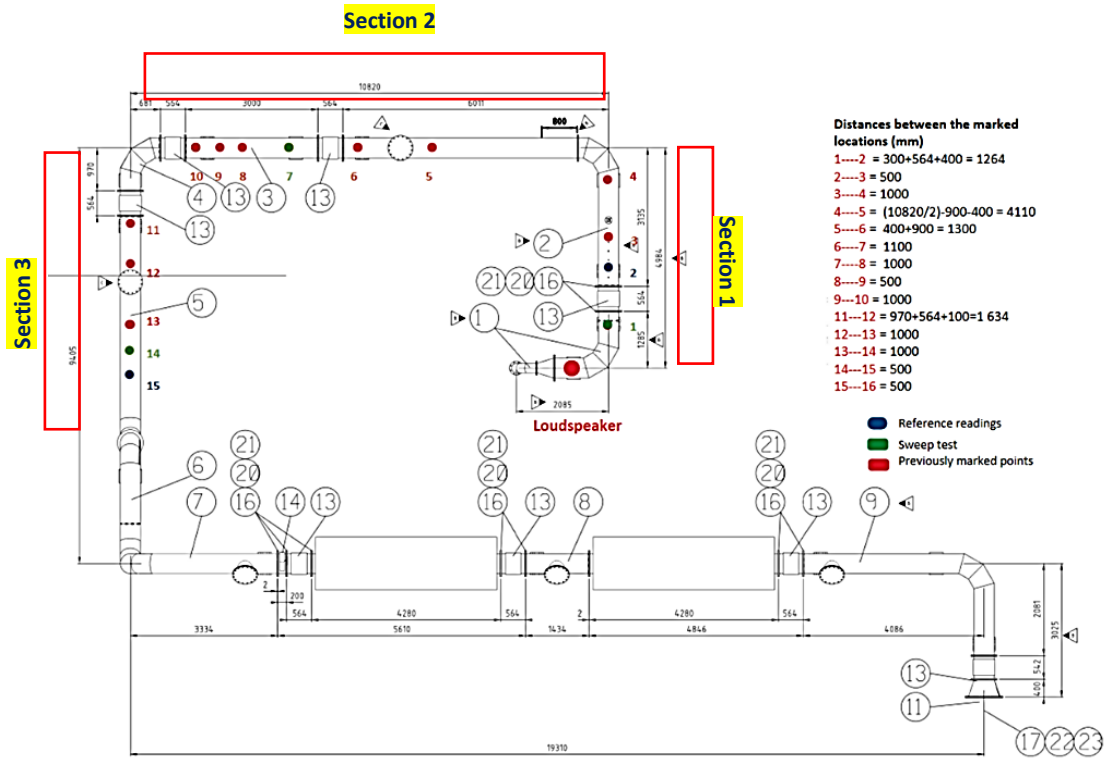

Figure 15. Layout drawing of the exhaust pipeline with marked holes.

3.1.3 Experimental Configurations of the Plastic Pipe

The reference experiment consists of components such as loudspeaker box, plastic flange connector and plastic pipe. The dimension of the experimental components can be seen in Tab. 7. These dimensions are very critical and important for the next phase of the thesis which comprise of the modeling this reference experiment in the GT-POWER.

Table 7. The dimensions of the components utilized in the experiment are displayed.

Components	Length (mm)	Width &Internal Dia.(mm)
Loudspeaker box	520	520
Plastic Flange Connector	160	65
Hose Pipe (PVC)	3190	76

Furthermore, this reference experiment consists of three different setups. Each of these setups is created by rearranging the experimental components. They serve different purposes. Set1 consists of a loudspeaker box and a flange connector, which serves as the source, as depicted in Fig 16. Set2 is attributed to a plastic pipe that is connected to this source setup and this plastic pipe would have a slight bend of 90 degrees. Similarly, Set3 is setup similar to Set2, but the pipe has oblique bend of 180°. The different angle of bend in Set2 and Set3 serves the purpose of studying the effect of these different bends on the behavior of the noise. The schematic diagram and some of the pictures taken during experimenting on each setup can be seen in Fig. 16 and Fig. 17.

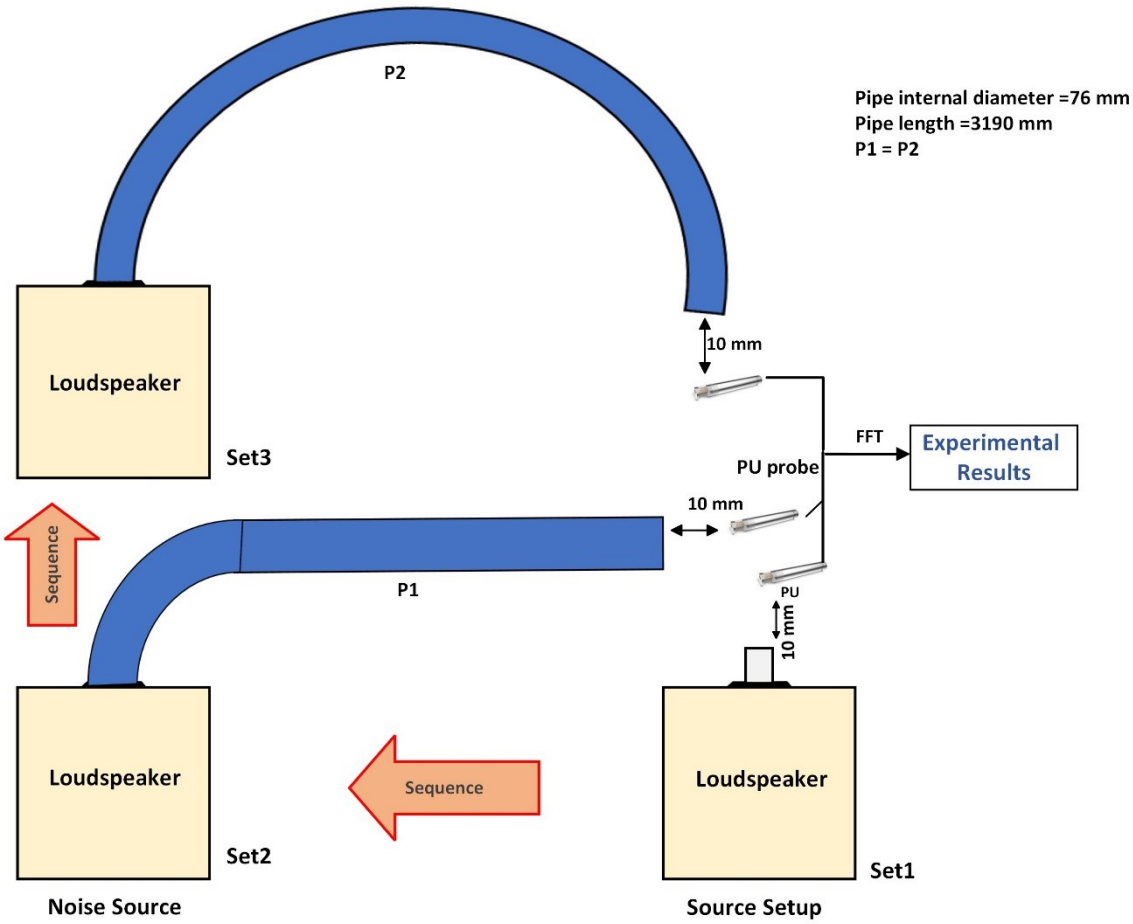

Figure 16. All the three experimental setups have been shown along the placement of PU Probe.

Table 8. Different setup with their arrangements is described.

Specific Setups	Arrangements
Set1	Loudspeaker box with lid and duct adaptor (connector)
Set2	Loudspeaker box connected to the pipe (PVC) with slight bend of $90°$
Set3	Loudspeaker box connected to pipe (PVC) with oblique bend of $180°$

Figure 17. An image is provided to illustrate all the setups used during this experimentation.

Sound pressure, sound intensity, pressure and particle velocity measurements were made in all three setups. The positions of the sensors are shown in Fig. 18.

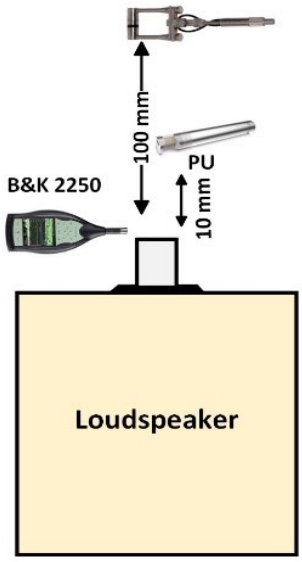

Figure 18. The setup of the source has been shown with the placement of the sensors.

The PU probe is of particular importance in this work because it provides essential data, including pressure and particle velocity values, that are critical to accurately determine the acoustic impedance of the source. This impedance data will be used for GT-POWER model-based simulations of the experiment. The pressure readings from the B&K 2250 handheld analyser have been used as a reference to normalize the pressure readings taken by the PU probe during the analysis. However, this analysis will not use data measured by the sound intensity probe.

3.2 Signal Processing of the Pressure and Particle Velocity data

This section analyzes the data obtained from the PU sensor, in the form of pressure and particle velocity signals. The first step is to collect the sensor data. The data is based on analog signals. These are converted into electrical signals according to the principle followed by the sensor. These analog signals are then pre-processed. This includes signal conditioning and amplification of weak signals. After conditioning, these signals are sent to the data acquisition system, which converts them from analog to digital using an analog-to-digital converter (ADC). These discrete signals are stored, displayed and processed in a computer system. This operation is performed using appropriate software. This step is also known as post-processing of the data. Digital processing techniques such as FFT can be applied at this stage to obtain the desired data. All of the signal-processing steps involved are shown in Fig. 19.

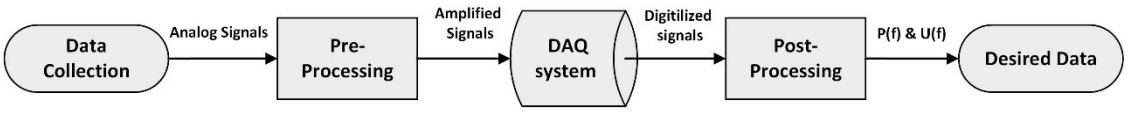

Figure 19. The signal processing of pressure and particle velocity data involves five different stages.

The main purpose is to determine the complex acoustic impedance and pressure values at the source setup along desired frequencies. This can be achieved by the post

processing of the data obtained by the PU probe. The resulting data will be used for source characterization of GT-POWER based model. In addition, the pressure data collected from all experimental setups as depicted in Fig. 16 will be processed by using FFT to represent the experimental results in the frequency domain.

3.2.1 Data Collection

The initial stage of signal processing involves data collection, where sensors or transducers are the main source of data acquisition. The PU probe was used to collect data from all three setups as described in section 3.1.3 of the thesis. The probe consists of two primary components: a pressure sensor, also known as a microphone, and a particle velocity sensor. Each of these components is designed to measure a specific aspect of the acoustic field. The pressure sensor uses capacitive sensing. It converts sound waves into electrical signals by detecting diaphragm vibrations.

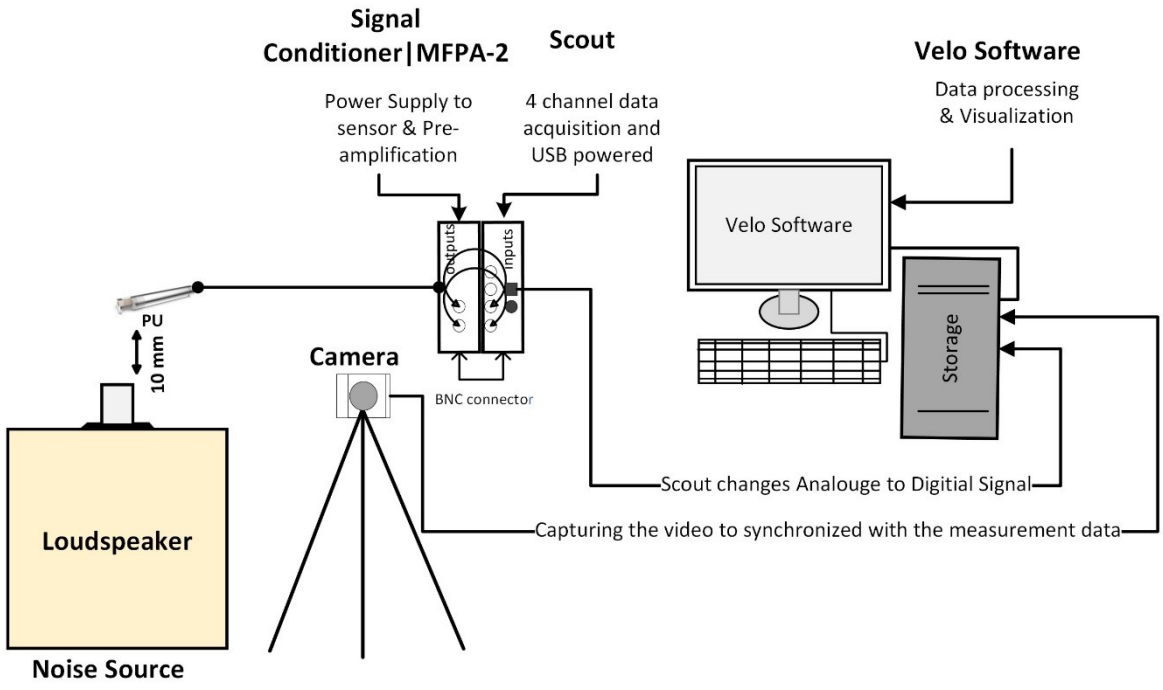

Figure 20. The schematic diagram shows measurement chain of the PU probe.

On the other hand, the particle velocity sensor is based on thermal principles. It uses temperature sensors (platinum wires) to monitor resistance changes. The data acquisition mechanism includes a four-channel scout followed by a two-channel signal conditioner and preamplifier. The probe collects acoustic data from the desired location and sends this data in the form of raw analog signals to the signal conditioner as shown in Fig. 20.

3.2.2 Pre-Processing

The signal conditioner plays a key role. It supplies power to the PU probe. It contains 2 channels to receive the analog pressure and particle velocity signals. It's important to note that the intrinsic frequency response of the Microflown PU probe is not perfectly flat. In order to compensate for this, the instrument's signal conditioning mechanism has a special equalization component. This element has been carefully tuned in order to correct the amplitude and phase response of the incoming signals. As a result of this adjustment, the probe exhibits a balanced response in both amplitude and phase. This greatly improves the fidelity of the sound intensity measurements (Microflown Technologies). A preamplifier inside the signal conditioning unit significantly amplifies the analog signals of both pressure and particle velocity. This amplification prepares the signals for subsequent processing. It also improves the accuracy of the data collected.

3.2.3 Data Acquisition System

Conditioned analog signals from the signal conditioners are received by the Scout unit. The Scout unit is a data acquisition system developed by Microflown to interface its PU probes. It is a high-precision, 24-bit, 4-channel data acquisition system. It is powered by a USB port. The main function of this device is to receive conditioned analog signals via the BNC connector and digitize these signals. These digitized pressure and particle velocity signals are processed and stored. Data can be stored temporarily in the device's internal memory. The data is then transferred in real time to a computer or external storage device. The computer system uses specialized software called VELO to process

and analyze the acquired data. This software enables the user to visualize particle pressure and velocity signals, perform various signal processing operations and extract useful information from the data.

3.2.4 Post processing of data by using Fast Fourier Transform

The built-in VELO software does not have the capability to directly calculate acoustic impedance. However, it can provide access to raw pressure and particle velocity data in the time domain for further analysis. It is essential that the pressure and particle velocity data be in phase to accurately determine acoustic impedance. This is where the design of the PU Probe comes into play. It captures these signals simultaneously, preserving their phase relationship and ensuring accurate data for acoustic impedance calculations. Pressure and particle velocity raw data has been obtained in the time domain. These data sets contain the information about the time steps and sampling frequency. FFT has been applied to both pressure and particle velocity data by using MATLAB code. The code was developed by the Wartsila and it could not be shared in this thesis due to the confidentiality. All the steps followed during the code have been detailed in the subsequent section.

3.2.4.1 Time Domain

Time domain provides some basic information about the signals. But it is very important to understand it to perform the analysis in the frequency domain. The terms used in the time domain are given below.

Sampling rate (Fs): The sampling rate is important for determining the maximum amplitude and correct waveform of the signal. The sampling frequency is set to 25000 Hz for all the measurements taken by the PU probe, meaning 25000 samples per second. The more the number of the samples, better the waveform will be. It is calculated by the formula given in Eq. (34).

$$F(s) = \frac{1}{\Delta t} \tag{34}$$

Whereas Δt is known as time step between two data points or samples. If the sampling frequency is 25000 Hz, the time interval between two sample will be given by Eq. (35).

$$\Delta t = \frac{1}{25000} = 0.00004\ sec \tag{35}$$

Block Size (N) is the total number of the data present in the frame. It is also known by the data length and is 338584 for given data sets.

Frame Size (T) is the amount of time in which the data has been collected for the FFT. It is the product of the block size and the time step and can be given by Eq. (36).

$$T = \Delta t \times N = 13.54\ sec \tag{36}$$

The pressure and particle velocity signal plotted along the time axis based on the block size and time steps are displayed in Fig. 21. The frame size is same as calculated 13.54 sec and the data contains 338584 samples. It shows that the magnitude of pressure fluctuation is way more than the that of the particle velocity.

This is because pressure fluctuations are spread over a larger volume and affect more air molecules, while particle velocity fluctuations are localized around the equilibrium position. Sometimes, observing the phase relationship between two signals is simpler in the time domain, particularly when there isn't a substantial difference in the magnitude of both signals.

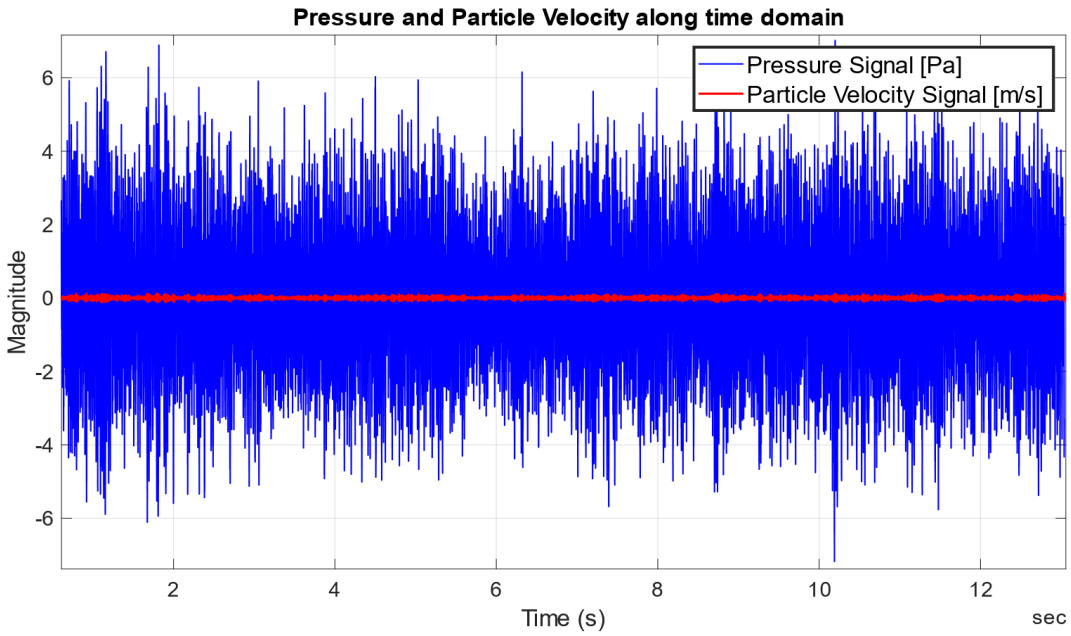

Figure 21. The graph displays the variations in pressure and particle velocity over the frame size.

Contrarily, in the case of the pressure and particle velocity signal, it is difficult to see the phase relationship by looking at the waveform alone as shown in Fig. 22. This is due to huge difference present between the magnitude of both signals.

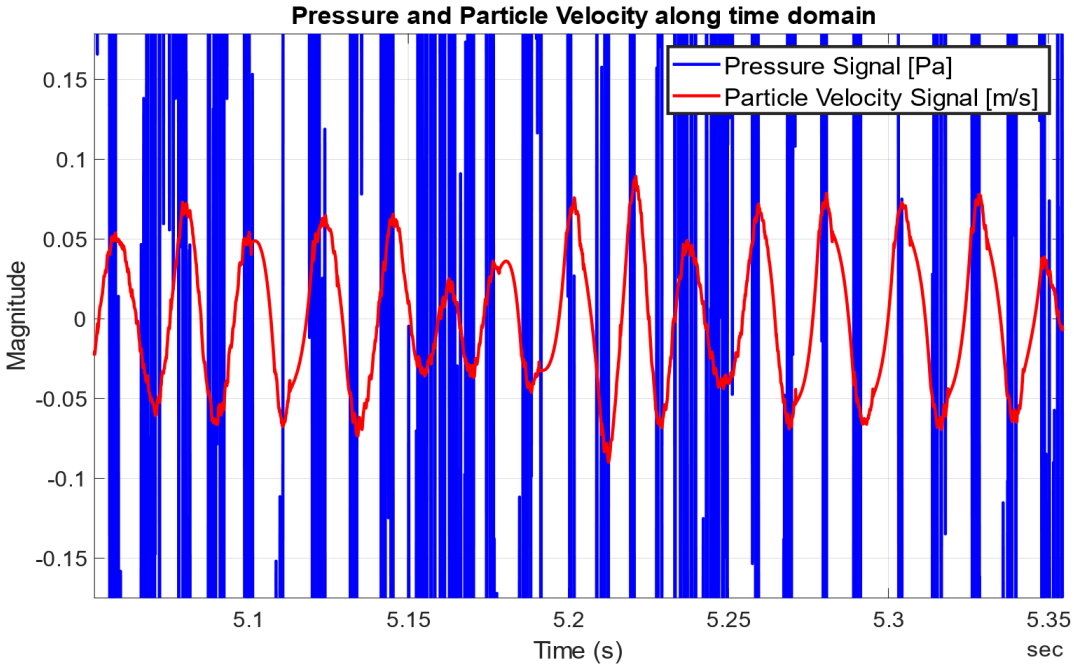

Figure 22. Fluctuations can be seen in the particle velocity signal (red), corresponding with variations in the pressure signal (blue).

A MATLAB code is used to perform the FFT to analyse the data. The code is based on the subsequent sections.

3.2.4.2 Input Parameters and Initialization

This is the main function that serves by accepting different input parameters like pressure and particle velocity signals, sampling rate, maximum frequency, window type, and averaging method. It then generates multiple outputs, including averaged FFT for both pressure and particle velocity signals, accompanied by additional relevant information.

3.2.4.3 Signal Parameters Calculation

This section assigns variables and calculates various parameters required for the FFT and further processing. Parameters like the number of samples, frequency resolution, window size, overlap step and the number of frames is assigned to appropriate variable and calculated. For instance, the frequency resolution is calculated by Eq. (37).

$$res = \frac{F_{max}}{n_{lines}}; \tag{37}$$

Where, F_{max} is the bandwidth or maximum frequency considered for analysis. It plays a critical role in signal processing. F_{max} must be set to half the sampling frequency, as defined by the Nyquist sampling criterion. The anti-aliasing filter is another crucial aspect to consider when determining the bandwidth. This conventional filter reduces aliasing effects in the signal. The sampling frequency should be at least 2.5 times the maximum frequency considered for analysis to ensure effective anti-aliasing. The given sampling

frequency is 25000 Hz, so F_{max} is set to 10000 Hz. This ensures compliance with the Nyquist criterion and the anti-aliasing filter. Moreover, n_{lines} indicates the number of spectral lines which is analogous to the N, number of samples in the time domain. The spectral lines represent the total number of data points in the frequency domain. Each spectral line has two different data values, an amplitude and a phase value. The frequency resolution also depends on the numeric value of the spectral lines. For an instance, if n_{lines} are 32000 then resolution will be given by Eq. (38).

$$res = \frac{10000}{32000} = 0.3125 \tag{38}$$

The frequency resolution for the narrow band spectrum is primarily chosen based on its intended application. A resolution of 0.3125 is most commonly used when displaying linear SPL in the frequency spectrum. It is worth noting that selecting the frequency resolution directly affects the detail and accuracy of the results. A narrower band of frequencies will result in higher frequency resolution, allowing for the display of more intricate and detailed results.

Window Size: The window size is a critical parameter that determines the frequency resolution of the spectrum. It represents the number of samples used in each FFT calculation. The choice of window size affects the frequency and time resolution of the FFT analysis. A larger window size improves frequency resolution (narrower frequency bins) but compromises time resolution (worse time localization of frequency components). A common approach to determining the appropriate window size is to balance the tradeoff between frequency resolution and the number of samples in the signal. The window size is often set as the sampling frequency divided by the desired frequency resolution, mathematically represented in Eq. (39).

$$winsize = \frac{F(s)}{res} = \frac{25000}{0.3125} = 80000; \tag{39}$$

The window size must be smaller than the number of samples in the signal to avoid overlapping data segments and artifacts in the frequency analysis.

Overlap Step: The overlap step represents the number of samples the analyzing window shifts between successive frames. The overlap step is usually expressed as a percentage of the window size. It lies in the range of 0 to 100 and is selected as 66.7 as expressed in Eq. (40) and Eq. (41).

$$Overlapstep = 100 - selected\ overlapstep = 100 - 66.7 = 43.3 \tag{40}$$

$$Overlap = \frac{overlapstep \times winsize}{100} = \frac{43 \times 80000}{100} = 34640 \tag{41}$$

In this scenario, the next frame uses the last 34640 data points from the previous frame and combines them with new data points to form the next frame of 80000. This overlapping process will continue for all subsequent frames until the end of the signal data has been reached. Overlapping helps avoid abrupt changes between successive frames and can improve the accuracy of selected signal-processing techniques. The overlap step is the same as the window size if no overlap step is chosen. It has a direct effect on the trade-off between frequency resolution and time resolution in the analysis. A large overlap step results in higher time resolution, allowing for more frames, but may introduce redundant computations. Conversely, a small overlap step results in better frequency resolution at the expense of more frame count. The number of frames can be determined using Eq (42).

$$nFrames = \left(\frac{number\ of\ samples}{overlap}\right) - 1 = \frac{338584}{34640} - 1 \cong 8; \tag{42}$$

The subtraction of 1 account for the initial frame. In addition, there will be about 8 overlapping windows in the signal data. Each window uses 34640 samples of the previous window. The last window overlaps the end of the signal data, but the fraction of the window beyond the data is ignored.

3.2.4.4 Application of Windowing Function to Avoid Spectral Leakage

Windows plays a critical role in reducing spectral leakage during FFT analysis. Understanding spectral leakage is essential when dealing with signals acquired in a periodic or non-periodic manner. The data can be categorized based on the measurement time (frame size). Unlike periodic signals, pink noise lacks regular and repeating patterns because it is non-periodic.

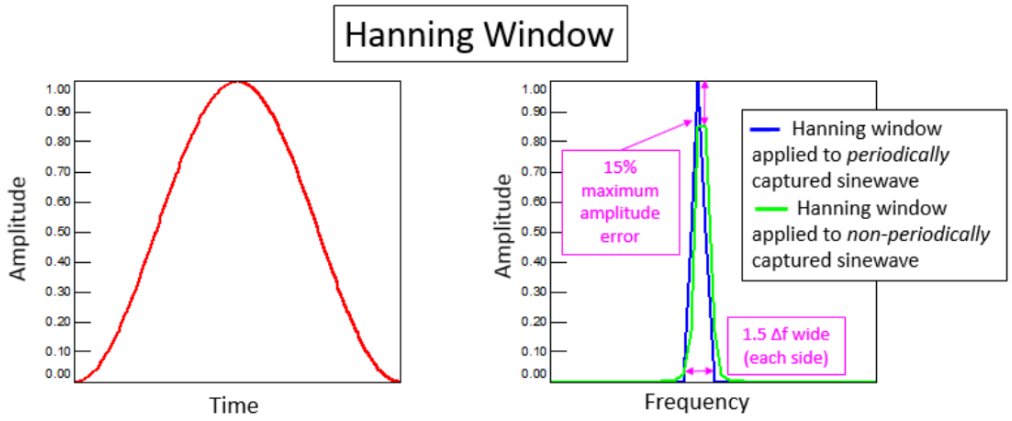

Figure 23. Hanning window in the time domain, and its frequency effect on periodic and non-periodic sine waves with respect to the measurement time (Window Types: Hanning, Flattop, Uniform, Tukey, and Exponentia, 2019).

Hanning windows are often chosen to analyze random data because of their moderate effect on frequency resolution and amplitude accuracy in the resulting frequency

spectrum. The Hanning window gradually transitions between zero and one, providing smooth amplitude changes as it multiplies the measured signal. This effectively reduces spectral leakage, as shown in Fig. 23. The Hanning window ensures a maximum amplitude error of 15%. It typically limits frequency leakage to 1.5 spectral lines on either side of the original sinusoidal signal.

The application of windowing to the signal can introduce distortion. It reduces the amplitude and energy of the original signal. Therefore, windowing correction factors must be applied after the FFT is performed on the data. These correction factors, multiplied by the corresponding absolute values, effectively correct the amplitude and energy. The Hanning window is used. It is conveniently available as a built-in function in MATLAB. The method for calculating the correction factors for the window using its RMS and mean values is given in Eq. (43).

$$a_f = \frac{1}{mean(w)} \quad e_f = \frac{1}{rms(w)}; \tag{43}$$

The correction factor for the signal's amplitude is denoted as a_f while the correction factor for the energy level is represented by e_f.

3.2.4.5 FFT Processing and Linear Averaging

This section of the code encompasses the following steps:

a. The code starts by calculating the FFT for each frame of the signal separately. Two frames of data (pressure and particle velocity) are extracted from the main signals of the pressure and particle velocity based on the window size. A frame is a segment of the signal of fixed size, and the FFT converts the time-domain data of each frame into its frequency-domain representation. This step is performed in the while-loop, where the code processes one frame at a time.

b. During the while-loop, the FFT is calculated for both the pressure signal and the particle velocity signal. The instantaneous spectra of pressure and particle velocity are stored in **InstSpec** and **InstSpecVelocity,** respectively. However, the amplitudes of the both signals are multiplied by **sqrt (2)** to scale the amplitude for RMS conversion. These arrays hold the complex amplitudes of the sinusoidal components at discrete frequencies for each frame.
c. After calculating the FFT for each frame, the averaging process begins. The switch averaging block is responsible for different types of averaging methods applied to the instantaneous spectra along different frames of windows.
d. Linear averaging is performed along the columns of **InstSpec** and **InstSpecVelocity**, which correspond to different time frames. For example, **mean(abs(InstSpec), 2)** calculates the mean of the absolute values of the instantaneous spectra along each frequency bin for all frames.
e. The averaged spectra obtained from the averaging process are then multiplied by the corresponding phase values, **cos (Phase (: 1)) + 1i * sin (Phase (: 1)).** This step ensures that the phase information, which is important in signal analysis, is preserved in the averaged spectra.
f. The final averaged spectra are stored in **FFTaveraged (: 2)** for pressure and **FFTaveragedVelocity (: 2)** for particle velocity. These spectra represent the main characteristics of the signals across different frames, providing a more stable and representative representation of the frequency-domain data.

3.2.5 Desired Output

The post-processing of the measured data was performed to obtain two main outcomes. The first was to obtain the narrowband frequency spectrum for all experimental setups. This allows a detailed analysis of these experimental results. This is accomplished by performing an FFT on the pressure data obtained from the PU probe at the end of all three setups.

The second outcome was to determine the complex acoustic impedance of the source setup. This allows the noise source to be characterized in GT-POWER. This involves finding both the complex pressure and the complex particle velocity. This is accomplished by applying an FFT to both the pressure and particle velocity data, from which the acoustic flow impedance values can be calculated.

3.2.5.1 Frequency spectrum derivation from experimental setups

The complex averaged pressure is obtained by taking the FFT of the data collected from all three setups. It contains both magnitude and phase information. The RMS of this averaged complex pressure is taken along the frequencies of interest. This is done by taking the absolute value of each of the elements of the pressure vector along the corresponding frequencies. These values are then divided by the reference pressure. The result is expressed in decibels. The formula for the conversion is given by Eq. (44).

$$Sound\ Pressure\ (dB) = 20\log\left(\frac{abs(\mathbf{FFTaveragedPressure}\ (:\mathbf{2})\ )}{20e^{-6}}\right); \tag{44}$$

The resulting sound pressure level is plotted against frequency. This frequency spectrum shows experimental results for three setups. They will be presented in the results section 4.1 of the thesis.

3.2.5.2 Acoustic Impedance Calculation Using FFT Results

The concept of acoustic impedance was explained in detail in section 2.1.7 (page 32) of this thesis. The calculation of the acoustic impedance involves the use of the flow impedance formula, which is dependent on the specific pipe geometry. This relationship is expressed by Eq. (45).

$$Complex\ Acoustic\ Impedance = \frac{complex\ pressure}{complex\ particle\ Velocity \times area}\ [pa - s/m^3] \quad (45)$$

Complex pressure and particle velocity are obtained by performing an FFT on the source data, and the area is calculated using the internal diameter of the connector.

3.2.6 Application of Normalization Technique for correcting the pressure value

The placement of the PU probe at a distance of 10 mm from the connector opening of the source setup may not represent the actual pressure values. Likely, the pressure and particle velocity values inside the connector will not be the same as measured outside the pipe. These differences could be due to pipe geometry, wave interactions in the confined space, and impedance variations which affect particle pressure and velocity inside the connector. Conversely, the pressure measured in an open space would be different. It could not benefit from the same geometric effects as the confined pipe space. The impedance characteristics of these measurements are different.

In support of these assertions, the inverse distance law formula can be used to estimate pressure values closer to the source. This formula is applicable under free-field conditions, but it still provides a rough approximation in an enclosed environment, albeit with a deviation of about 2 dB. The concept of the inverse distance law and its practical use in evaluating sound pressure levels near the source is illustrated by Eq. (46).

$$L_2 = L_1 - 20\log\left(\frac{r_2}{r_1}\right) dB,\ \ r_2 = 1\ mm\ and\ r_1 = 10\ mm \quad (46)$$

In Eq. (46) L_2 is the value of pressure taken at a 1 mm distance from the connector. The result is presented in the result section 4.1 of the thesis.

In addition, the normalization process is used to account for any differences between the measured values and those expected in the close vicinity of the source. The normalization process adjusts the data within a specified range or relative to a reference value. The peak pressure value within the pressure vector has been selected as the reference point. This reference value is divided by the entire pressure vector to obtain the normalized pressure, as shown in Eq. (47).

$$Normalized\ Complex\ Pressure = \frac{complex\ FFT\ Pressure}{max(abs(Complex\ FFT\ Pressure)} \quad (47)$$

Where, $\max(abs(Complex\ FFT\ Pressure)$ is 0.19 Pascals. This normalization procedure serves to adjust the amplitude of the measured pressure signal. It aims to bring the signal's amplitude into better alignment with the expected pressure values near the source.

3.3 1D Modeling of Reference Experiment

Reference experiment including the configurations of Set2 and Set3 is modeled by using the acoustic components of GT-POWER software. The software solves the fluid flow by solving the Navier-Stokes equations in only one dimension. This implies that it can capture sound waves traveling along the discretized direction, commonly known as plane waves (see Fig. 24). However, the waves that travel across the discretized lengths are considered to be cross or radial waves. These waves can only be captured when a 3D discretization is carried out. Flow splits can be used to discretize the volume along multiple axis. This allows the plane waves to be captured in more than one direction during the simulation. This approach is most useful for larger volumes where the possibility of cross waves exists, such as resonators and silencers. For instance, for a sound wave passing through an expansion chamber. The resonance mode for the plane wave can be traced along the length, width and diagonal of the expansion chamber. It shows that 1D solver can capture the complex geometries (Acoustics Application Manual, 2023).

In this experiment, however, a simple pipe geometry was used. The pipe diameter is smaller than the wavelength of the highest frequency analyzed (500 Hz). These conditions imply only an axial flow of the waves, so the pipe is only discretized in the axial direction as depicted in Fig. 24. Furthermore, GT-POWER supports only plane wave analysis, which meets the requirements and conditions of this analysis. In most of the cases, the plane wave mode dominates the other modes of wave propagation. The dominance of the other modes, depends on the geometry. A good way to determine this is to make a comparison between the simulated results and the measured results. It is possible that the results may agree well for a certain frequency range, and then start to diverge due to domination of the radial modes.

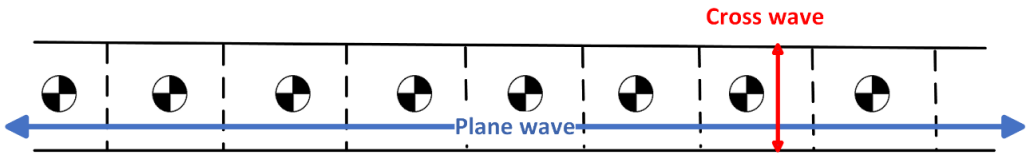

Figure 24. Plane waves are traveling along the discretized horizontal length of the pipe.

3.3.1 The Simulation model

The Transfer Matrix (TM) method has been used for the modeling of the reference experiment. It uses a set of linearized equations to characterize the acoustic properties and flow within the system. The TM method is not based on the linearized Navier-Stokes equation. Instead, it is derived from the solution of the Helmholtz equation as expressed in Eq. (48), which is related to plane wave theory.

$$\frac{\partial^2 P}{\partial x^2} - \frac{2jkM_0}{1-M_0^2}\frac{\partial P}{\partial x} + \frac{k^2}{1-M_0^2}P = 0 \tag{48}$$

Where P is the pressure, x is the flow coordinate, j is the imaginary number, k is the wave number, and M_0 is the Mach number. The Mach number refers to the ratio of the

fluid's flowing velocity to the speed of sound. This Eq. (48) is termed the convective acoustic equation. It describes the behavior of acoustic waves in a fluid with uniform velocity and steady flow. This equation considers the convection effect, where the motion of the fluid (mean flow) influences the propagation of acoustic waves in the medium. The first term in the equation describes how the sound pressure changes in space. The second term reflects the mean flow convection M_0. The third term describes the wave behavior (István L. Vér, 2005).

The TM approach simplifies the characterization of a system by relying on geometric dimensions, boundary conditions, and initial conditions, without the need for detailed time-based simulations. It operates in the frequency domain, contrary to non-linear standard GT-POWER solver which uses the mathematical tools like FFT to transform results from time domain to the frequency domain. It can be applied to many of the same flow components used in flow simulations, making it convenient to analyze acoustic properties within their existing models. Moreover, one of the significant advantages of TM analysis is its computational speed. It can provide approximate results for the system's response in a fraction of the time it takes for a non-linear GT-POWER acoustic simulation. The limitation of this method is that it doesn't provide a detailed physical flow simulation, and it may not capture fine details of the system's components. Instead, it provides a general system response. It doesn't calculate pressures, velocities, or other detailed information for individual components. It only computes the overall system response (Acoustics Application Manual, 2023).

This method is only applicable when the frequency of interest is below the cutoff frequency. The TM method involves constructing matrices that represent the acoustic properties and interfaces of each component. These matrices relate state variables from one end of the component to the other. The most commonly used state variables are pressure and volumetric flow rate. The overall response of the acoustic system is calculated by multiplying the matrices of all system components. The components refer

to the source, pipe interfaces and the boundary condition of the system. For example, the TM for a component with two ends is given in Eq. (49).

$$\begin{pmatrix} p_1 \\ u_1 \end{pmatrix} = \begin{bmatrix} T_{11} & T_{12} \\ T_{21} & T_{22} \end{bmatrix} \begin{pmatrix} p_2 \\ u_2 \end{pmatrix} \tag{49}$$

In Eq. (49), the coefficients T_{11}, T_{12}, T_{21}, and T_{22} of TM describe the relationship between the state variables and depend on the chosen format. For example, GT-POWER offers three different formats depending on the application: Pressure/Volume Flow, Progressive/Reflective, and Transmission/Reflective. The pressure/flow format is the most widely used and is considered the default in GT-POWER (Acoustics Application Manual, 2023).

The reference experiment, is modeled in GT-POWER to validate the accuracy of model with the experimental results. It mainly consists of four main components, as shown in Fig. 25.

1. AcoustTMSource (Source template)
2. PipeRound (Pipe model)
3. BoundaryPressure (End-Environment)
4. AcoutTMExtMic-1 (Microphone)

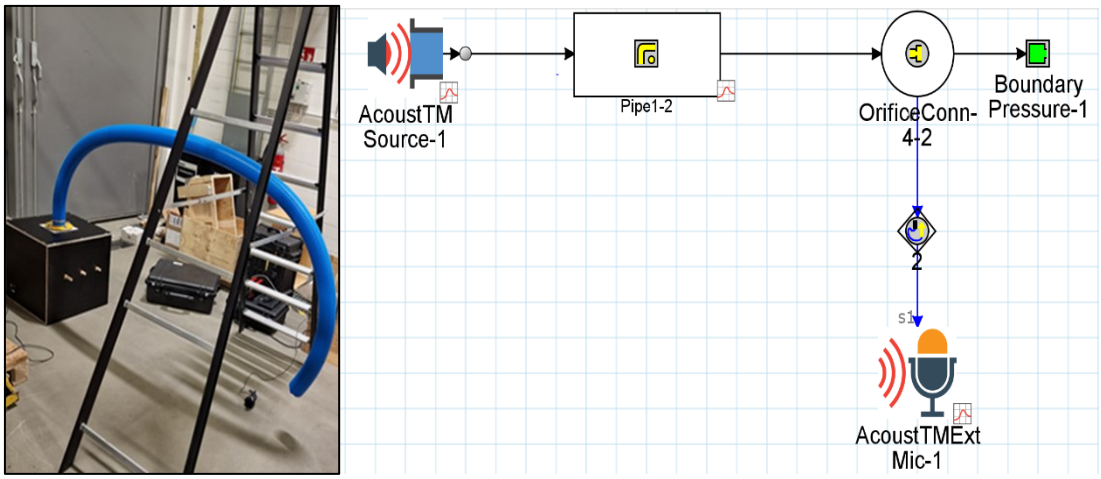

Figure 25. Set3 (left) mapped in GT-POWER (right) with AcoustTMSource by using the link arrows directing towards the flow direction of system.

3.3.1.1 AcoustTMSource (Source Template)

This template is used to characterize a source using the acoustic properties of the experimental source. These properties are obtained from post processing of measured data such as pressure and particle velocity. The 'AcoustTMSource' is the main template that should be present on the map for all TM acoustic simulations. When the solver detects this template, it performs the TM acoustic analysis on the components attached to the source. These components can be the common flow components. The list of flow components that can be part of the acoustic TM method is in Tab. 9.

Table 9. The following flow components are suitable for TM acoustic simulations (Acoustics Application Manual, 2023).

PipeRound	PipeRectangle	PipeCrossSection	PipeTable
FlowSplitTRight	FlowSplitTAngle	FlowSplitY	FlowSplitSphere
FlowSplitGeneral	FlowSplitAbsorbing	OrificeConn	BoundaryFlowCap
AcoustTMSource	BoundaryPressure	AcoustTMBoundary	BoundaryAnechoic

GT-POWER provides three different formats for source characterization using this template. These formats include input data in the form of amplitude/reflection, volume/admittance, and pressure/impedance formats. The pressure/impedance format is the default format used by GT-POWER to perform most of its calculations. This format was selected and provided the necessary data to simulate the model. These data included the complex acoustic flow impedance and complex pressure computed during the post data processing part of the thesis. The data is already transformed to the frequency domain, which is the main requirement of the TM method. The equation used by GT-POWER for this format is given in Eq. (50).

$$P_s = p_0 + Z_s u_0 \tag{50}$$

Equation (50) shows how source pressure (P_s) and source impedance (Z_s) relate to other state variables such as volumetric flow (u_0) and pressure (p_0) during TM analysis.

3.3.1.2 PipeRound (Pipe model)

The 'PipeRound' is not an acoustic component, as it is an element of the fluid flow. However, as explained before, the TM method considers only the initial conditions, the geometry and the boundary conditions of the system. The role of this component is to provide geometric information about the pipe. Even the discretization of the pipe is not considered in this method. The consideration of the discretization depends on the need and the nature of acoustic TM template being used. For an instance, 'AcoustTMEigen' is template that provides the option to include the discretization factor for the analysis of the eigen frequencies.

Furthermore, the mean flow effects, viscous and thermal effects can be included in the TM analysis. It depends on the acoustic component being used such as 'AcoustLinTransLoss', 'AcoustLinInsLoss', and 'AcoustLinEigen' provides an option to turn on these effects. The mean flow is calculated by the correction of the Mach number effects while viscous and thermal effects by correcting the viscosity and thermal conductivity of fluid both as the function of temperature. The details of these corrections can be seen in the Eq. (51).

$$\begin{pmatrix} p_0 \\ u_0 \end{pmatrix} = \begin{bmatrix} T_{11}(k) & T_{12}(k) \\ T_{21}(k) & T_{22}(k) \end{bmatrix} \begin{pmatrix} p_1 \\ u_1 \end{pmatrix} \tag{51}$$

Equation (51) is a general transfer function equation expressed as the function of the wave number. The Eq. (52) expresses the same general matrix with an exponential term as a correction and the TM is function of now modified wave number(k_c).

$$\begin{pmatrix} p_0 \\ u_0 \end{pmatrix} = \exp\left(-j\frac{kM}{1-M^2}L\right)\begin{bmatrix} T_{11}(k_c) & T_{12}(k_c) \\ T_{21}(k_c) & T_{22}(k_c) \end{bmatrix}\begin{pmatrix} p_1 \\ u_1 \end{pmatrix} \quad (52)$$

Where, $k_c = \frac{k+\alpha}{1-M^2}$ with $a = (1-j)\frac{k}{2R}\sqrt{\frac{2v}{\omega}}\left(1+\frac{\gamma-1}{\sqrt{Pr}}\right)$, k_c is the modified wave number. M is the Mach number, R is the geometric radius, v is the dynamic viscosity and Pr is the Prandtl number. Equation (52) is the general matrix form that includes the effects of mean flow and viscous thermal flow. However, if only mean flow effects are included, the alpha (a) term of the modified wave number is omitted. Conversely, if only the viscous thermal effect is included, the whole exponential term is omitted and the modified wavenumber would have a denominator of 1 (Acoustics Application Manual, 2023).

None of these effects were considered due to the nature of the experiment and the requirement of analysis. As loudspeaker is used as noise source. The thermal and viscous flow effects of the air would be minimal in this case and there is no mean flow. The geometric parameters of the pipe that are measured from the experiment are fed into the input table of the ''PipeRound'' component of the GT-POWER. As shown in Fig. 26, these parameters include the length, diameter, bend radius, and bend angle of the pipe. The experiment is based on the two different bending angles of the pipe. Set2 has a bending angle of 90°, while Set3 has a bending angle of 180°. However, both pipes have the same diameter and length. By simply changing the bending angle, these configurations can be modelled and analysed in GT-POWER. A temperature of approximately 21°C is imposed on the inner wall of the pipe. This temperature is the same as the ambient temperature. Therefore, no boundary conditions were applied across the pipe wall. In addition, only thermal conductivity is affected by changing the

material of this flow component. Acoustic effects like absorption of sound waves are not considered.

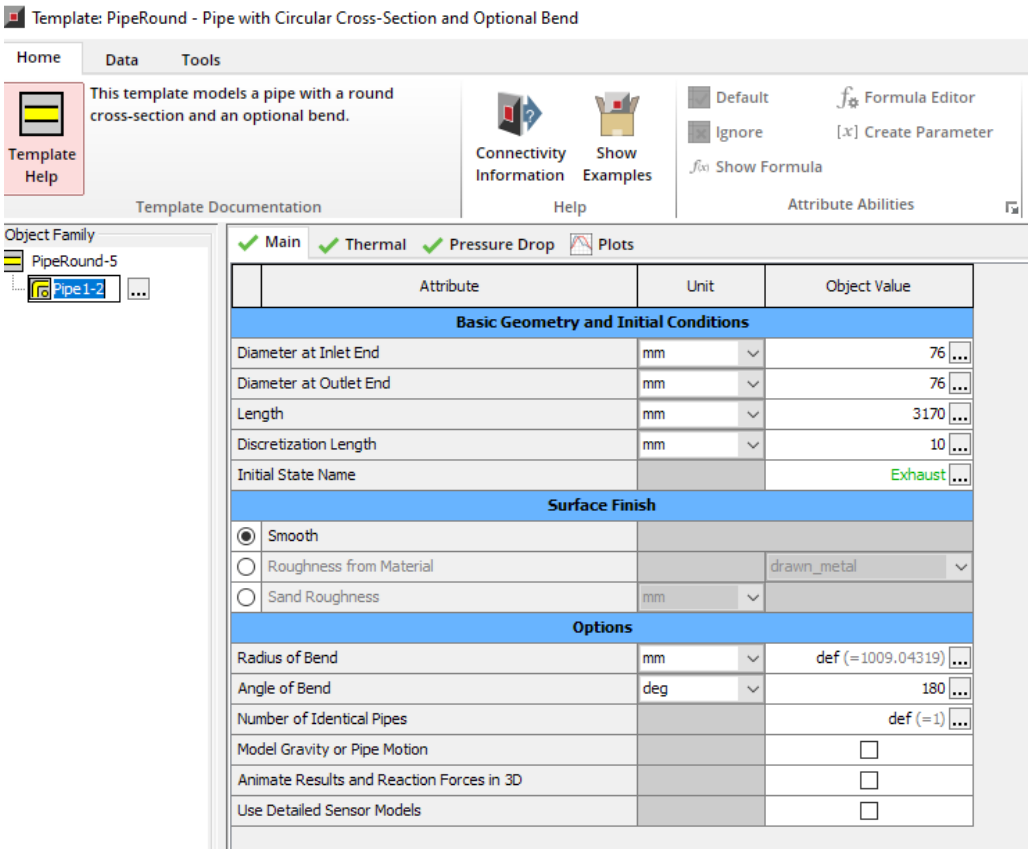

Figure 26. The figure shows the format for adding the pipe's geometric parameters.

3.3.1.3 BoundaryPressure (End-Environment)

The 'BoundaryPressure' is a component of flow. It is used to define the end-environment in GT-POWER, mirroring the experimental setup. This template sets the boundary conditions for the environment at the end of the pipe. Its purpose is to replicate the experimental conditions, including temperature, pressure, and air composition. The only difference is that this recreated environment represents a free field, meaning it is an open and unobstructed space where sound waves propagate without any reflective surfaces. The downside of using this template is that it does not include the impedance of the surrounding environment.

GT-POWER offers two acoustic components, namely 'BoundaryAnechoic' and 'AcoustTMBoundary,' which can also be used to specify the boundary conditions at the downstream end of a system. The 'BoundaryAnechoic' template can be employed to define an anechoic outlet boundary. The pressure assigned to this anechoic end will be pre-determined and is often referred to as the 'anchoring pressure.' Typically, it is set equal to the ambient pressure or to another specific pressure based on the experimental requirements. This template is primarily used for analyzing transmission losses. On the other hand, 'AcoustTMBoundary' provides the ability to impose an impedance at the open end of the pipe. This impedance can. simulate the influence of the atmosphere. Acoustic parameters such as pressure and particle velocity of the atmosphere need to.be measured, so the impedance can be calculated to use this template.

3.3.1.4 AcoutTMExtMic-1 (Microphone)

This is a component of TM and is used to predict the SPL at the microphone located at some distance from the source opening. It is connected to the orifice that connects the outlet of pipe with a sensor connection. At the orifice end the sensor senses the velocity. The orifice acts like a monopole pulsating source for which the velocity is transformed to the pressure at any location in the free field by using Eq. (53) (Acoustics Application Manual, 2023).

$$P = \frac{\rho * S}{const * \pi * r} * \frac{d(u[TM])}{d\omega} \tag{53}$$

In Eq. (53), ρ is the density of the free field, S is the cross-sectional area of the orifice, const. is the value that is 4 for spherical radiation and $2\sqrt{2}$ for hemispherical radiations. ω is the frequency, r is the distance of microphone from orifice and $(u[TM])$ represents the velocity calculated by the transfer matrix.

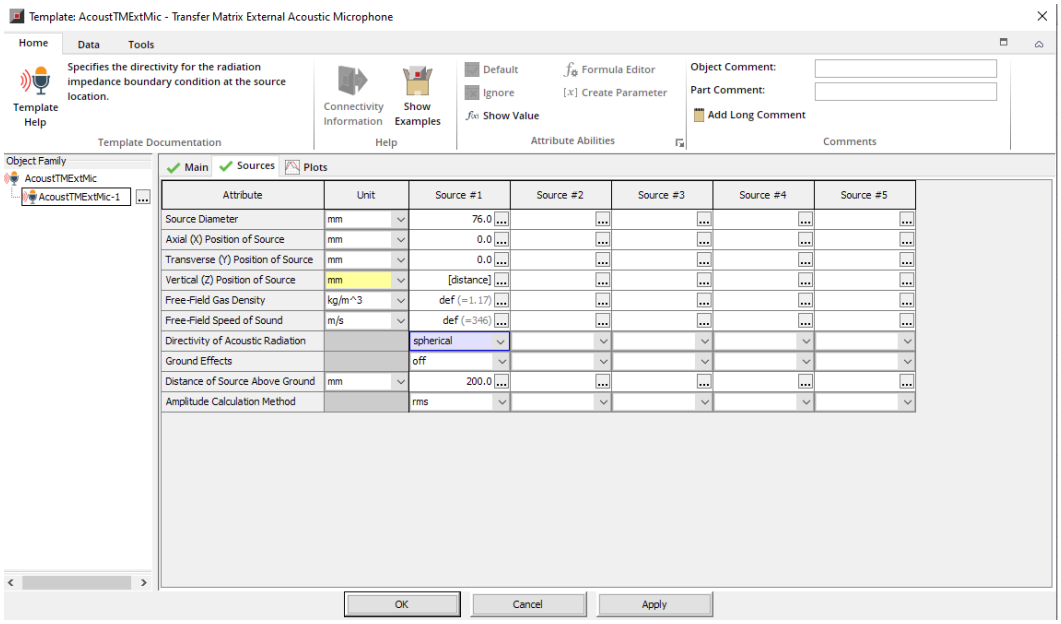

Figure 27. The input parameters for configuring the microphone settings are displayed.

The microphone is positioned 10 mm away from the pipe opening. This distance is given along the z-axis. This is the perpendicular distance from the surface of the pipe. This distance is equal to the distance of the PU probe during the experiment. Furthermore, the position of the microphone relative to the sound source follows the principles of the inverse square law. In other words, a doubling of the distance from the sound source will have a 6-dB reduction in sound pressure level. The template also provides the option of determining the directivity of the source, as shown in Fig. 27, classified as spherical, hemispherical, and hemi-6. A spherical radiation direction corresponds to the fact that the pipe is open-ended and ends with a circular opening in the free field. Conversely, a hemispherical radiation pattern is obtained when the pipe terminates with a flange. RMS is selected as the amplitude calculation method.

4 Results and Discussion

4.1 Validation of the Post-processing methods

Data obtained from PU probe in all the three setups has been analyzed during the post processing stage of signal processing. The FFT has been performed on the data and the SPL measured at end of each pipe setup is available in frequency domain. Frequency spectrum of the pressure emitted from the source setup has been depicted in Fig. 28. The source setup consists of a loudspeaker box with a small connector opening (see section 3.1.3 for details). This connector (duct adaptor) is connected to the plastic pipe for the subsequent setups. Referred to as the "source setup," it acts as the source of pink noise, which will be analyzed through the other setups.as well.

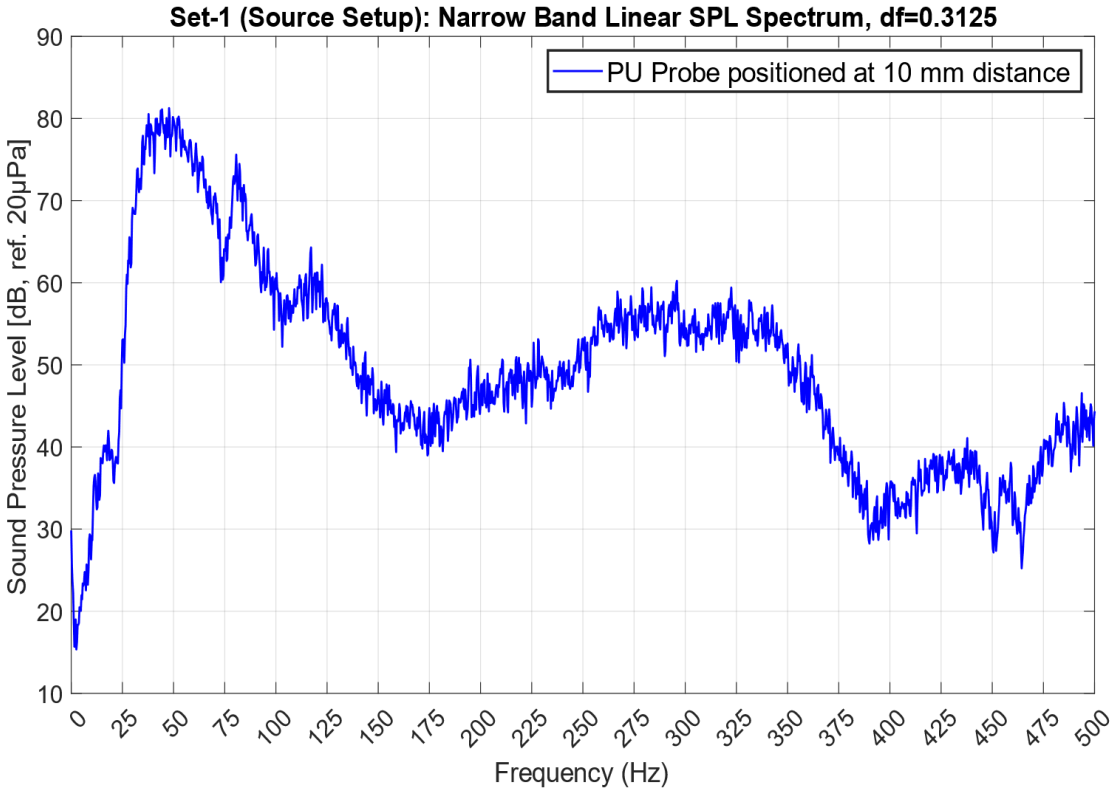

Figure 28. Frequency spectrum of source setup at 10 mm from the connector opening.

In this graph, distinct high-pressure curves were observed in the frequency spectrum at different frequency ranges. This prominent peak in the low-frequency region is

attributed to the response of the subwoofer. As low-frequency sounds are intended to be generated by subwoofers, the peak at 25 to 125 Hz indicates that a significant amount of sound energy within this range is being produced by the subwoofer, resulting in higher sound pressure levels. The shaping of this peak is influenced by the size and design of the loudspeaker box, along with the characteristics of the subwoofer. The sound pressure level in the frequency range of 125 Hz onward to 500 Hz shows that the sound output is being contributed by the speaker in the setup.

Following the initial readings with the sensor at the source setup, the connector of the source setup was subsequently attached to the pipe, featuring a slight 90° bend (refer to section 3.1.3 for detailed information). Further readings were acquired at the end of the pipe to investigate the potential influence of the pipe's geometry. The frequency spectrum obtained from the processed data has been shown in Fig. 29.

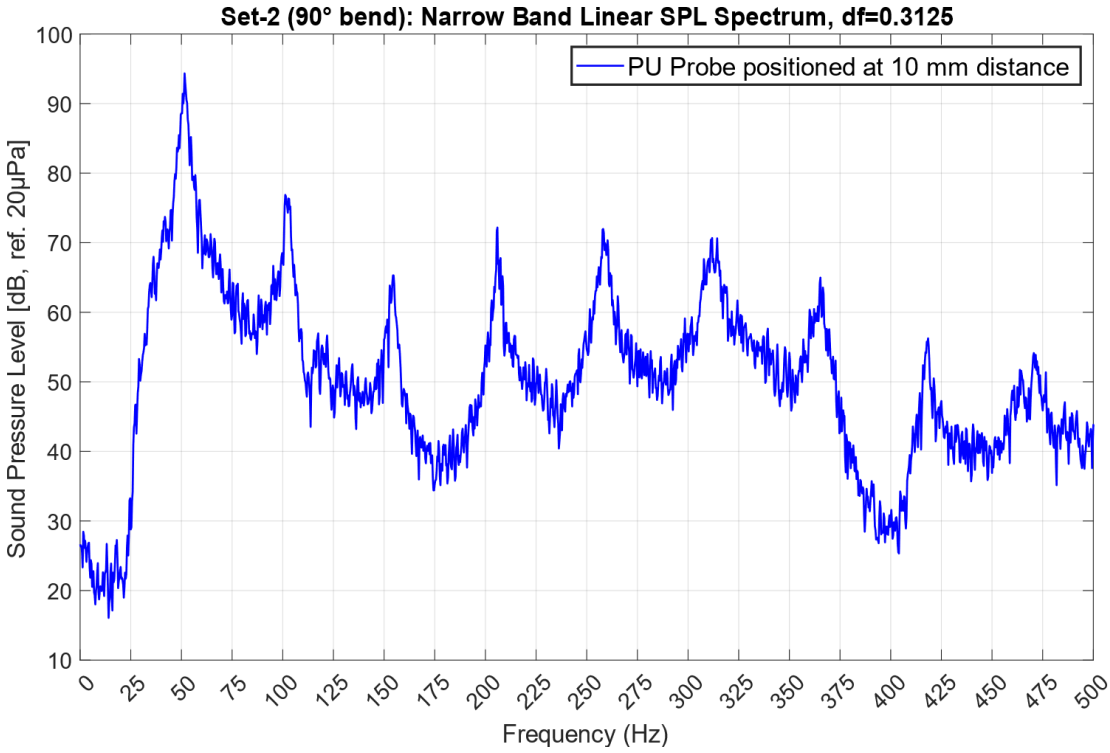

Figure 29. A noticeable presence of harmonics is evident in the observed spectrum.

The spectrum showed some harmonics which might have been caused due to resonant behavior of the pipe. A similar spectrum is observed when the pipe is subjected to a 180° oblique bend. The frequency spectrum obtained at the end of the pipe with the 180° oblique bend has been shown in Fig. 30.

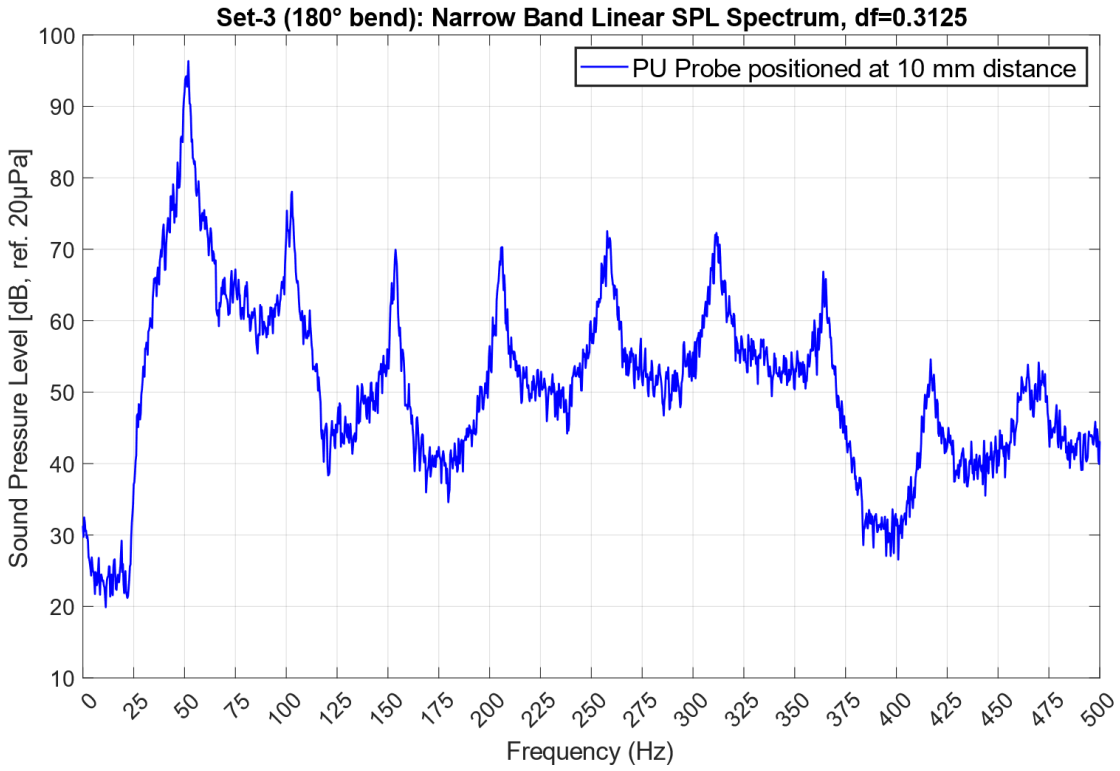

Figure 30. The frequency spectrum of Set3 is displayed, showing a striking resemblance in the pattern of harmonics as observed in Set2.

These are the frequency spectrums observed for all three setups. Moreover, to support this assertion that the pressure value measured at 10 mm away from the connector differs from the one inside the connector of source setup. A graph has been shown in Fig. 31 to depict a comparison among the pressure measurements acquired using the PU probe at 10 mm, and the B&K 2250 handheld analyzer at 1mm, and the estimated values calculated at 1 mm distance from the connector.

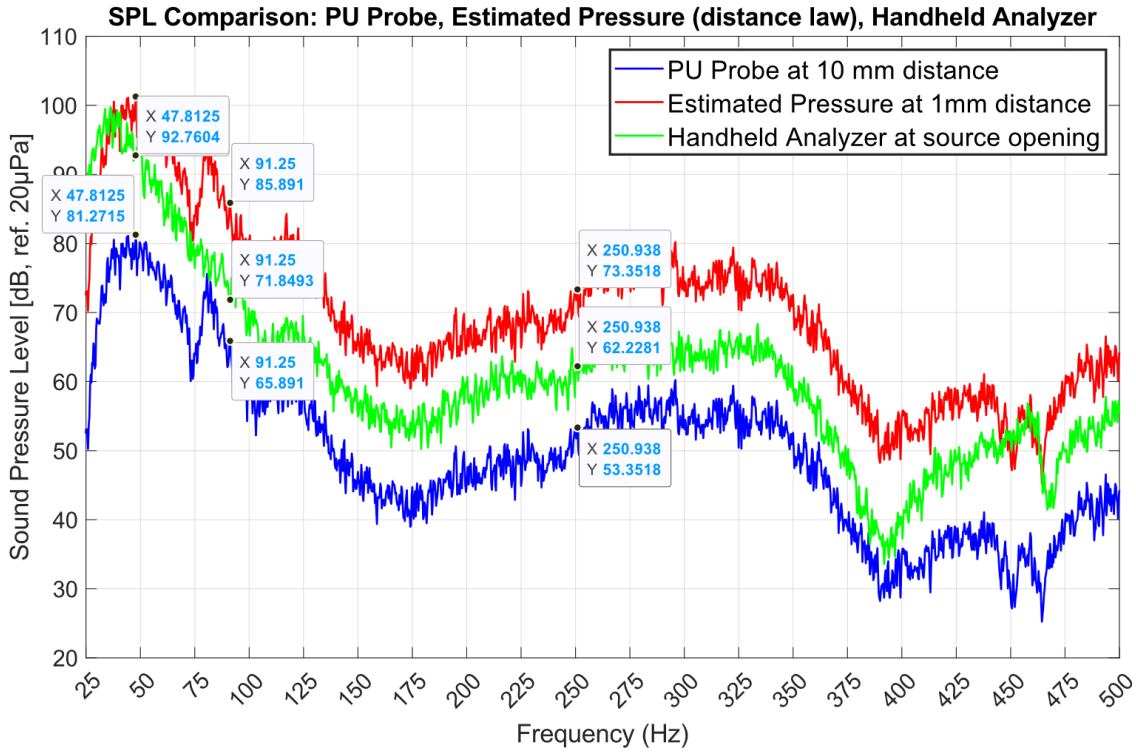

Figure 31. The comparison is shown among the estimated pressure (distance law), pressure measured by hand held analyzer and PU probe at source setup.

It is clear from Fig. 31 that the pressure value changes significantly depending on the placement of sensor from source. The estimated pressure calculated at a distance of 1 mm from the source setup, shows a 20 dB increase in SPL over the PU probe. Similarly, the SPL measured by the B&K 2250 at 1 mm from the source is approximately 10 dB higher than that of the PU probe. It is possible that the SPL inside the pipe is even higher. This implies that PU probe measured an underestimated pressure value when placed at a distance of 10 mm from the source setup. The normalization technique (see section 3.2.6 for details) is used to scale up these pressure values measured by the PU probe. To confirm the effectiveness of this normalization, a graph in Fig. 32 shows the agreement of the normalized pressure values with the pressure readings obtained using the B&K 2250 handheld analyzer.

The graph serves as a validation of the normalization process, confirming its ability to accurately align the measured pressure signal with the expected values in close proximity to the source. This normalized pressure value of the source has been used as an input for the simulation of the GT model.

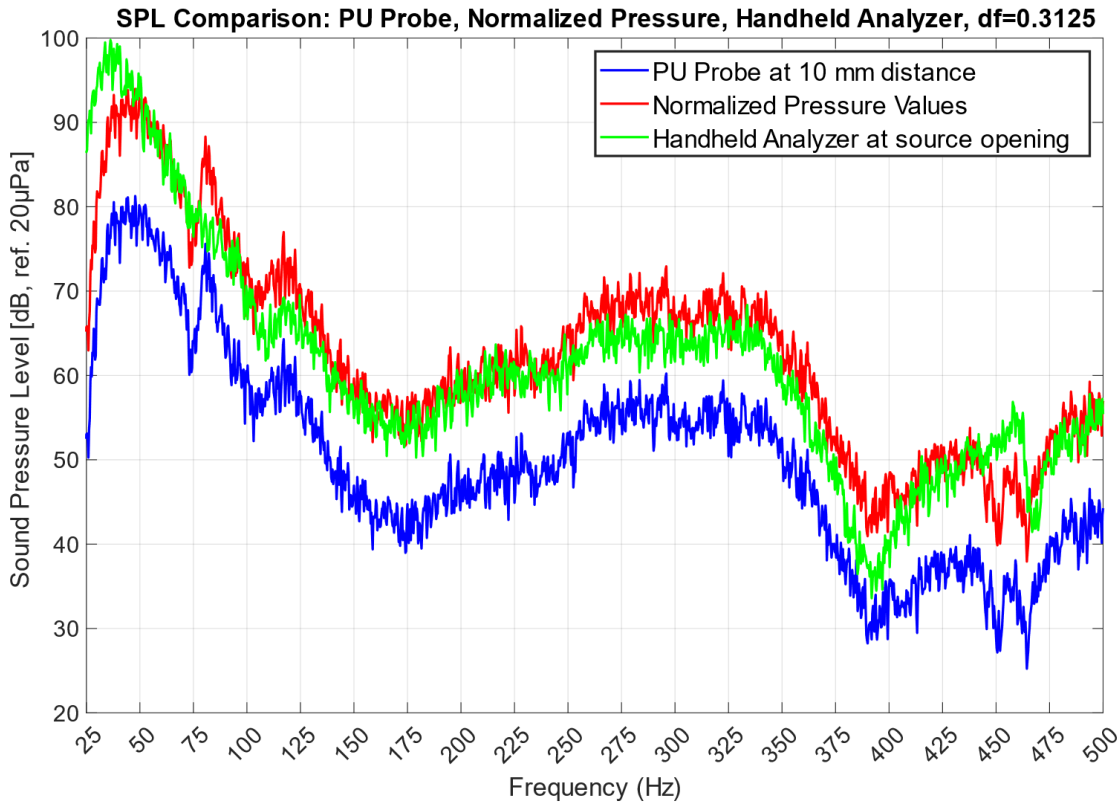

Figure 32. Given graph shows a close match between the normalized pressure values (red) and B&K 2250 analyser readings (green).

4.2 Spectrum Analysis of noise on plastic pipe setups

This section provides a comparative analysis of the post-processing results. As shown in the previous section, the frequency spectra of the sound pressure level have been presented for all three setups. Now the focus has shifted to a more detailed study of the phenomenon responsible for these spectral variations. In addition, the effect of changing the angle of the pipe bend on the frequency spectrum will be investigated.

4.2.1 Comparative Analysis of Frequency Spectra b/w Source Setup & Set3 (180°)

Figure 33 shows the results of the linear sound pressure level measured at both the source setup and the end of the plastic pipe. Specifically, it represents the sound pressure emitted by the source, propagated through the plastic pipe, and then measured at the end of the pipe. It is noticeable that distinct harmonics appear within its frequency spectrum. These harmonics indicate the presence of standing waves within the pipe. The presence of standing waves in a pipe can be attributed to several factors, including both the resonance characteristics of the pipe and the phenomenon of end reflection. Resonance and end reflection are related, and together they contribute to the formation of standing waves in the pipe.

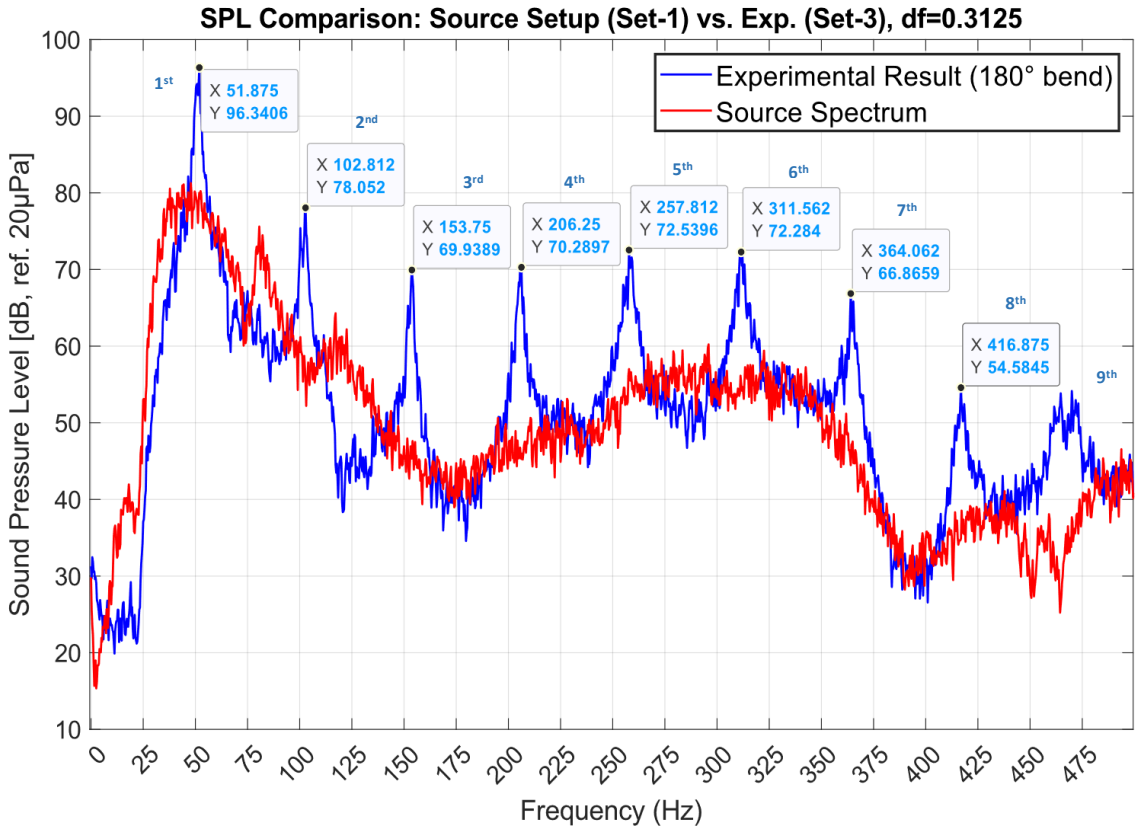

Figure 33. Comparative graph showing the frequency spectra of source setup vs. Set3 (180°).

4.2.1.1 Resonance of the pipe

Resonance in the pipe occurs when the dimensions of the pipe match certain wavelengths of sound waves. These resonant frequencies correspond to the conditions under which standing waves are formed in the pipe. At these frequencies, the reflected waves constructively interfere with the incident waves, resulting in stationary patterns of high- and low-pressure areas known as standing waves.

Nearly nine harmonics are observed at the end of the pipe in the frequency range from 0 to 500 Hz. Such harmonics are commonly found in musical instruments such as flutes, which are designed by their dimensions to produce specific harmonics. Open-ended resonance occurs due to the interaction between the pipe's vibrational characteristics and the sound waves it generates. The resonance of the pipe is calculated using Eq. (30) from section 2.1.8 of the thesis. This equation determines the pipe resonance based on theoretical principles. A comparison between the theoretical and experimental resonance values is given in Tab. 10.

Table 10. Comparing Experimental and Theoretical Resonant Frequencies**.**

Harmonics	Theoretical	Experimental	Percentage Error
1st	53.847 Hz	51.88 Hz	3.66 %
2nd	107.69 Hz	102.81 Hz	4.53 %
3rd	161.541 Hz	153.75 Hz	4.70 %
4th	215.388 Hz	206.25 Hz	4.11 %
5th	269.235 Hz	257.812 Hz	4.37 %
6th	323.082 Hz	311.562 Hz	3.49 %
7th	376.989 Hz	364.062 Hz	3.67 %
8th	430.776 Hz	416.875 Hz	3.04 %
9th	484.623 Hz	470 Hz	3.08 %
Overall Average Percentage Error			3.95 %

The calculated overall percentage error of 3.95% between the experimental and theoretical resonant frequencies is within the expected range. This discrepancy can be attributed to the differences between the actual experimental conditions and the idealized assumptions made in the theoretical framework. Hence the harmonics observed in the frequency spectrum are merely caused by the resonant frequency of pipe, which has further given rise to standing wave inside the pipe.

The deviation of the experimental resonant frequencies from the theoretical values could be traced to the loudspeaker box itself. While the theoretical model expects the pipe to be open at both ends to facilitate proper resonance, the practical setup involves the loudspeaker box. This incorporation of the loudspeaker box introduces its own Helmholtz resonance characteristics, which interact with the pipe's resonance. As a result, the combined system of the loudspeaker box and the pipe might exhibit resonance frequencies different from what the analytical model predicts.

4.2.2 Effect of Varied Pipe Bend Angles on Frequency Spectrum

In this study, two separate experimental setups were used, each sharing an identical pipe length and consistent geometric parameters. Set 2 was characterized by a smooth 90° bend, while Set 3 featured a 180° oblique bend. Figure 34 shows an interesting frequency spectrum observed at the end of the pipe. Notably, both configurations display remarkably similar amplitudes in the sound pressure level, underlining the consistent nature of the sound behavior in both pipe configurations.

A closer look reveals slight variations in SPL. The pipe with the 180° bend shows a 2 dB increase in SPL compared to the other configuration. Such small variations could be attributed to inherent measurement uncertainty. Variations of 2 to 3 dB are not uncommon in SPL measurements. Even repeated measurements at the same location can produce such differences due to factors such as environmental conditions. Specifically, the absence of an anechoic chamber or free-field conditions introduces reflections that can have an impact on SPL consistency.

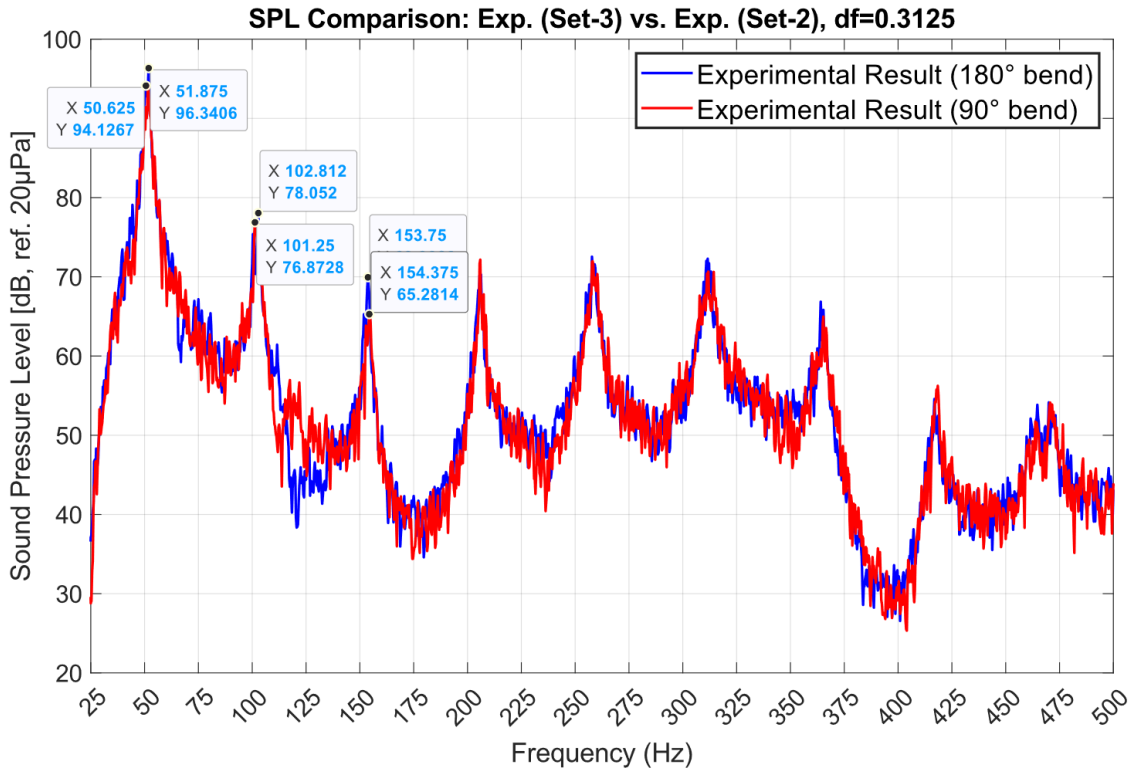

Figure 34. Spectral analysis of pipes with different bending angles.

It would therefore be premature to attribute these minor variations in sound pressure level solely to the change in bend angle. Changing the bend configuration shows no significant difference in frequency between the configurations; they retain a similar behavior. The lack of any significant impact from altering the bend angle may indicate the pipe's resilience to internal reflection and diffraction. A more comprehensive analysis awaits confirmation through simulation results to clarify whether changing bending angles has a significant effect on frequency.

4.3 Spectrum Analysis of noise on Exhaust Pipeline

4.3.1 Effects of Bend on the Frequency Spectrum in Exhaust Duct

The spatial averaging method is employed to investigate the sound characteristics within the duct. The duct is divided into three segments, and spatial averaging is conducted for

each segment following a bend (for detailed information, refer to section 3.1.2). During spatial averaging, sound pressure levels are initially converted to RMS values. These RMS values are then averaged across all designated points within a specific section of the pipe. The resulting averaged value covers a specified frequency range. Subsequently, this averaged value is converted into decibels, representing the SPL for that particular section of the pipe. This approach enables a comprehensive analysis of the sound behavior along different segments of the pipeline. The resulting frequency spectrum obtained by spatially averaging all three pipeline sections is displayed in Fig. 35.

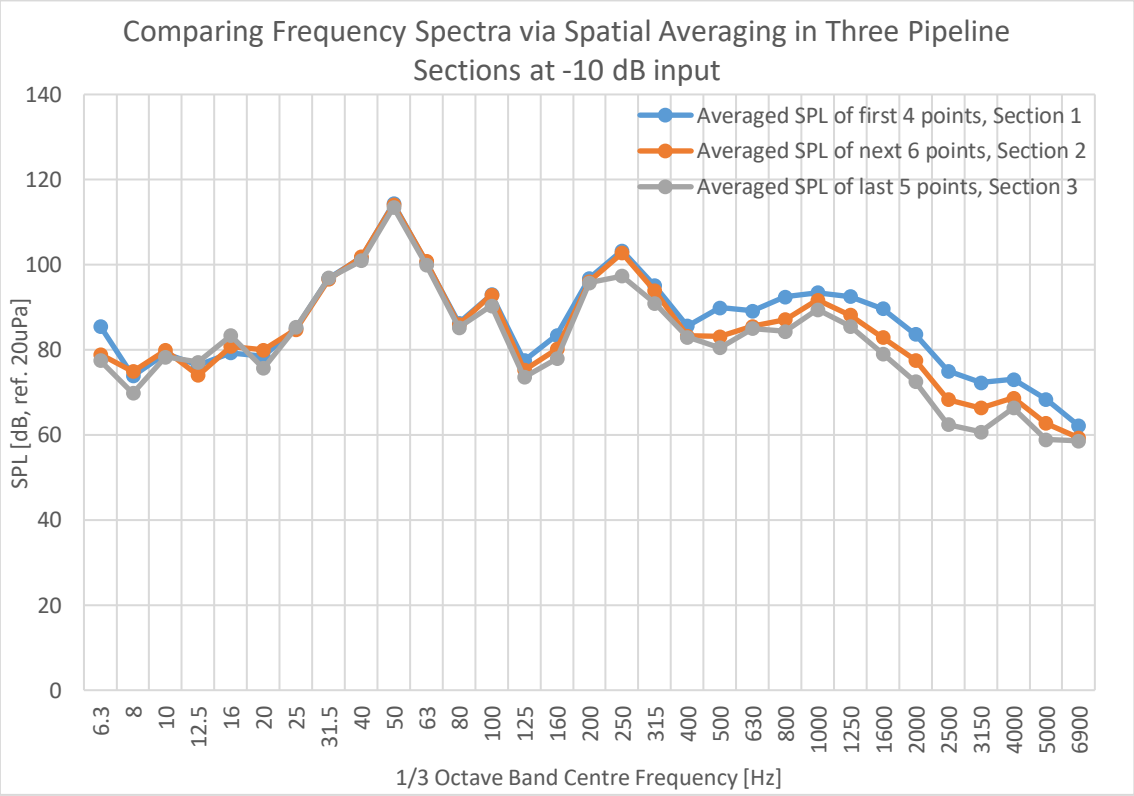

Figure 35. Comparative analysis of frequency spectra by spatial averaging over three sections of the exhaust pipe.

The frequency spectra of all three pipe sections after bends show minimal bending effects, especially in the low frequency range. However, a variation in the sound pressure level is observed in the frequency range from 400 Hz to 7000 Hz, which correlates with the distance of the pipe section from the source. This phenomenon can be attributed to sound energy loss during propagation, resulting in a decrease in amplitude and intensity,

especially at higher frequencies. As a result, the sound pressure level decreases the farther the sound waves travel from the source.

In particular, the bends in the exhaust pipe have an insignificant effect on the sound propagation behavior below the cut-off frequency of the pipe (about 446 Hz). This behavior occurs because when a sound wave encounters a bend, it may undergo partial reflection and scattering. Some of the energy may be redirected or dissipated as a result of a change in the direction of the pipe. However, this does not necessarily result in significant energy loss because the wave is already confined to the fundamental mode. Since this is first mode, most of the energy is conserved in this mode. In addition, below the cutoff frequency, the sound wave in the exhaust pipe behaves like a nearly perfect plane wave. This is because the observed frequency spectrum at different locations in the pipe shows minimal amplitude variation. The dominance of the fundamental mode is assessed by the absence of peak values above the cutoff frequency. This indicates that higher modes may exist, but have no particular influence on wave propagation.

4.3.2 Resonance Effect of the Exhaust Duct

The presence of resonant frequencies in the 1/3-octave frequency spectrum reflects the resonant frequencies of the plastic pipe (waveguide). These resonant frequencies, resulting from the fundamental mode of propagation, persist in all three sections of the exhaust pipe. This persistence is particularly noticeable in the low-frequency range, where attenuation is minimal, as shown in Fig. 36.

The yellow curve in the graph serves as a reference and represents the frequency spectrum observed at the end of the plastic pipe. It's important to note that the noise behavior in all three sections mirrors the trend of the reference curve, especially in terms of resonance. This is especially true in the low-frequency range. However, it is clear that as the frequency increases, there is an observable attenuation of the sound pressure level due to a higher rate of energy dissipation. There are two possible reasons for this energy loss. The first is the larger exhaust pipe diameter (450mm), which has lowered

the cutoff frequency. The second reason is related to the source input. The sound is directed at 90 degrees into the exhaust pipe. As a result, a significant amount of energy associated with high frequencies is dissipated.

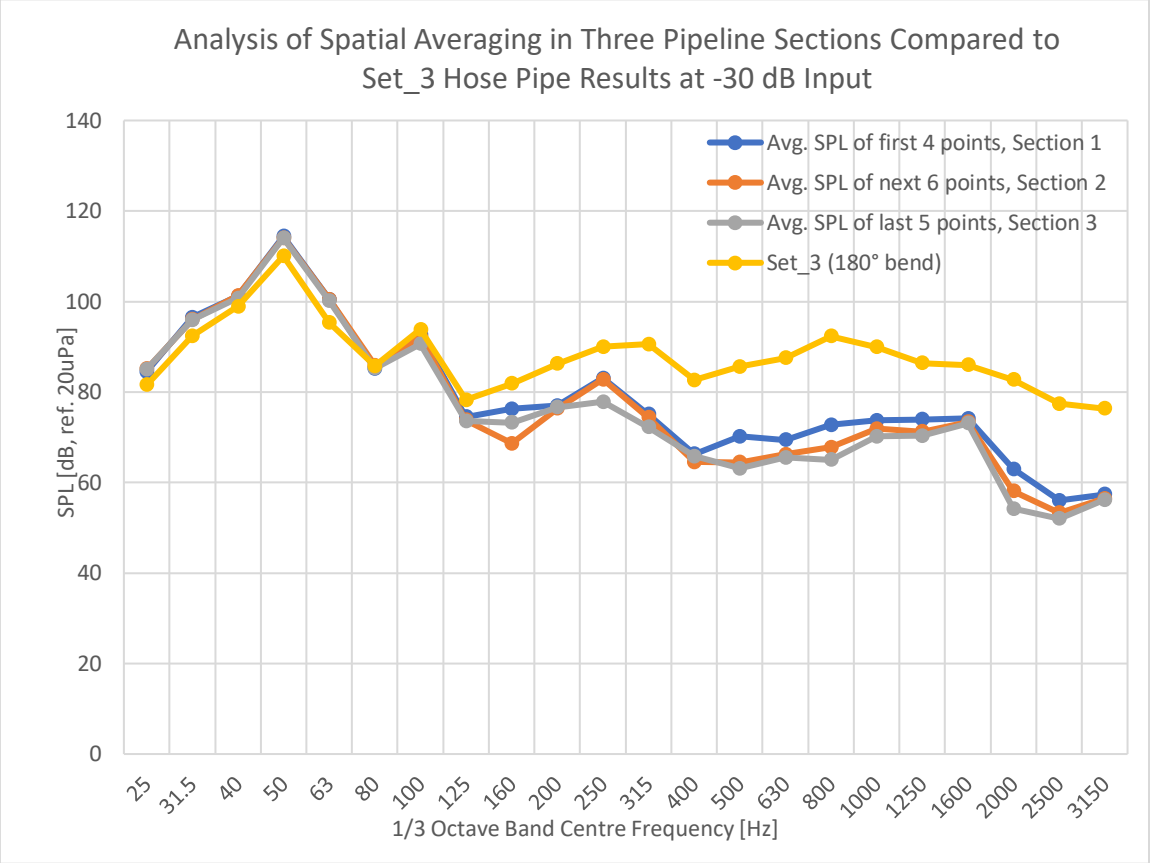

Figure 36. The graph clearly shows that the resonance effects of Set3 are still present within three pipe sections.

The exhaust pipe has effectively adopted the resonant characteristics of the connected plastic pipe. This implies the absence of inherent pipe resonance, which would otherwise have interfered with the incoming sound waves and consequently altered the trend of the observed spectrum. This shows that fundamental mode prevails in the exhaust pipe, though it could not excite the exhaust pipe's resonance but it conserves the enhanced energy transmitted by plastic pipe in this range. The absence of specific resonance frequencies in the exhaust pipe is due to the frequency range and type of noise applied to the exhaust pipe. It indicates that the resonance frequencies of the steel exhaust pipe

do not fall within the pink noise frequency range (25 Hz to 5000 Hz). As a result, the pipe does not exhibit much vibration or resonance in response to the pink noise signal. Infact, the energy of the pink noise signal may not be concentrated in the frequency band corresponding to the resonance frequency of the pipe. Also, the resonance of the pipe depends on the material properties and the boundary conditions (the way the pipe is mounted). The pipe may require a high energy input to excite its resonance.

Resonance can have a significant impact on complex exhaust systems, particularly when it comes to amplifying low frequencies. In multi-pipe scenarios, even the resonances of a single pipe play a critical role in increasing the overall sound pressure level. This amplification effect extends from duct to duct, even if a particular duct has no resonant frequencies of its own.

4.4 Simulation Results of Plastic Pipe setups

The previous section outlined the configuration and results obtained by the post processing the experimental data. This section focuses on the results generated by the simulation of the GT models on the basis of the plastic pipe setups. The results of the simulation are compared with the corresponding setup. This will provide insight into the accuracy of GT model-based acoustic predictions. It will also help identify causes of discrepancies in these results.

The comparison of results between the Set3 (180° bend) and its GT model is shown in Fig. 37. The graph shows a good agreement between the simulation and experimental results especially both of the curves follow the same pattern. However, a comparison of the harmonics between the results shows discrepancies of about 8 to 10 dB. The simulation result predicts the SPL about 8 to 10 dB lower than the experimental results. In particular, there is a noticeable frequency shift and the harmonics appear to be misaligned. The analysis first discusses the possible reasons for the observed amplitude discrepancies. Then, the potential factors behind the observed frequency shift are explained.

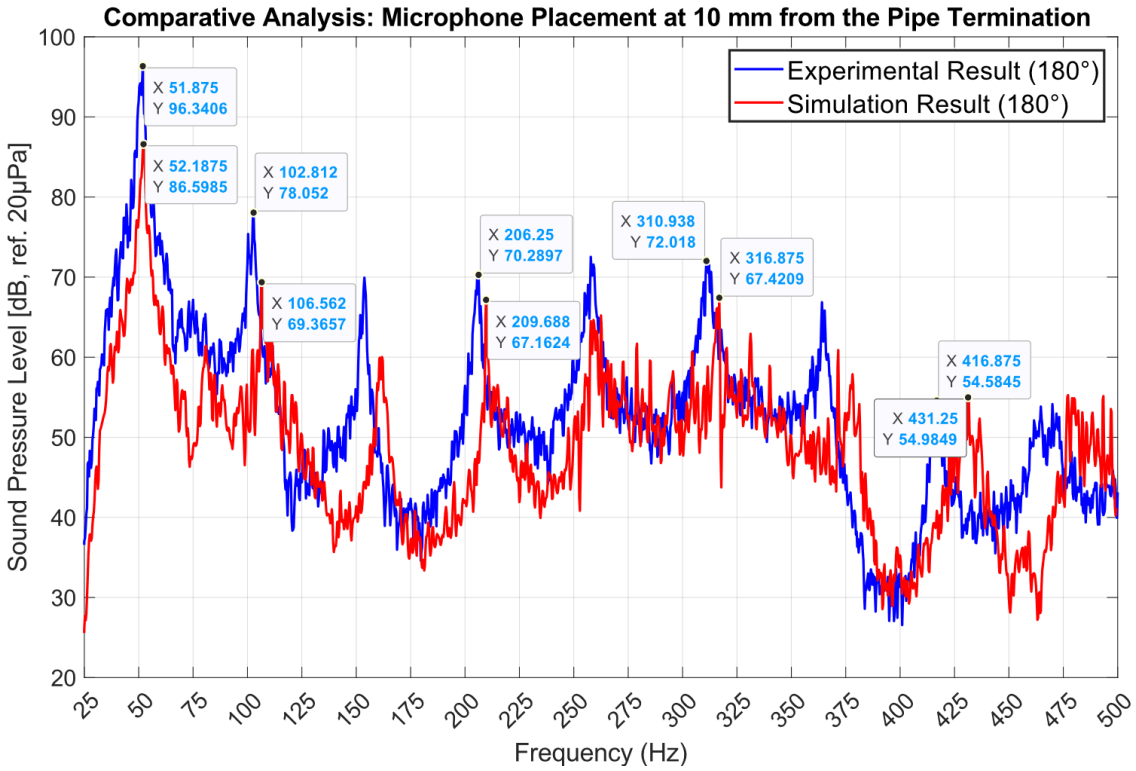

Figure 37. Comparison of narrow-band frequency spectrum between simulation and experimental result.

4.4.1 Factors contributing to the discrepancies in the amplitude

The lower SPL results of the simulation compared to the experimental results can be attributed to two possible reasons. The first is related to the positioning of the sensor during the experimental measurements. The other is linked to the accuracy of source data measured and used in the simulation.

4.4.1.1 Sensitivity of the positioning of the sensor

The placement of the sensor during the experiment can be responsible for the difference in amplitude of the sound pressure level. The experimental measurements were made 10 mm from pipe's end. The sensor was held by hand. During the measurements, the sensor was also moved across the pipe surface. Since 10 mm is a small distance, even a little nudge of the hand can bring the sensor closer to the pipe's end, potentially

increasing the readings. Therefore, to address this issue, a ±9mm error is allowed when positioning the GT model microphone from the actual microphone position at 10mm.

Figure 38 shows a graph in which the experimental results, indicated by blue curves, are within the defined margin of error. This agreement implies that the simulation results are quite good. The amplitude variation is most likely due to the movement of the sensor during the measurement. The green curve in the graph shows that moving the microphone only 9 mm closer to the pipe can increase the SPL from 10 to 12 dB. This illustrates the sensitivity of the microphone positioning to even small changes.

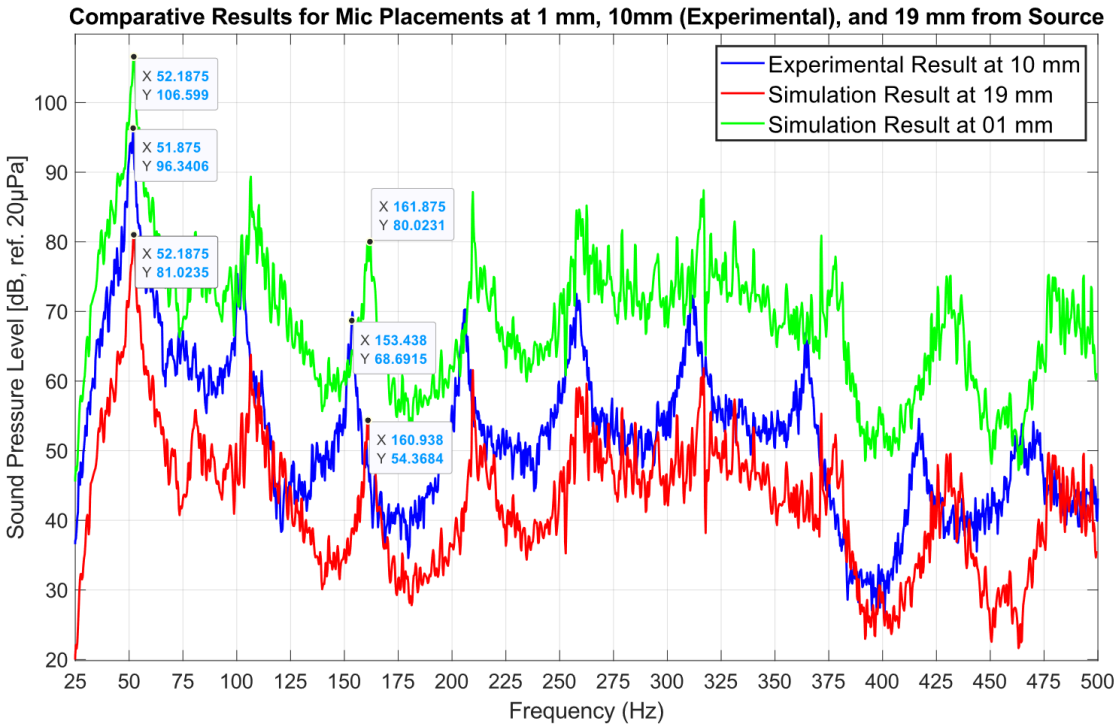

Figure 38. The experimental result (blue) lies between the simulation results generated at a distance of ±9 mm from the actual microphone placement (10 mm).

4.4.1.2 Acoustic Pressure Data used for Source Characterization

The accuracy of input data used for the source characterization in GT-POWER is possibly another factor for the lower SPL values of the simulation results. The measured

experimental results were obtained when the connector of the source setup was connected to the plastic pipe. However, the input data used were measured at a distance of 10 mm from the connector of the source setup. The sensitivity of the sound pressure to the distance from the source has already been verified (see Fig. 32 in section 4.1 of the thesis). It shows how the pressure value changes when measured at a 10 mm distance with a PU probe and at a 1 mm distance with a B&K 2250 handheld analyzer. The pressure value increases by 8 dB to 10 dB as the sensor is moved just 9mm closer to the source setup. However, the pressure value captured by the PU probe from the source is normalized to the value closest to the source. This normalized pressure value cannot correspond exactly to the value inside the connector. The normalization process has its limitations since it can approximate amplitude to some extent but cannot precisely capture the phase information of the pressure signal.

GT-model based simulations rely on both amplitude and phase information of the pressure signal to accurately characterize the source. Therefore, the input pressure data must be measured inside the connector to achieve accurate acoustic predictions.

4.4.2 Factors contributing to observed frequency shift

There are a number of factors that contribute to the observed frequency shift in the simulation results. These factors include the differing geometric parameters, the impedance data used to characterize the source, and the differing end conditions between the experiment and the simulation.

4.4.2.1 Disparities in Geometric Parameters

One of the reasons for these frequency shifts is the difference in geometric parameters between experimental setups and GT-models. Open pipes exhibit inherent resonant behavior, resulting in the emergence of multiple resonant frequencies. The frequency spectrum observed at the end of the pipe primarily embodies the characteristics of these

resonant frequencies. These significantly shape the overall phenomenon occurring inside the pipe.

The spectrum observed at end of the pipe during the experiment is influenced by several factors, including the dimensions of the connector, its base length and the size of the lid hole, as shown in Tab. 11. As the main plastic pipe overlaps the connector, it contributes to an effective length of 3,000 mm for the main pipe. Furthermore, the combined dimensions of the connector give a total length of 190 mm. Together, they contribute to the pipe like behavior of the entire assembly.

Table 11. Contributing dimensions of the pipe and connector to the total length of the pipe.

Attributes	Length	Diameter
Connector	160 mm	65 mm
Connector base	10 mm	65 mm
Lid Hole	20 mm	65 mm
Plastic Pipe (PVC)	3000 mm	76 mm
Experimental pipe length	3190 mm	76 mm

In GT-POWER, only the plastic pipe is represented with a uniform diameter, as the source is defined after the connector. However, to include same parametric effects in the simulation as the experimental ones. The length of the plastic pipe is extended to 3190 mm in GT-POWER, similar to the sum of the pipe lengths in the experiment. The difference between the diameter of the connector and that of the main plastic pipe is around 10 mm. Such a small variation in pipe diameter does not affect resonance frequencies significantly, so this difference in diameter can be ignored for a short length of 190 mm.

The graph in Fig. 39 shows that the frequency mismatch between simulation and experimental results has been reduced. This is because length and frequency are inversely proportional to each other. As pipe length increases in GT-POWER, resonance

frequencies shift towards lower frequencies. Despite this, there are still some difference in frequency alignment between the experimental and simulation results. A plausible factor contributing to this discrepancy could be the impedance effect.

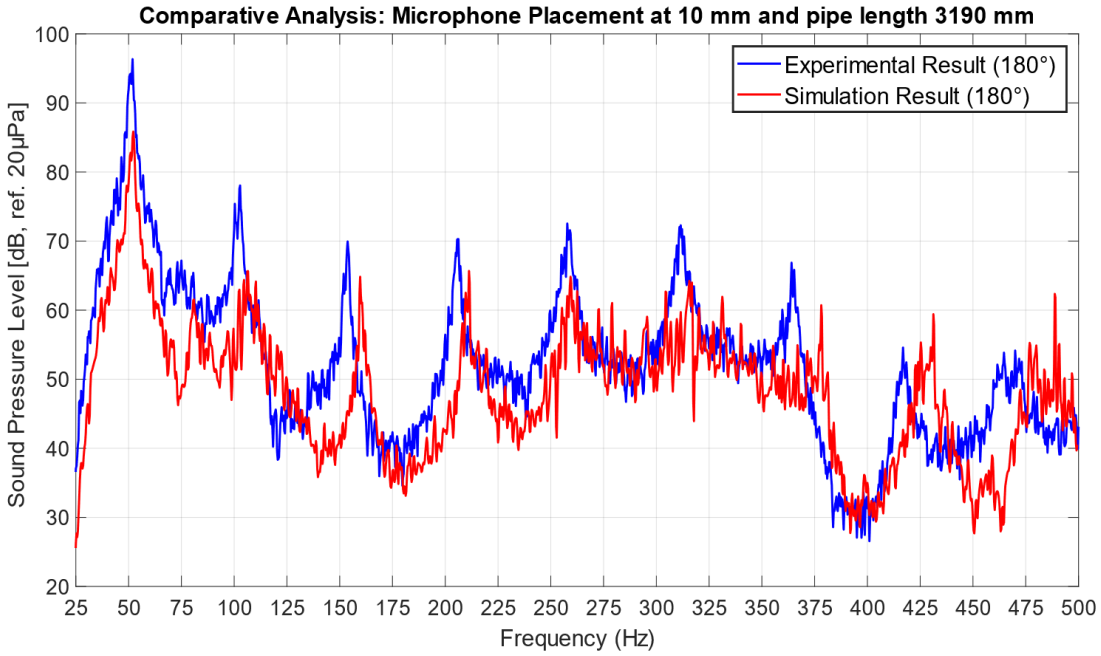

Figure 39. Simulation and experimental results considering the same pipe lengths.

4.4.2.2 Acoustic Impedance Data used for Source Characterization

It is important to understand the effect of impedance on the distribution of resonant frequencies. The resonant frequency of a system is determined by the interaction of its mass, stiffness, and damping. Impedance, which represents resistance to the flow of energy, affects damping and energy dissipation within the system. Higher impedance values tend to increase energy dissipation, potentially shifting resonant frequencies to lower values. Conversely, lower impedance values increase the efficiency of energy transfer, causing resonant frequencies to shift to higher values. In essence, impedance shapes the distribution of resonant frequencies by modulating energy dissipation and transfer within the system.

The impedance data used for the simulation is underestimated because it's computed from pressure and particle velocity measurements taken 10 mm outside the connector. However, the actual impedance inside the connector would be higher and have different phase information than the one computed from the parameters measured outside the connector. This is because the high pressure inside the pipe increases the air density, and the geometric factors inside the connector can further increase the impedance value. As a result of the lower input impedance data, the resonant frequencies observed during simulation tend to shift to higher frequencies.

4.4.2.3 End-Environment-Induced Frequency Shift

Boundary Pressure template has been used in GT-POWER during the modeling of experiments. This template defines the boundary environment using the ambient temperature and pressure in GT-POWER (see section 3.3.1.3 for details). The template supports the free field environment, where the sound propagates unhindered according to the inverse square law. In addition, the template does not define the impedance present in the environment. This is in contrast to real-world experimental conditions where reflections from walls, floors, and obstacles introduce complexities. The real environment has its own characteristic impedance depending on the properties of the medium. Because of this characteristic impedance, the value of the end reflection during the experiment would be different from that of the GT-POWER environment. This can differ the formation of the resonance frequencies of experimental results from the simulation one’s.

4.5 Parametric study by means of GT-model

Acoustic behavior is sensitive to changes in geometric parameters. This is particularly true when sound is propagated through a pipe. Even small changes in pipe length can significantly affect the frequency response of the entire system. In this section, a parametric study is carried out by changing geometric parameters such as pipe length

and diameter using GT-model. In addition, the pipe is subjected to different bending angles to see their effect on the frequency spectrum.

4.5.1 Effect of change in pipe length on the observed frequency spectrum

The length of the pipe plays a critical role in determining the resonant frequency, following the inverse relationship given by Eq. (55) for the open-ended pipe.

$$f = \frac{v}{2L};\ \lambda = 2L \tag{54}$$

Longer pipe length increases the spatial extent of the standing wave. As a result, the fundamental frequency of the first harmonic decreases, allowing more harmonics to be accommodated in the pipe. For example, in GT-POWER, increasing the pipe length from 3180 mm to 3500 mm results in an observable increase in the number of harmonics in the pipe, as shown in Fig. 40.

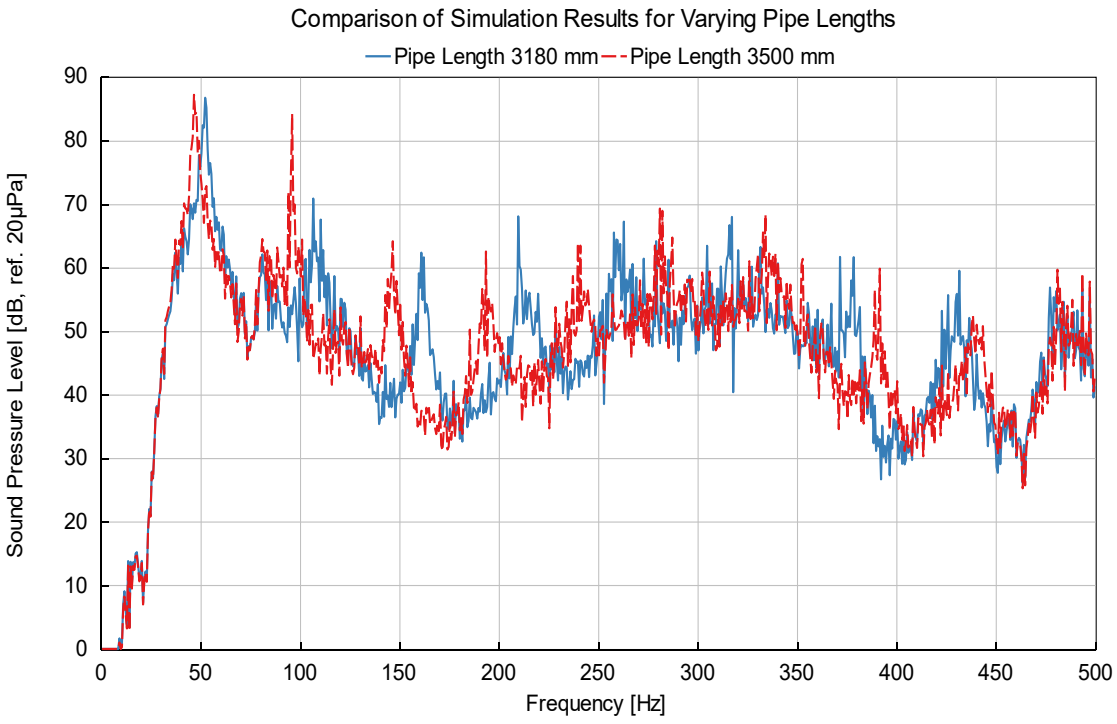

Figure 40. The blue curve shows the SPL at 3180mm, while the red dotted lines show the frequency spectrum at an increased length of 3500mm.

The dotted line in the graph indicates an additional harmonic. This harmonic is generated by increasing the pipe length by only 320 mm. The graph demonstrates that pipe elongation shifts resonant frequencies towards lower frequencies. This is consistent with Eq. (55) and reinforces the idea that increasing pipe length reduces the frequency of the first harmonic and its corresponding harmonics. In general, as the fundamental frequency decreases, the energy associated with the first harmonic is spread over a wider frequency range. Consequently, this shift can potentially affect the amplitude of frequencies adjacent to the fundamental.

4.5.2 Effect of change in pipe diameter on the observed frequency spectrum

The change in the diameter of the pipe does not result in a significant change in the resonant frequencies, as shown in Fig. 41.

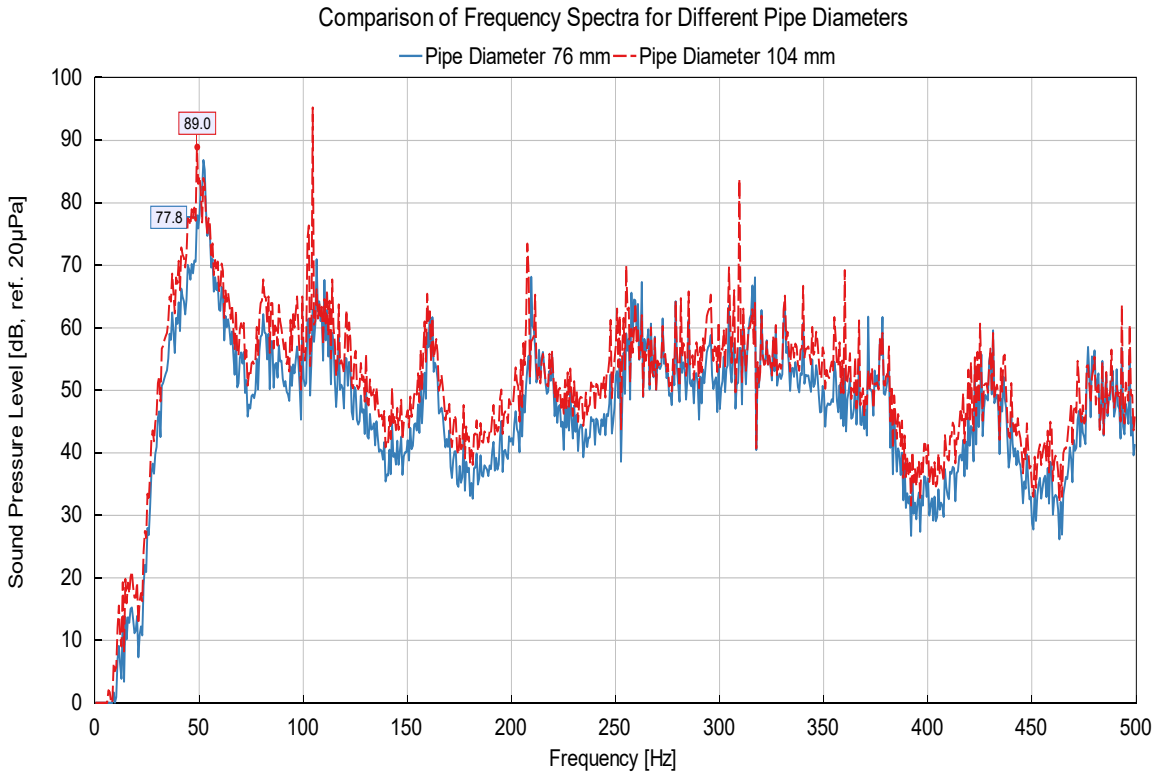

Figure 41. Influence of the change in diameter on the SPL and the resonance frequencies.

The acoustic impedance of the medium changes as the diameter changes. The impedance is inversely proportional to the cross-sectional area of the pipe So, increasing the diameter reduces the impedance. This decrease in impedance can result in an increase in sound pressure level. For example, when the pipe diameter is increased from 76 mm to 104 mm, the larger diameter pipe shows a gain of 5 to 7 dB at various frequencies, as shown in Fig. 41. There is also a slight shift in the resonant frequencies. The change in pipe diameter has an indirect effect on the end reflections of the pipe due to the change in impedance. The impedance mismatch between the pipe's medium and its environment determines this end reflection and its influence on resonant frequencies.

4.5.3 Effect of change in pipe angle on the observed frequency spectrum

The GT models based on the experimental configuration of Set2 (90°) and Set3 (180°) were simulated using pipes with different bending angles. Three cases with different bend angles were created in GT-POWER. These were used to examine the effect of the bend on the acoustic flow. A different bend angle but the same pipe geometry was used in each case. The simulation results for all these cases are shown in Fig. 42. The results indicate that changing the bend angle has a negligible effect on the sound pressure level in pipes with a constant cross-sectional shape. This observation holds for both simulation and experimental conditions, where the frequency spectrum remains unaffected by the presence of bends in both the exhaust pipes and the reference experimental setups.

The overall conclusion is that the bends do not affect the sound behavior under the dominance of the fundamental propagation mode. Bends may have caused partial dispersion and reflection of the sound waves, resulting in some energy being dissipated and redirected. But the total energy was conserved. The fundamental is the lowest mode of propagation, and most of the energy is concentrated in this mode. Therefore, a little dissipation does not affect the overall spectrum. Additionally, it's worth mentioning that

the bends in both cases do not possess a sharp geometry significant enough to induce noticeable effects on the observed frequency spectra.

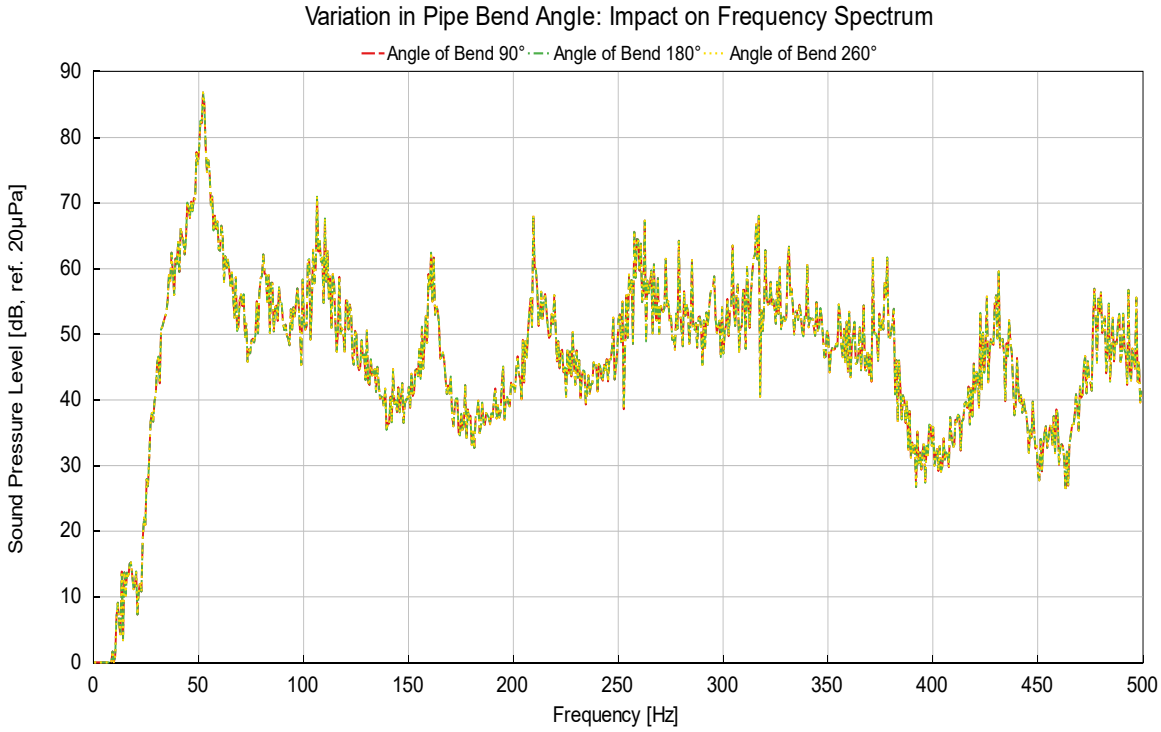

Figure 42. The frequency spectrum of the pipes with different bend angles does not differ.

5 Summary and Outlook

The thesis aimed to analyze the acoustic effects of the complex pipe geometries at low frequencies. The analysis of the experimental results of the exhaust pipeline and the reference experiment showed negligible influence of bends on the SPL. Moreover, certain resonant frequencies were generated during the reference experiment. These resonant frequencies enhanced the SPL and elaborated the existence of standing waves inside the ducts. However, the main exhaust pipeline did not show any inherent resonant behavior under the influence of the pink noise. The fundamental mode of propagation existed throughout the experimentation.

In the thesis, a comprehensive investigation was carried out to identify the factors impacting the precision of noise measurements, with a specific focus on calibrating airflow simulation models. It was found that the primary challenge lay in obtaining accurate experimental measurements essential for the simulation process. The reliability of predictions using the GT model is predominantly contingent on the precision of the input data. An analysis clearly revealed that measuring SPL outside the pipe can lead to unfavorable outcomes. In fact, there can be a substantial increase in SPL, ranging from 8 to 10 dB, simply by moving the sensor 9 mm closer to the sound source. Therefore, to ensure the fidelity of simulation outcomes, it is imperative to position the sensor inside the connecting pipe during data measurement. Moreover, the parametric study performed with the GT model showed that the resonant frequencies decrease as the pipe length increases. However, increasing the pipe diameter did not have a significant effect on the frequency spectrum.

Addressing research question 1,

The difference in SPL amplitude can be related to the sensitivity of the microphone position during the experiment and the pressure data used to characterize the source.in GT model. The experimental results showed an increase of 8-10 dB in SPL as compared to the simulation. In both cases, the sensor was placed 10 mm from the source. A similar gain was observed when the B&K 2250 probe was placed closer to the source opening

at 1 mm compared to the SPL observed with the PU probe at 10 mm. In addition, a 10-15 dB gain was observed when a microphone was moved 9 mm closer to the source in the GT-POWER. Such a substantial gain in SPL by moving the probe such a short distance demonstrates probe position sensitivity during the experiment. The difference in SPL amplitude could be due to the probe's position during the measurement. A slight jerk in the hand movement during reading may have inadvertently brought the PU probe closer to the pipe opening. As a result, the experiments showed an increased SPL. Another reason for the difference is related to the accuracy of the simulation results. The pressure data used to define the source of GT-POWER was measured at a distance of 10 mm from the connector. Pressure data has been normalized to the value closest to the source. However, this data is not as accurate as it should be when measured inside the connector pipe. The pressure data measured outside was underestimated and contained imprecise phase information, resulting in a lower SPL amplitude in the simulation results.

The disparity in frequency shift could be linked to three distinct factors: the geometric parameters of the pipe, the input impedance for source characterization, and the state of the end environment. First, there was a difference between the pipe length during the experiment and that simulated in GT-POWER. This discrepancy was due to the characterization of the source after the connector. This was resolved by using the same pipe length in both scenarios. As a result, the frequency offset between the results was reduced. However, a minor difference in frequency agreement remained. This was related to the impedance data used for source characterization in GT-POWER. The impedance data was taken from the outside of the connector. However, the impedance value inside the pipe is expected to be higher. The higher impedance value dissipates more energy and shifts resonance frequencies to lower frequencies. Due to the low value of measured input impedance, the difference between the frequency mismatch of experimental and simulation results persists. The third factor is attributed to the boundary conditions. There is a difference between the end environment of the GT-POWER and the experiment. In GT-POWER, the end environmental was considered a free field. On the other hand, the real-world environment had its impedance characteristics.

This dissimilarity in the end environments impacted the end reflection of the pipe in both scenarios, consequently affecting the resonant frequencies accordingly.

Addressing research question 2,

The results of this study have helped to determine the optimal location for obtaining input data for accurate source characterization within GT-POWER. The input data, such as pressure or particle velocity, should be obtained from measurements taken inside the duct or pipe. Data obtained from external measurements will not faithfully represent the phenomena occurring inside the pipe. In particular, when sound waves interact with the boundaries of the duct, they can scatter and undergo phase shifts, resulting in noticeable changes in wave behavior. As a result, externally obtained pressure and particle velocity measurements may not accurately capture these complex effects. There are phase and magnitude discrepancies between external and internal measurements. Moreover, during the source characterization within GT-POWER, data should be obtained at the point closest to the experimental source. In the case of pipe, the data should be taken from the lowest point available in the pipe. This approach ensures a harmonious match between the resonant frequencies observed during the experiment and those generated by the simulation.

Regarding research question 3,

The exhaust pipe was divided into three sections following the bends. All sections showed an almost similar trend in the observed frequency spectrum. No significant differences were observed in the frequency spectra of the noise after the bends, particularly below the cut-off frequency (446 Hz). The reason for this phenomenon can be attributed to the fundamental mode of wave propagation. The bends in exhaust pipe do not possess a sharp geometry significant enough to induce noticeable effects on the observed frequency. Bends may have caused partial dispersion and reflection of the sound waves, resulting in some energy being dissipated and redirected. But the total energy was conserved. The fundamental is the lowest mode of propagation, and most

of the energy is concentrated in this mode. Therefore, a little dissipation does not affect the overall spectrum.

Addressing research question 4,

During the parametric study using the GT model, it was observed that as the pipe length increases, the resonant frequencies decrease and shift to lower frequencies. Generally, when the fundamental frequency decreases, the energy associated with the first harmonic spreads over a wider range of frequencies. Consequently, this shift can affect the amplitudes of frequencies neighboring the fundamental frequency. Moreover, an increase in pipe diameter did not significantly impact resonance frequencies. However, when the diameter was increased by half compared to the original diameter, there was a noticeable increase in SPL of 5 to 6 dB. This can be attributed to the reduction in impedance resulting from the increased diameter, leading to a higher acoustic pressure. Furthermore, the presence of different bend angles in the pipe did not show any significant influence on the SPL during the simulation. The same phenomenon was observed in the experimental results of the exhaust and plastic pipe. Bends did not affect the SPL, especially in the low-frequency range. This is primarily due to the dominance of the fundamental mode of wave propagation. The combined evidence from simulations and experiments supports this finding.

Outlook

The findings from this study have practical implications for precise source characterization and exhaust pipeline modeling using the GT-SUITE platform. Specifically, it is advisable not to rely on acoustic parameters, such as pressure and particle velocity, measured externally to the pipe for source characterization. Discrepancies can arise due to significant variations that occur in these acoustic parameters once they exit the pipe. The recommended approach is to utilize acoustic parameters measured internally within the pipe as the input for source characterization in the GT model. This approach enhances the accuracy of the modeling and simulation process. One way of doing this is by imposing the internal measured pressure as source in GT model.

Furthermore, for subsequent simulations, it is suggested to use a non-linear method to predict acoustic behavior. Non-linear methods provide a more detailed analysis based on the calculation acoustic properties for each individual component. For instance, in case of running engine, pressure and temperature readings can be acquired after the exhaust turbine. This data can be subsequently utilized as a source by imposing a pressure boundary condition within the established GT model of the exhaust pipeline. Consequently, this model can be further fine-tuned and optimized to minimize noise emissions.

In addition, if impedance needs to be measured, it is suggested to perform these measurements inside the duct using the two-microphone method. This method involves determining the reflection coefficient and then calculating the impedance value from these measurements. This approach, particularly in open pipe scenarios, provides more accurate impedance data and gives an idea of the extent of end reflections.

From a measurement point of view, it is recommended to take readings in an open environment at least three times to reduce potential discrepancies. This practice improves the reliability of the data collected and ensures consistency of results. Moreover, for source characterization, it is recommended to measure acoustic data at a point inside the pipe that is nearest to the experimental source. This approach guarantees harmonious resonant frequencies between the simulation and the experimental outcomes.

6 Conclusions

The outcomes of this study are as follows:

- It is observed that the SPL measured outside the pipe end is very sensitive to the positioning of the sensor. A gain of 8 to 10 dB in SPL has been observed experimentally by moving the sensor only 9 mm closer to the source. However, a gain of 10 to 15 dB is observed using the GT SUITE due to its idealized and free field environment.
- The deviation of the GT model-based results from the experimental ones shows the inaccuracy of the input data used for the simulation. The pressure and impedance data should be measured inside the source pipe. The measured values taken outside the source connecter were underestimated and did not contain the correct phase information.
- The experimental results of the exhaust pipe showed that the exhaust duct does not inherit its resonance under the influence of pink noise. However, the resonance of the transmission pipe (plastic pipe) was transferred to the exhaust pipe and persisted below the exhaust pipe's cut-off frequency.
- Throughout the experiment, the first mode, also known as the fundamental mode of wave propagation, prevailed. This can be related to the type of noise used in the analysis. Since pink noise was used, its energy is concentrated in the lower frequency range.
- The exhaust pipe is divided into three sections, followed by the number of bends. No significant bend effect is observed on the frequency spectrum of these sections. The reason for this can be related to the dominance of the fundamental mode. Since the energy remains conserved in this mode, the energy lost due to scattering and reflection at the bends does not contribute enough to affect the total mode energy.
- The experimental results based on the plastic pipe setups did not show any effect of the bend. The same frequency spectrum was observed in the case of pipe with smooth 90° and 180° bends. Similarly, in the simulations based on the GT model,

no effect of pipe bend was observed even when the pipe was subjected to a 240° bend.

- The parametric study using the GT model showed that the resonant frequencies shift towards the lower frequencies in case of increasing the pipe length.
- In contrast, increasing the diameter had no noticeable effect on the resonant frequency. However, the SPL was increased by 5 to 6 dB by increasing the diameter by half of its original diameter. This increase in SPL can be related to a decrease in impedance since impedance is inversely proportional to the cross-sectional area of the pipe.

References

(XII), I. R. (1981). *Code on noise levels on board ships.*

5040A Active Subwoofer. (2008, 6). Retrieved from GENELEC: https://assets.ctfassets.net/4zjnzn055a4v/11Z9iD8ILw2EQi2kCOE62i/70de42ba81bc579aa865740fb292ad72/5040A_opman.pdf

Acoustic Impedance. (2009). Retrieved from UWSP: https://www4.uwsp.edu/physastr/kmenning/Phys115/Link5-09_acoustic_impedance.pdf

Acoustic impedance. (2023, July 27). Retrieved from WIKIPEDIA The Free Encyclopedia: https://en.wikipedia.org/wiki/Acoustic_impedance

Acoustic Resonance. (2023, June 5). Retrieved from WIKIPEDIA: https://en.wikipedia.org/wiki/Acoustic_resonance

ACOUSTIC SENSORS & MEASURING SOLUTIONS. (2021). Retrieved from MicroFLown TECHNOLOGIES: https://www.microflown.com/products

(2023). *Acoustics Application Manual.* Westmont: GT-SUITE.

Authority, D. M. (2002). *Technical Regulation on Noise in Ships, Technical Regulation no. 4.*

Basic Concepts of Digital Signal Processing. (2008). In L. Tan, *Digital Signal Processing* (pp. 19-20). United States of America: ELSEVIER.

Basics: What is a decibel (dB) anyway? Why is it used? (2021, 01 11). Retrieved from community.sw.siemens: https://community.sw.siemens.com/s/article/basics-what-is-a-decibel-db-anyway-why-is-it-used

Brüel & Kjær. (1984). *Measuring Sound.* Retrieved 06 06, 2023, from https://www.bksv.com/doc/br0047.pdf

Clean Propulsion technologies. (2023). Retrieved from Project Website.

Crocker, M. J. (2007). *Handbook of Noise and Vibration Control.* John Wiley & Sons, Inc.

Danish Environmental Protection Agency. (2010). *Noise from ships in ports. Possibilities for noise reduction.* Denmark: Lloyd's Register ODS. Retrieved from https://mst.dk/media/mst/66165/978-87-92668-35-6.pdf

Dokumacı, E. (2021). *Duct Acoustics.* CAMBRIDGE UNIVERSITY PRESS.

F. Alton Everest, K. C. (2015). New York: McGraw-Hill Education.

Finn Jacobsen, H.-E. d. (2005). A comparison of two different sound intensity. *Acoustical Society of America*, 1513.

Finn Jacobsen, P. M. (2013). *Fundamentals of General Linear Acoustics.* WILEY.

G.R:A:S SOUND & VIBRATION. (2022). *Instruction Manual.* © 2016-2022 GRAS Sound & Vibration A/S. Retrieved from https://www.grasacoustics.com/component/dc/?dc_id=114

GRAS 40SC CCP Probe Microphone. (2023). Retrieved from grasacoustics: https://www.grasacoustics.com/products/special-microphone/probe-microphones/product/189-40sc

https://www.microflown.com/products/sound-localization-systems/scan-paint-2d. (2023). *SCAN&PAINT 2D*. Retrieved from MICROFLOWN TECHNOLOGIES.

IMO Resolution A.343(IX). (1975). *Recommendation on methods of measuring noise levels at listening posts.*

(1974). *International Convention for the Safety of Life at Sea.* International Maritime Organization (IMO). Retrieved 08 29, 2023, from IMO – the International Maritime Organization: https://www.imo.org/en/About/Conventions/Pages/International-Convention-for-the-Safety-of-Life-at-Sea-(SOLAS),-1974.aspx

ISO 1999:1990. (1990). *Acoustics — Determination of occupational noise exposure and estimation of noise-induced hearing impairment.* Retrieved from https://standards.iteh.ai/catalog/standards/sist/515cd798-ed1c-4190-99d4-dabaa7b41d48/iso-1999-1990

István L. Vér, L. L. (2005). *Noise and Vibration Control Engineering: Principles and Applications.* John Wiley & Sons, Inc.

Jaouen, L. (n.d.). *Octave and one-third octave frequency bands*. Retrieved from Acoustical Porous Material Recipes: https://apmr.matelys.com/Standards/OctaveBands.html

MATHIAS, K. (n.d.). *White Noise vs Pink Noise [Audio Engineering & Music Production]*. Retrieved from Audio University: https://audiouniversityonline.com/white-noise-vs-pink-noise/

Microflown Technologies . (n.d.). *PRODUCT CATALOG.* Arnhem.

(2023). *Nor150 Sound Intensity Option.* Norsonoc.

Norsonic. (n.d.). *Product data Norsonic noise excitation.* Lierskogen. Retrieved June 16, 2023, from http://norsonic.nl/assets/assets/1/noise-excitation.pdf

Octaves in Human Hearing. (2020, 09 17). Retrieved from community.sw.siemens: https://community.sw.siemens.com/s/article/octaves-in-human-hearing

(2019). *OPERATING MANUAL MR-PRO.* NTi AUdio. Retrieved from NTI-Audio: https://www.nti-audio.com/Portals/0/data/en/Minirator-MR-PRO-MR2-Manual.pdf

Particle velocity. (2021, November 18). Retrieved from WIKIPEDIA: https://en.wikipedia.org/wiki/Particle_velocity

Peters, R. J. (2011). *Acoustics and Noise Control.* London: Routledge.

(2019). *PU REGULAR.* Microflown Technologies. Retrieved 09 16, 2023, from https://www.microflown.com/assets/uploads/Product-Data/Product-Data-PU-Regular.pdf

PU Regular Particle Velocity Probe. (n.d.). Retrieved from AcSoft Noise, Vibration & Air Quality: https://acsoft.co.uk/product/pu-regular-particle-velocity-probe/

R. J. Peters, B. J. (2011). *Acoustics and Noise Control.* Routledge.

Ruby, R. (2023). *How to Use Pink Noise to Tune/EQ a Room*. Retrieved from Range of Sounds: https://rangeofsounds.com/blog/how-to-use-pink-noise-to-eq-a-room/

SCAN&PAINT 2D. (2021). Retrieved from MICROFLOWN TECHNOLOGIES: https://www.microflown.com/products/sound-localization-systems/scan-paint-2d

SCAN&PAINT 2D. (2023). Retrieved from MICROFLOWN TECHNOLOGIES: https://www.microflown.com/products/sound-localization-systems/scan-paint-2d

SilentEngine. (2022, october 1). Retrieved from Project: https://sites.uwasa.fi/silentengine/project/

Sound Intensity. (2020, Feburary 20). Retrieved from community.sw.siemens: https://community.sw.siemens.com/s/article/Sound-Intensity

Sound Intensity Probe Nor1290. (2023). Retrieved from Norsonic: https://web2.norsonic.com/product_single/sound-intensity-probe-nor1290/

Sound Pressure Level (SPL). (2023). Retrieved from SVANTEK Academy: https://svantek.com/academy/sound-pressure-level-spl/

Sound Pressure, Sound Power, and Sound Intensity: What's the difference? (2019, August 29). Retrieved from community.sw.siemen: https://community.sw.siemens.com/s/article/sound-pressure-sound-power-and-sound-intensity-what-s-the-difference

Sound Pressure, Sound Power, and Sound Intensity: What's the difference? (2019, August 19). Retrieved from community.sw.siemens: https://community.sw.siemens.com/s/article/sound-pressure-sound-power-and-sound-intensity-what-s-the-difference

WIKIPEDIA The Free Encyclopedia. (2023, Feburary 20). Retrieved from Cutoff frequency: https://en.wikipedia.org/wiki/Cutoff_frequency

Window Types: Hanning, Flattop, Uniform, Tukey, and Exponentia. (2019, August 29). Retrieved from community.sw.siemens: https://community.sw.siemens.com/s/article/window-types-hanning-flattop-uniform-tukey-and-exponential